SEARS FOUNDATION FOR MARINE RESEARCH
BINGHAM OCEANOGRAPHIC LABORATORY, YALE UNIVERSITY

JOURNAL OF
MARINE RESEARCH

VOLUME 13 1954 NUMBER 1

SOURCE OF WATER IN BASINS OFF SOUTHERN CALIFORNIA[1]

By

K. O. EMERY

University of Southern California

ABSTRACT

Water temperature and salinity measurements from most of the 14 basins off southern California, when compared with older data, show no detectable changes. The water in each basin is nearly isothermal and isohaline from the bottom to near the sill depth. Water temperatures indicate that the bottom water of most basins must have travelled from basin to basin in a general northwesterly direction while that of the outermost basins came directly from the open sea on the west. Each sill in the path of the water acts as a submerged dam which holds back the water that is deeper than the sill itself. The densest water which can cross, that near the sill depth, occupies each basin from its bottom to near its sill depth.

INTRODUCTION

An investigation of sediments from the floors of basins off southern California (Emery and Rittenberg, 1952) has indicated that certain characteristics of the sediment, such as the amount of organic matter and the depth of zero oxidation-reduction potential, are controlled in part by the nature of the overlying basin water. Conversely, the hydrogen-ion concentration, oxygen content, and sulphate-chloride ratio of the overlying water may be influenced by the sediment. Since the sediment and water are inter-related, additional work on the sediment could not be effective without more complete knowledge

[1] Contribution of Allan Hancock Foundation, No. 134.

of the water. For convenience, study of the water was divided into two parts: (1) An examination of the origin of the water mass, and (2) a study of the peculiar chemical properties near the bottom. The part on water origin has been completed and is presented herewith.

Most of the data for this study were obtained during the winter of 1952–1953 aboard the University of Southern California research vessel, VELERO IV. During four short cruises, vertical series of Nansen bottle samples were taken from nine basins as well as from five main basin sills and four secondary sills. Because of the importance attached to the interface between water and sediment, the samples at each station were spaced widely near the surface and more closely near the bottom, and usually an attempt was made to trip one Nansen bottle at the bottom. This spacing is the reverse of the usual oceanographic procedure. Supplementary data for two deep-sea stations and one station near a basin sill were obtained from records of fisheries research cruises made during 1949, 1950, and 1951 by vessels of the Scripps Institution of Oceanography (Staff, 1950, 1951, 1952).

In order to ascertain whether or not changes in the water of the basins had occurred during the past years, a search was made for older data. Unpublished data from three basins and a trough were obtained by John Lyman during 1940 while he was engaged in work at the Scripps Institution of Oceanography. In 1937 Sverdrup and Fleming (1941) obtained one observation below the sill depth of each of two other basins. Serial temperatures in another basin were measured by the U. S. Coast and Geodetic Survey in 1933 during a study of sound transmission in the water (Swainson, McIlwraith, and Dyk, 1934). Unpublished bottom temperatures for one of the basins that was sampled by Sverdrup and Fleming in 1937 were provided by Manley L. Natland, who had obtained them during 1931 and 1932 for a study of the depth distribution of Foraminifera (Natland, 1933).

TOPOGRAPHY

The sea floor off southern California is well sounded for such a large area, there being about 280,000 soundings in areas deeper than 100 m, mostly obtained by the U. S. Coast and Geodetic Survey between the years 1932 and 1938. From all available soundings, Shepard and Emery (1941) prepared charts at 50-fathom contour intervals. Fig. 1, simplified from the contour charts, shows the characteristics which are probably of greatest importance to bottom water circulation.

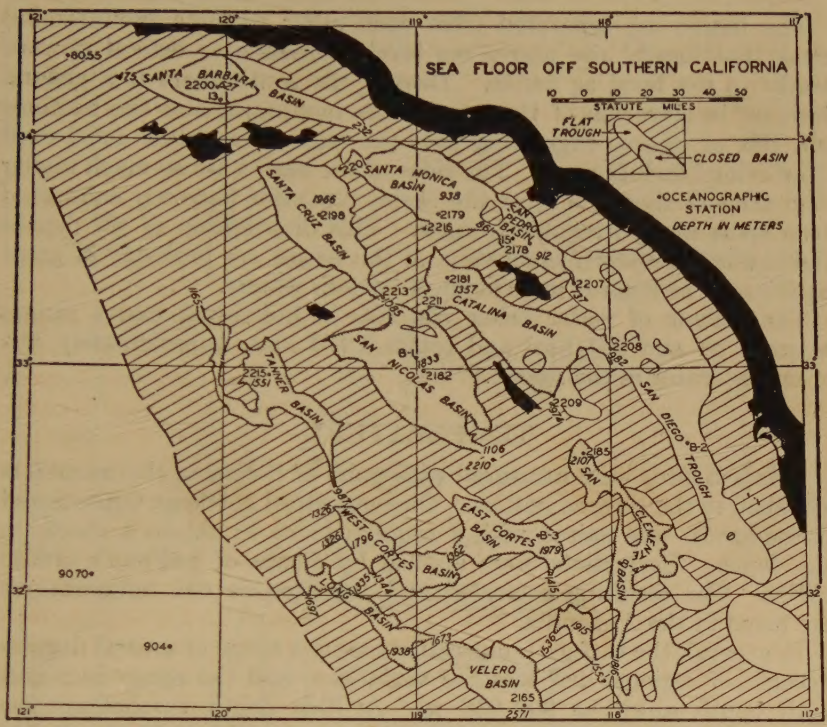

Figure 1. Topographic relations of basins off southern California. Stations between 2100 and 2300 are those of the Allan Hancock Foundation; most others are of Scripps Institution of Oceanography. Italicized numbers show the deepest point of basin floors and sills in meters.

In the 80,000 km² area bounded by the southern California shoreline on the east, Lat. 34° 30′ N on the north, the continental slope on the west, and Lat. 31° 30′ N on the south, there are 12 closed basins as well as parts of two more at the southern boundary (see Fig. 1). Thus, the region contains 14 basins, the bottom depths of which range from 627 to 2,571 m and the sill depths from 475 to 1,902 m below the sea surface. The differences between sill depth and basin depth for given basins vary from 152 to 881 m. Depth data for individual basins are presented in Table I and Fig. 1. Of the indicated depths, that of the sills is least certain because of the difficulty of determining the deepest point of a sill in the absence of extremely detailed surveys. Thus it is possible that reported sill depths have an accuracy no better than plus or minus 50 m. Curiously, each of four basins contains two sills that have indicated depths within 100 m of each other, and one basin has five sills of approximately equal depth.

The basins are separated from each other by high mountainous areas that locally rise above sea level as islands or extend upward nearly to sea level as banks. Toward the south there is a general decrease in elevation of the tops of the mountains and the bottoms and sills of basins, suggesting that the region was tilted southward after being block-faulted. The sides of the basins are so much higher than the sills that in a sense the basins represent narrowly connected deep spots along irregular troughs. This distribution of sill depths and the northwesterly elongation of the basins are probably of great significance as regards movement of bottom waters.

The volume of water below the sills in individual basins ranges between 43 and 961 km^3 and totals 3,470 km^3, approximately 5% of all the water in the region.

TEMPERATURE

Temperatures were measured with pairs of reversing thermometers attached to the Nansen bottles. On every third bottle an unprotected thermometer was paired with a protected one to obtain a check on the depth. Corrections were applied by means of LaFond's (1951) tables. The resulting corrected and averaged *in situ* temperatures are listed in the Appendix.

In general, the surface temperatures show a range of several degrees because of regional and seasonal variations, and the range decreases with depth down to 900–950 m. At this depth throughout the region all of the temperatures were identical within 0.2° C. Below 950 m the temperature-depth measurements again present a spread of values due to basin conditions. Below the sills, the water in a given basin approaches thermal uniformity except for the first hundred meters or so. The straight lines in Fig. 2 show a best fit through the points well below each basin sill. The mean difference between these lines and the 63 measurements is only 0.02° C, which is close to the limit of accuracy of the thermometers. Absence of secular or seasonal changes in temperature below the sills is indicated by the fact that 15 earlier (1931–1940) temperature measurements below the sills have a mean difference of only 0.01° C from the same straight line. The temperature is so constant with depth and time in fact that these areas may even prove useful for checking the calibration of thermometers.

In several of the basins a temperature decrease amounting to a few hundredths of a degree occurs in the first hundred meters below the sill, and in one basin (San Nicolas) it amounts to 0.13° C. Probably this gradient can be attributed to mixing. At greater depths, the

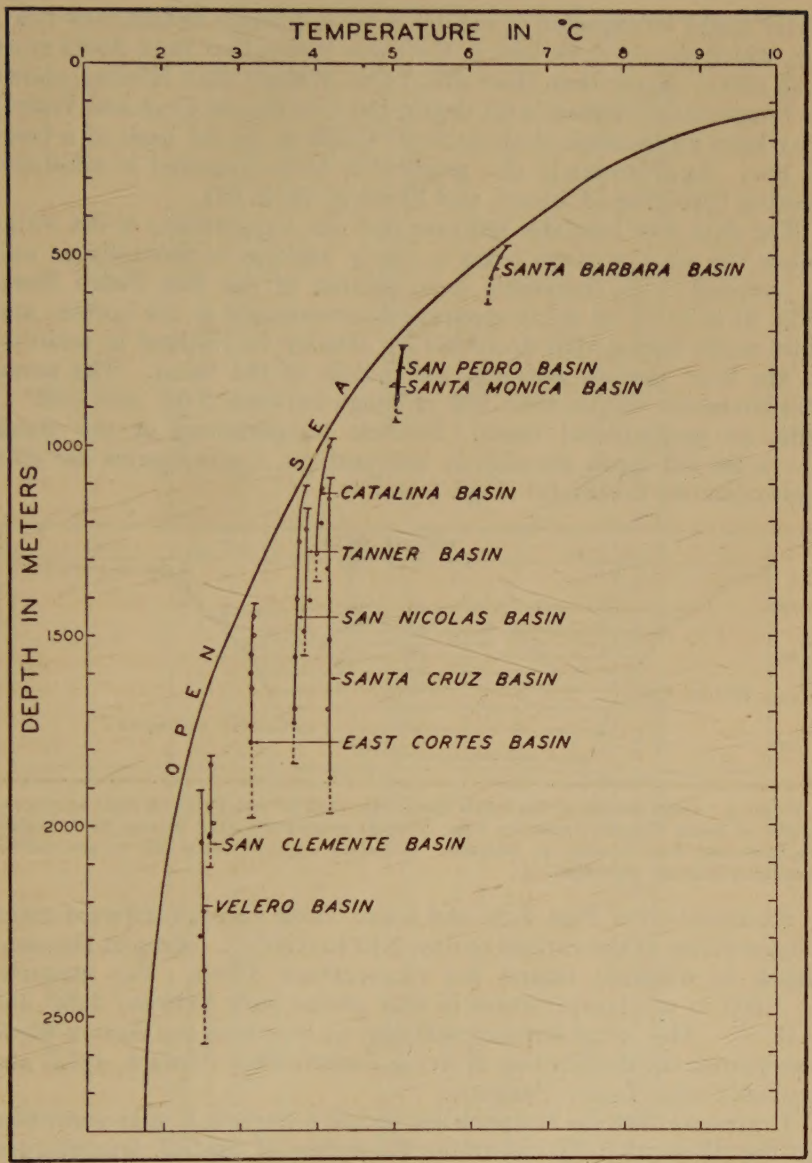

Figure 2. Temperature-depth curves for the open sea (St. 904) and for basin water below sills. Short horizontal lines indicate sill and bottom depths of basins. The dashed lines indicate water below lowest sample bottle plus difference in depth between station location and deepest part of basin.

water might be expected to exhibit some indication of adiabatic heating, which should show best in the three basins that have floors more than 650 m deeper than their sills. One of these (San Nicolas) shows no temperature increase with depth, but two (Santa Cruz and Velero) may have an increase of about 0.04° C/500 m on the basis of a best-fit line. Approximately this gradient is to be expected in adiabatic heating (Sverdrup, Johnson, and Fleming, 1942: 63).

The data now available indicate that the temperature of the water below the sill of a given basin is nearly uniform horizontally as well as vertically. A transverse cross section of the San Pedro Basin (Fig. 3) is based on many separate measurements at the bottom and sides made during 1931 and 1932 by Manley L. Natland in addition to the later vertical series in the middle of the basin. The seven measurements deeper than 800 m range between 5.04° and 5.09° C with no geographical trend. Because temperatures of the water above the sill depth are slightly less uniform, the isotherms are only approximately horizontal (Figs. 3 and 4).

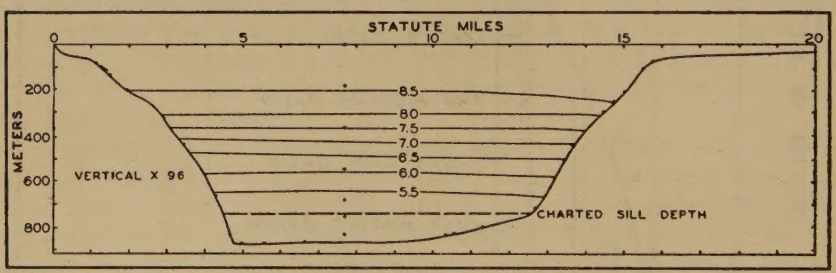

Figure 3. Cross section of San Pedro Basin from shelf off San Pedro on right to shore at middle of Santa Catalina Island on left. Vertical series from AHF Station 2178; bottom measurements from Manley L. Natland. Isotherms shallower than 200 m are omitted because of seasonal variations.

Examination of Figs. 2, 4, and 5 and Table I shows different mean temperatures in the various basins: 2.52 to 6.26° C. Even at the same depth in different basins the temperature differs. For example, at 1,900 m the temperatures in four basins vary between 2.52° and 4.15° C. This range appears sufficient to be one of the factors which can control the distribution of living Foraminifera (Crouch, 1952) and probably other faunal elements.

It appears that the temperature within a basin is largely controlled by the sill depth. To determine the degree of control, temperature-depth series were obtained as near as possible to the position of the lowest sill at each of five basins. The lowermost Nansen bottle was still 3 to 51 m above the lowest charted sill depth, and therefore the sill

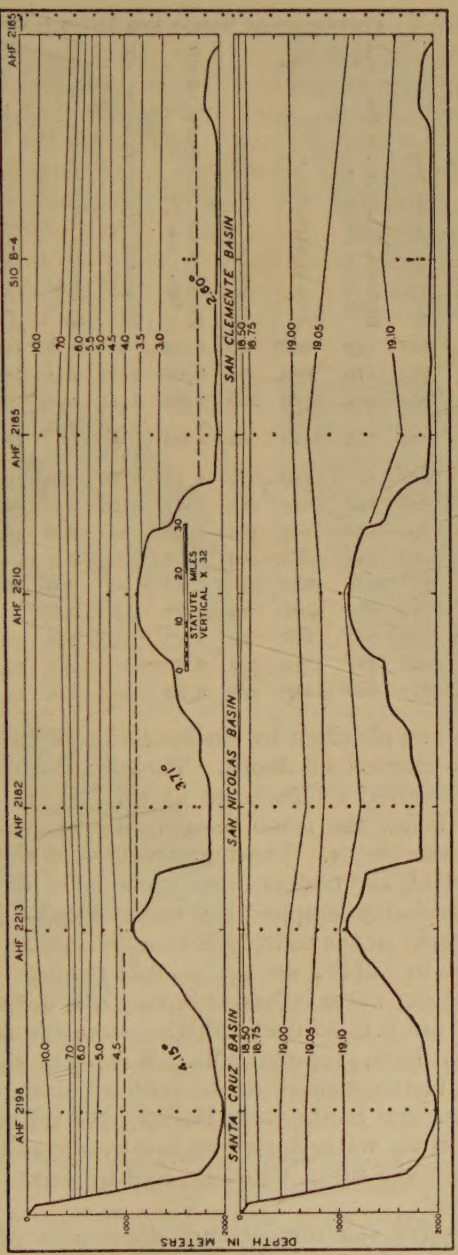

Figure 4. Longitudinal sections of San Clemente, San Nicolas, and Santa Cruz Basins. Isotherms in °C at top; isochlores in °/₀₀ at bottom. Horizontal dashed lines indicate effective sill depth. Water at extreme right is assumed to be like that of Velero Basin.

TABLE I. Properties of Basins and Their Water

	Lowest sill depth from sea surface (m)	*Depth of bottom (m)*	*Difference between sill depth and bottom depth (m)*	*Area of basin (km²)*	*Volume of basin (km³)*	*Temperature of basin water below sill (°C)*	*Measured temperature at sill (°C)*	*Estimated temperature at sill (°C)*	*Chlorinity of basin water below sill (‰)*	*Effective sill depth (m)*	*Sonic minus effective sill depth (m)*
Santa Barbara	475	627	152	660	45	6.26	—	6.5	18.96	510	−35
San Pedro	737	912	175	655	78	5.06	5.11	5.1	18.98	750	−13
Santa Monica	737	938	201	1805	210	5.05	5.11	5.1	18.99	750	−13
Catalina	974 982	1357	383	2140	89	4.02	3.90 4.17	4.1 4.2	19.05	1010	−36
Santa Cruz	1085	1966	881	1780	879	4.15	3.85	3.9	19.11	980	+105
San Nicolas	1106	1833	727	2660	961	3.71	3.76	3.7	19.11	1100	+6
Tanner	1165	1551	386	1260	183	3.85	—	3.6	19.13	1060	+105
West Cortes	1362	1796	434	1005	160	3.3?	—	3.2	—	—	—
East Cortes	1415	1979	564	1055	216	3.13	—	3.0	19.11	1370	+45
No Name	1553	1915	362	307	43	2.9?	—	2.8	—	—	—
Long	1697	1938	241	830	63	2.7?	—	2.5	—	—	—
San Clemente	1816	2107	291	1490	120	2.60	—	2.5	19.13	1750	+66
Velero	1902	2571	669	1310	420	2.52	—	2.3	19.14	1700	+202

temperature had to be obtained by extrapolation of the temperature-depth curve to the charted sill depth. The extrapolations, indicated in Table I as "measured temperature at sill," range from 0.05° C above to 0.30° C below the mean temperature of the water deeper than sill depth in the basins. The temperatures at the depth of the sills were also read off the temperature-depth curve of the adjoining water mass that probably supplied the water which crossed the sill, usually the next basin to the south. These "estimated temperatures at sill," shown also in Table I are 0.1° to 0.3° C lower than the temperature of the bottom water in basins having sills deeper than about 1000 m, but they are 0.1° to 0.2° C higher than the temperature of water in basins that have shallower sills. Where the sill temperature is lower than that at the same depth in both adjoining basins (as in sills of the Catalina and Santa Cruz Basins), the difference must be due to a slight rise of the water during its flow over the sill, as discussed by Schott (1928) for the sill at Gibraltar and by Parr (1937) for sills in the Caribbean Sea.

Attempts to resolve the temperature differences of basin water and sill water led to the conclusion that the water which enters a

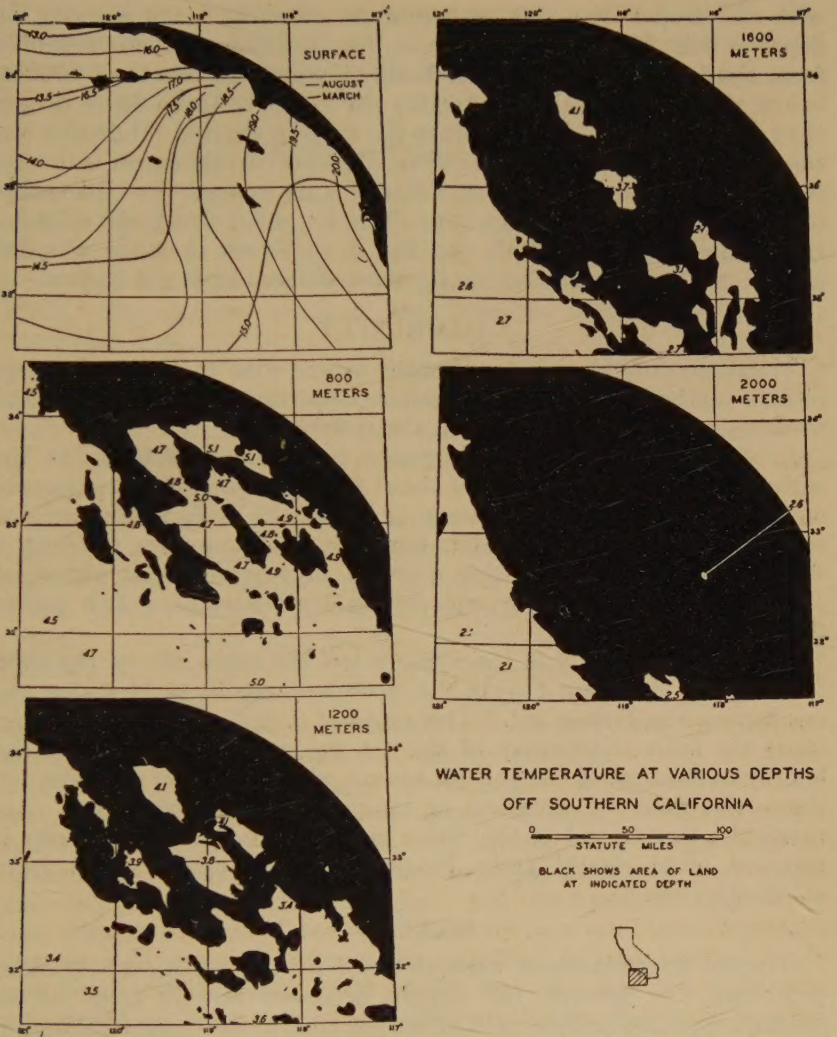

Figure 5. Maps of sea floor at 0, 800, 1200, 1600, and 2000 m. The solid black represents land areas at the various levels. Temperature in °C. Generalized isotherms for March and August at surface from Leipper (1947).

basin may come from some depth other than that of the exact lowest point of the sill. The average water temperature in any given basin is the same as that at some depth in an adjoining basin, and this depth was taken as the effective sill depth (see Table I). For basins

with sills deeper than 1000 m below the sea surface, the effective sill depth is 6 to 202 m shallower than the sill depth that was accepted from available soundings. For basins having sills less than 1000 m below the sea surface, the effective sill depth is 13 to 36 m deeper than the charted sill depth. Since the error in charted sill depths was considered to be plus or minus 50 m, the effective sill depth is in substantial agreement with the soundings for six basins. For four other basins (San Clemente, Santa Cruz, Tanner, and Velero), the effective sill depths are 66, 105, 105, and 202 m shallower than the sounded sills, respectively. The reason for these differences is not known.

CHLORINITY

Titrations for chlorinity were done ashore with the ordinary silver nitrate method standardized against Copenhagen sea water. The method is considered accurate to about 0.02 ‰.

In general, the chlorinity increases from about 18.40 ‰ at the surface to 18.90 ‰ at a depth of about 300 m, below which it increases more gradually to values between 19.10 and 19.15 ‰ within most of the basins. Near the bottom, however, there appears to exist a slight decrease. Because this decrease may indicate an abnormal salinity-chlorinity ratio, the chlorinities are reported as such rather than as salinities.

The mean chlorinity of the water below the basin sills ranges from 18.96 ‰ for the basin having the shallowest sill to 19.14 ‰ for the one having the deepest sill. This range of 0.18 ‰ is only about nine times the limit of accuracy of the determination, in contrast to the temperature range of the bottom waters, which amounts to about 190 times the limit of accuracy of temperature determinations. Accordingly, the control of the water movement exerted by the sills is revealed more clearly from temperature observations than from chlorinity (Fig. 4).

OXYGEN

Oxygen determinations were obtained by the customary Winkler procedure. In general, the oxygen decreases rapidly from 5.5 to 6.0 ml/L near the surface to less than 0.5 ml/L at the oxygen minimum between 500 and 600 m. Below the oxygen minimum in the open sea the oxygen again increases to about 2.0 ml/L at 2,000 m. Wherever the water is trapped in a basin, the bulk of it retains the approximate oxygen content that occurs at the sill depth; thus, if the sill is near the depth of oxygen minimum the oxygen content is low; if the sill is well below the depth of oxygen minimum the oxygen content of the basin water is higher. Accordingly, the oxygen content

of waters below basin sills ranges between 0.2 and 2.5 ml/L. Near the basin floors the oxygen content of the water may again decrease, owing to complex alteration of the water by the sediment and organisms living at the bottom.

SOURCES OF BASIN WATER

Pattern. In Fig. 4 it is obvious that the water near the bottom of San Nicolas Basin must have come from the mid-depths above San Clemente Basin rather than from Santa Cruz Basin, for there is no water in Santa Cruz Basin which is as cold as that in San Nicolas Basin. The deepest water of San Clemente Basin is so cold and dense that it cannot rise up to the level of the sill of San Nicolas Basin, and consequently it remains behind, marking the direction from which the water of San Nicolas Basin came. Similarly, the bottom water of San Nicolas Basin cannot rise to the level of the still shallower sill of Santa Cruz Basin, and it marks the direction from which Santa Cruz Basin was supplied.

The general path of the water is shown by isolated masses of trapped basin water of progressively higher temperature. Examined from this viewpoint, the temperature measurements show that the waters of the Santa Barbara, Tanner, and Long Basins have been supplied entirely or primarily from the open sea beyond the continental slope. Possibly some of the water in West Cortes Basin also came from the open sea. Velero Basin may have furnished some of the water in Long Basin and in the small unnamed basin just south of Sixtymile Bank. It appears probable that the waters in all of the remaining basins have funnelled through the unnamed and unexplored basin east of Velero Basin above its sill depth. From this unnamed basin two tongues extend northward. The left-hand one enters the small basin south of Sixtymile Bank and proceeds thence to East Cortes and finally to west Cortes Basin. The right-hand tongue enters San Clemente Basin, from whence it divides into three branches. One branch turns northwestward into San Nicolas and continues into Santa Cruz Basin. The middle branch continues northward into Catalina Basin, where it may partly leave that basin through the sill southeast of Santa Catalina Island to rejoin the third branch which left San Clemente Basin to proceed northward up the San Diego Trough. The two rejoined branches thereupon proceed northwestward into San Pedro and thence into Santa Monica Basins.

The sides of most of the basins extend upward to form islands or rise at least to depths that are much shallower than the sills; thus, the sides confine the movements of water at the depth of most down-current

sills. Only the sills of the San Pedro Basin and Catalina Basin are sufficiently shallow with respect to the surrounding topography to permit water to enter by a number of routes. The current axes leading to these sills are shown as dashed lines in Fig. 6.

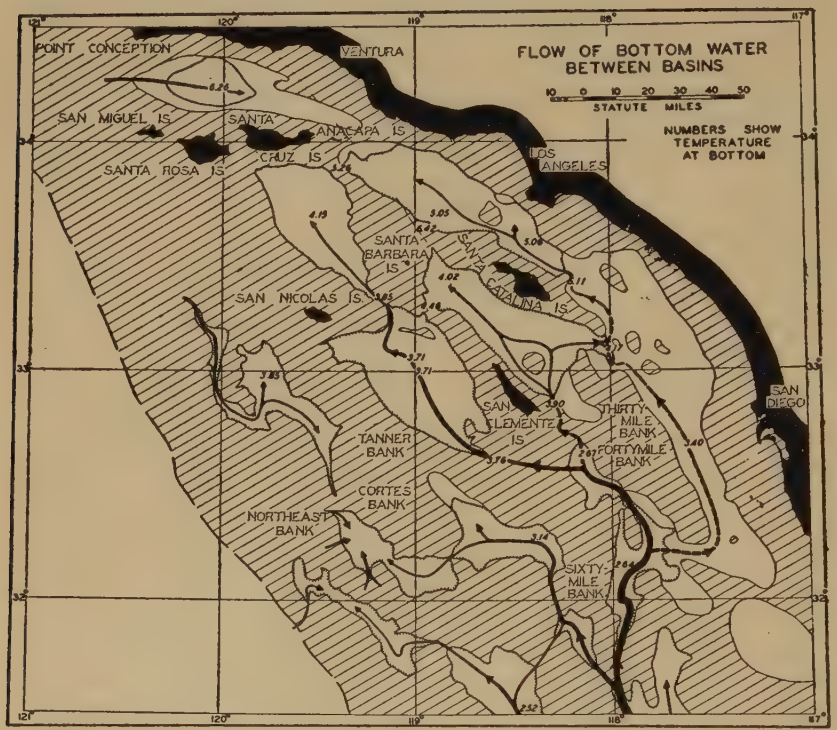

Figure 6. Pattern of water flow from basin to basin. Width of arrow serves as rough indicator of relative transport volume.

In its travels through the basins, the water appears to have followed a general northwesterly course that is opposed for the most part to the surface current, especially during winter. The latter is shown by the generalized map of surface isotherms (Fig. 5), if we assume that the current flows along the isotherms in a direction such that the warm water is on the right-hand side of the current. Because of the current which exists near the surface, there must be continual mixing across the interface between the water masses. As a result of this mixing, some of the water below the basin sills becomes less dense in the course of time, thus permitting the flow of additional

water across the sills. Because of the slow mixing and replacement, the water within the basins does not become stagnant and devoid of oxygen.

The relationship of the water to topography off southern California is similar to that observed in basins of the East Indies (van Riel, 1934; van Riel, Hamaker, van Eyck, 1950) and in the West Indies (Parr, 1937). Thus, in a sense, the basins off southern California are small scale parallels of the basins of the East Indies and West Indies.

Velocity. The many surveys of temperature and salinity of the near-surface waters off southern California, when converted to dynamic topography, yield surface current speeds that locally range up to about 50 cm/sec and average between 10 and 15 cm/sec. Though such computations are subject to many errors, these computed currents show good agreement with the results of drift bottle experiments (Sverdrup and Fleming, 1941: 273).

Thus far indirect methods have not been applied to the problem of currents within the basins and below their sills, but brief measurements with current meters have been made just above the floors of Santa Cruz and San Pedro Basins (Shepard, 1948: 65). In Santa Cruz Basin, currents between 8 and 15 cm/sec were obtained, the speeds just above the bottom often being greater than those of currents slightly above them; thus the presence of turbulent motion is indicated. In San Pedro Basin the speeds ranged between 7 and 18 cm/sec. Since the measurements are not very complete, the origin of these currents is uncertain, but they may be related to seiches.

ACKNOWLEDGMENTS

Appreciation is due Captain Allan Hancock for making Velero iv available for the field work. Aid in the collection and analysis of samples was rendered by Messrs. B. L. Conrey, J. R. Grady, J. W. Marlette, and F. C. Ziesenhenne. John Lyman and Manley L. Natland kindly contributed unpublished data, part of which is listed in the Appendix.

REFERENCES

Crouch, R. W.

1952. Significance of temperature on Foraminifera from deep basins off southern California coast. Bull. Amer. Ass. Petrol. Geol., *36:* 807–843.

Emery, K. O. and S. C. Rittenberg

1952. Early diagenesis of California basin sediments in relation to origin of oil. Bull. Amer. Ass. Petrol. Geol., *36:* 735–806.

LaFond, E. C.
1951. Processing oceanographic data. Publ. Hydrographic Office, No. 614. 114 pp.
Leipper, D. F.
1947. Sea surface temperature variations influencing fog formation in southern California. Rep. Scripps Inst. Oceanogr., Oceanogr. *9:* 13 pp. (mimeo.).
Natland, M. L.
1953. The temperature and depth distribution of some recent and fossil Foraminifera in the southern California region. Bull. Scripps Inst. Oceanogr., *3:* 225–230.
Parr, A. E.
1937. A contribution to the hydrography of the Caribbean and Cayman seas based upon the observations made by the research ship "Atlantis," 1933–34. Bull. Bingham Oceanogr. Coll., *5* (4): 1–110.
Schott, G.
1928. Die Wasserbewegungen im Gebiete der Gibraltarstrasse. J. Cons. int. Explor. Mer, *3:* 139–175.
Shepard, F. P.
1948. Submarine Geology. Harper & Bros., New York. 348 pp.
Shepard, F. P. and K. O. Emery
1941. Submarine topography off the California coast: Canyons and tectonic interpretation. Spec. Pap. Geol. Soc. Amer., *31:* 171 pp.
Staff
1950. Physical and chemical data. Marine Life Research Program. Cruise 7, Sept. 5 to Sept. 18, 1949. Rep. Scripps Inst. Oceanogr., No. 7. (mimeo.)
1951. Physical and chemical data. Marine Life Research Program. Cruise 14, May 3 to May 18, 1950. Rep. Scripps Inst. Oceanogr., No. 14. (mimeo.)
1952. Physical and chemical data. Marine Life Research Program. Cruise 23, March 8 to March 23, 1951. Scripps Inst. Oceanogr., Ref. 52–9. (mimeo.)
Sverdrup, H. U. and R. H. Fleming
1941. The waters off the coast of southern California, March to July, 1937. Bull. Scripps Inst. Oceanogr., *4:* 261–378.
Sverdrup, H. U., M. W. Johnson, and R. H. Fleming
1942. The Oceans. Prentice-Hall, Inc., New York. 1087 pp.
Swainson, O. W., C. G. McIlwraith, and K. Dyk
1934. The velocity and ray paths of sound waves in deep sea water. U. S. Coast and Geodetic Survey, 37 pp. (mimeo.)
Van Riel, P. M.
1934. The bottom configuration in relation to the flow of the bottom water. The Snellius Expedition, *2* (2) ch. 2: 60 pp.
Van Riel, P. M., H. C. Hamaker, and L. Van Eyck
1950. Serial and bottom observations. Temperature, salinity, and density. The Snellius Expedition, *2* (6): 44 pp.

APPENDIX

Allen Hancock Foundation Stations made by VELERO IV, showing depth, temperature, and chlorinity.

AHF 2165
Oct. 11, 1952 Lat. 31°31.1′ Long. 118°27.0′ 2484 meters

Depth	*Temp.*	*Cl °/₀₀*	*Depth*	*Temp.*	*Cl °/₀₀*
0	18.5	18.43	1497	2.87	19.09
91	10.12		1679	2.65	19.11
186	10.70	18.91	1859	2.48	19.15
369	8.95	19.00	2042	2.50	19.14
552	6.76	19.00	2225	2.52	19.15
744	5.38	19.04	2289	2.47	19.13
926	4.38	19.03	2380	2.52	19.12
1109	3.78	19.04	2472	2.53	19.11
1314	3.30	19.08			

AHF 2178
Nov. 7, 1952 Lat. 33°32.7′ Long. 118°24.9′ 862 meters

Depth	*Temp.*	*Cl °/₀₀*	*Depth*	*Temp.*	*Cl °/₀₀*
0	17.75	18.41	679	5.31	18.93
183	8.63	18.70	752	5.11	18.98
365	7.52	18.92	828	5.09	
547	6.04	18.88			

AHF 2179
Nov. 7, 1952 Lat. 33°40.9′ Long. 118°53.0′ 893 meters

Depth	*Temp.*	*Cl °/₀₀*	*Depth*	*Temp.*	*Cl °/₀₀*
0	17.6	18.52	743	5.13	19.05
183	8.88	18.87	808	5.06	18.96
367	7.49	18.97	883	5.03	18.99
550	5.90	19.02			

AHF 2181
Nov. 8, 1952 Lat. 33°24.2′ Long. 118°51.0′ 1295 meters

Depth	*Temp.*	*Cl °/₀₀*	*Depth*	*Temp.*	*Cl °/₀₀*
0	18.0	18.52	821	4.52	19.04
184	8.44	18.85	1006	4.15	19.06
367	7.43	18.97	1112	4.11	19.06
550	5.99	18.99	1204	4.05	19.00
669	5.40	19.02	1286	4.00	18.99

AHF 2182
Nov. 8, 1952 Lat. 32°59.6′ Long. 118°58.3′ 1731 meters

Depth	*Temp.*	*Cl* °/₀₀	*Depth*	*Temp.*	*Cl* °/₀₀
0	17.3	18.52	1252	3.76	19.11
183	8.30	18.86	1402	3.74	19.11
366	7.30	18.96	1554	3.71	19.11
549	5.88	18.95	1692	3.71	19.06
732	4.99	19.03	1731		19.00*
914	4.35	19.06	1731	3.71	18.95†
1097	3.88	19.07			

*Clear: †Muddy.

AHF 2185
Nov. 9, 1952 Lat. 32°37.5′ Long. 118°08.0′ 2030 meters

Depth	*Temp.*	*Cl* °/₀₀	*Depth*	*Temp.*	*Cl* °/₀₀
0	16.1	17.88	1840	2.61	19.13
186	8.42	18.87	1950	2.60	19.13
370	6.89	18.93	1994	2.66	19.12
556	5.96	18.83	2025	2.60	19.13
921	4.34	19.08	2030	2.60	19.12*
1291	3.19	19.08	2030	2.61	19.11*
1660	2.65	19.10			

*Muddy

AHF 2198
Dec. 19, 1952 Lat. 33°40.5′ Long. 119°31.2′ 1893 meters

Depth	*Temp.*	*Cl* °/₀₀	*Depth*	*Temp.*	*Cl* °/₀₀
0	13.9	18.43	1138	4.15	19.12
361	7.65	18.98	1323	4.12	19.11
546	5.91	19.03	1509	4.15	19.09
729	4.85	19.06	1691	4.13	19.10
956	4.34	19.09	1874	4.17	19.09

AHF 2200
Dec. 20, 1952 Lat. 34°13.5′ Long. 120°02.5′ 589 meters

Depth	*Temp.*	*Cl* °/₀₀	*Depth*	*Temp.*	*Cl* °/₀₀
0	13.1	18.46	445	6.61	18.96
124	9.79	18.66	505	6.37	18.96
246	8.68	18.89	561	6.26	18.94
399	7.48	18.95			

AHF 2201
Dec. 20, 1952 Lat. 33°52.9′ Long. 119°24.3′ 677 meters

Depth	*Temp.*	*Cl* °/₀₀	*Depth*	*Temp.*	*Cl* °/₀₀
472	6.34	19.00	655	5.30	19.04
594	5.48	19.04			

AHF 2207
Jan. 28, 1953 Lat. 33°22.3′ Long. 118°10.7′ 722 meters

Depth	*Temp.*	*Cl* °/₀₀	*Depth*	*Temp.*	*Cl* °/₀₀
596	5.78	19.05	722		18.93†
722	5.20	19.00*			

*Muddy. †Clear.

AHF 2208
Jan. 28, 1953 Lat. 33°04.9′ Long. 117°59.1′ 935 meters

Depth	*Temp.*	*Cl* °/₀₀	*Depth*	*Temp.*	*Cl* °/₀₀
642	5.47	19.07	916	4.41	19.09
825		19.08			

AHF 2209
Jan. 29, 1953 Lat. 32°51.1′ Long. 118°17.9′ 939 meters

Depth	*Temp.*	*Cl* °/₀₀	*Depth*	*Temp.*	*Cl* °/₀₀
681	5.33	19.06	924	4.14	19.12
831		19.11			

AHF 2210
Jan. 29, 1953 Lat. 32°35.9′ Long. 118°35.5′ 1118 meters

Depth	*Temp.*	*Cl* °/₀₀	*Depth*	*Temp.*	*Cl* °/₀₀
0	15.4		1012	4.01	19.07
829	4.59	19.05	1103	3.77	19.12

AHF 2211
Jan. 30, 1953 Lat. 33°17.1′ Long. 118°56.0′ 845 meters

Depth	*Temp.*	*Cl* °/₀₀	*Depth*	*Temp.*	*Cl* °/₀₀
0	14.9		735	5.44	19.03
552	6.14	18.99	826	4.72	19.05

AHF 2213
Jan. 30, 1953 Lat. 33°18.6′ Long. 119°10.4′ 1051 meters

Depth	*Temp.*	*Cl* °/₀₀	*Depth*	*Temp.*	*Cl* °/₀₀
0	15.0	18.45	777	4.91	19.05
213	8.38	18.94	960	4.29	19.09
396	7.25	18.98	1051	3.93	19.05*
579	5.85	19.02			

*Muddy.

AHF 2215
Jan. 31, 1953 Lat. 32°58.8′ Long. 119°46.2′ 1490 meters

Depth	*Temp.*	*Cl* °/₀₀	*Depth*	*Temp.*	*Cl* °/₀₀
0	13.5	18.42	913	4.34	19.09
183	7.97	18.86	1097	3.90	19.11
366	6.62	19.01	1221	3.85	19.14
549	5.60	19.03	1405	3.90	19.13
732	4.86	19.06	1490	3.82	19.09*

*Muddy.

AHF 2216
Feb. 1, 1953 Lat. 33°36.4′ Long. 118°58.0′ 454 meters

Depth	*Temp.*	*Cl* °/₀₀	*Depth*	*Temp.*	*Cl* °/₀₀
0	14.2	18.40	350		18.87
166	8.55	18.83	442	6.80	18.92

Scripps Institution of Oceanography Stations. The Name of the Vessel Is Listed in Parentheses After the Station Number

SIO 80.55 (Horizon)
May 3, 1950 Lat. 34°21′ Long. 120°50′ 859 meters

Depth	*Temp.*	*Cl* °/₀₀	*Depth*	*Temp.*	*Cl* °/₀₀
0	12.26	18.67	300	7.57	18.92
50	9.93	18.71	400	7.05	18.95
100	8.84	18.81	500	6.32	18.97
150	8.48	18.88	600	5.64	18.97
200	8.13	18.88	700	5.05	19.02
250	7.82	18.90	800	(4.54)	(19.04)

SIO 90.70 (Black Douglas)

March 19, 1951 Lat. 32°04.5′ Long. 120°39′ 3743 meters

Depth	*Temp.*	*Cl* °/₀₀	*Depth*	*Temp.*	*Cl* °/₀₀
0	14.27	18.36	600	5.34	18.99
50	12.65	18.41	700	4.96	19.05
100	9.55	18.50	800	4.53	19.10
150	8.83	18.74	1000	3.87	
200	8.25	18.80	1200	3.37	
250	7.67	18.86	1500	2.77	
300	7.10	18.90	2000	2.07	
400	6.31	18.94	2500	1.79	
500	5.69	18.96			

SIO 904 (Crest)

Sept. 15, 1949 Lat. 31°46′ Long. 120°15′

Depth	*Temp.*	*Cl* °/₀₀	*Depth*	*Temp.*	*Cl* °/₀₀
0	18.30	18.49	600	5.62	19.01
50	16.05	18.47	700	5.11	19.04
100	11.07	18.51	800	4.69	19.06
150	9.24	18.71	1000	4.03	19.10
200	8.52	18.84	1200	3.51	19.13
250	7.96	18.89	1500	2.84	19.15
300	7.52	18.92	2000	2.12	19.17
400	6.85	18.96	2500	1.81	19.18
500	6.22	18.99	3000	1.70	19.18

SIO B-1 (E. W. Scripps)*

Sept. 4, 1940 Lat. 33°03′ Long. 119°00′ 1737 meters

Depth	*Temp.*	*Cl* °/₀₀	*Depth*	*Temp.*	*Cl* °/₀₀
0	18.04	18.67	618		19.03
26	14.87	18.61	824	4.77	19.04
77	9.84	18.71	1030	4.11	19.05
129		18.84	1236	3.91	19.09
206	8.39	18.89	1442		19.10
309	7.78	18.98	1648	3.71	19.10
412	7.15	18.98			

*John Lyman (personal communication)

SIO B-2 (E. W. Scripps)*
Sept. 5, 1940 Lat. 32°40′ Long. 117°35.5′ 1152 meters

Depth	*Temp.*	*Cl* °/₀₀	*Depth*	*Temp.*	*Cl* °/₀₀
0	20.22	18.54	298		18.94
26	16.04	18.50	398	7.83	18.96
77	10.88	18.46	410		18.96
128	10.28	18.78	497	6.87	18.97
140		18.84	696	5.45	19.01
199	9.54	18.90	895		19.04
249	9.13	18.92	1094	3.66	19.09

*John Lyman (personal communication).

SIO B-3 (E. W. Scripps)*
Sept. 28, 1940 Lat. 32°16′ Long. 118°23′ 1773–1847 meters

Depth	*Temp.*	*Cl* °/₀₀	*Depth*	*Temp.*	*Cl* °/₀₀
0		18.54	1600	3.14	19.12
1000		19.09	1610		19.11
1350	3.24		1640	3.15	19.11
1400	3.20	19.10	1740	3.14	19.11
1450	3.17	19.10	1780	3.13	19.15
1500	3.17		1790		19.10
1550	3.15	19.15			

*John Lyman (personal communication).

SIO B-4 (E. W. Scripps)*
Sept. 28, 1940 Lat. 32°08′ Long. 117°58′ 1929 meters

Depth	*Temp.*	*Cl* °/₀₀	*Depth*	*Temp.*	*Cl* °/₀₀
1625	2.74	19.17	1775		19.15
1675	2.70		1825		19.15
1725	2.64	19.19	1875		19.19
1735		19.13	1885		19.15

*John Lyman (personal communication).

SIO 13 (Bluefin)*
June 27, 1937 Lat. 34°10′ Long. 120°02′

Depth	*Temp.*	*Cl* °/₀₀	*Depth*	*Temp.*	*Cl* °/₀₀
0	15.21	18.61	250	7.90	18.92
50	9.56	18.68	300	7.65	18.94
100	8.85	18.82	400	7.03	18.95
150	8.50	18.87	500	6.40	18.96
200	8.20	18.91			

*Sverdrup and Fleming, 1941: 371.

SIO 15 (BLUEFIN)*
March 31, 1937 Lat. 33°34′ Long. 118°30′

Depth	*Temp.*	*Cl* °/₀₀	*Depth*	*Temp.*	*Cl* °/₀₀
0	13.80	18.49	300	7.43	18.96
50	10.54	18.61	400	6.70	18.98
100	9.34	18.75	500	6.16	18.99
150	8.85	18.83	600	5.67	19.02
200	8.38	18.89	800	5.08	19.02
250	8.06	18.94			

*Sverdrup and Fleming, 1941: 351.

OTHER OBSERVATIONS

SANTA CRUZ BASIN*
U. S. C. & G. S. (U. S. S. PIONEER) November, 1933

Depth	*Temp.*	*Cl* °/₀₀	*Depth*	*Temp.*	*Cl* °/₀₀
0	15.55	18.4	732	5.1	19.0
55	10.95	18.4	823	4.6	19.0
110	9.2	18.7	915	4.3	19.0
201	8.4	18.9	1006	4.2	19.1
292	7.9	18.9	1097	4.15	19.1
366	7.3	18.9	1280	4.15	19.1
457	6.7	18.9	1462	4.15	19.1
548	6.2	18.9	1700	4.15	19.0
640	5.6	18.9	1829	4.15	18.9

*Swainson, McIlwraith, and Dyk (1934: 20).

SAN PEDRO BASIN*
July 1931 to June 1932 Lat. 33°22.0′ to 33°45.8′ Long. 118°11.5′ to 18°20.5′

Depth	*Bottom Temp.*	*Depth*	*Bottom Temp.*
0	24.50	667	5.46
55	12.52	720	5.29
102	10.23	796	5.10
202	8.51	829	5.07
255	8.52	835	5.05
296	8.30	864	5.07
322	7.85	872	5.04
437	6.79	874	5.05

*Manley L. Natland (personal communication).

A COMPARISON OF CERTAIN NORTH ATLANTIC WIND, TIDE GAUGE AND CURRENT DATA[1]

By

JOSEPH CHASE

Woods Hole Oceanographic Institution

ABSTRACT

Wind components from large areas within the zones of the trades and westerlies of the North Atlantic Ocean are determined by means of a geostrophic template and mean weather maps. These wind speeds are compared with current speed data from the trade-wind zone as well as the Gulf Stream and to tide gauge data from Bermuda-Charleston, Galveston, and Miami. In long-term averages, the trade winds undergo monthly fluctuations which are similar to those of the current speeds. The monthly fluctuations of the trades plus westerlies are similar to those of sea level slope between Bermuda and Charleston and to those of sea level height at Galveston. While short-period average winds may be measured easily by the template method, their correlation with the corresponding current and tide gauge data is relatively poor.

INTRODUCTION

Oceanographers have long sought means of using data collected in related fields to supplement the observations obtained on oceanographic cruises. Data on winds and on heights of sea level have been suggested for this purpose, and certainly the low cost of obtaining such data plus the fact that they are continuous for long periods make such an idea attractive. The studies of Montgomery (1938), Iselin (1940) and Fuglister (1951) are pertinent. More knowledge of the relationships between winds, sea level heights and hydrographic events is needed, and it is with the hope of adding to the present understanding that this paper is written.

WINDS, CURRENTS AND MEAN SEA LEVEL

In a mathematical treatment, Munk (1950) has shown that a circulatory current system, such as the North Atlantic eddy, responds to the curl of the wind stress acting upon it. Similarly, Stommel (1951) and Hidaka (1952) have used the stress of both the trades and the westerlies in explaining features of oceanic circulations.

[1] Contribution No. 652 from the Woods Hole Oceanographic Institution. This work was performed under the auspices of the Office of Naval Research Contract N6onr-27701.

For the actual ocean, it has not been established that the major currents are totally dependent upon the winds. Clearly the winds do exert an influence, but there remains the possibility of a direct contribution to current from the earth's heat budget and consequent thermal distribution.

The density distribution which is normally associated with an ocean current is reflected in the slope of sea level across the current, and, in the absence of other influences, two suitably located tide gauges could record this slope. In actuality, other influences, such as atmospheric pressure and local winds, have an independent effect and the distances of the gauges from the edges of the current allow for heights not identical with those at the edges.

DATA

The tide gauge data used here were obtained from U. S. Coast and Geodetic Survey records and from a comprehensive compilation of records gathered by Walter H. Munk of Scripps Institution of Oceanography. The data have been corrected for atmospheric pressure. The current data are based on U. S. Navy Hydrographic Office (1946) charts.

The normal pressure maps and monthly mean pressure charts of the U. S. Weather Bureau (1946, 1943) are the sources of the long- and short-period wind values. The geostrophic template used in conjunction with the maps is shown in Fig. 1.

LONG-TIME MONTHLY AVERAGES

Fuglister's (1951) values for observed and calculated (harmonic analysis) current speeds for his segment 1 (trades) are shown at the top of Fig. 2. The calculated values have been included because of the paucity of observed values in this segment. The next curve in Fig. 2 shows the template-measured trade winds. The outstanding feature in each of these three curves is the July maximum. Slight fall and spring minima and a winter maximum are also present. Fuglister found similar seasonal fluctuations in wind components from an area near the segment. It is interesting that the template-measured trades, which represent a much larger area, agree as well with the current as do the more local winds of Fuglister. This agreement of wind and current fluctuations does not preclude a direct contribution to current from the earth's thermal distribution.

The next curve in Fig. 2 gives the northbound components of current for an area covering four degrees of latitude from the U. S. coast

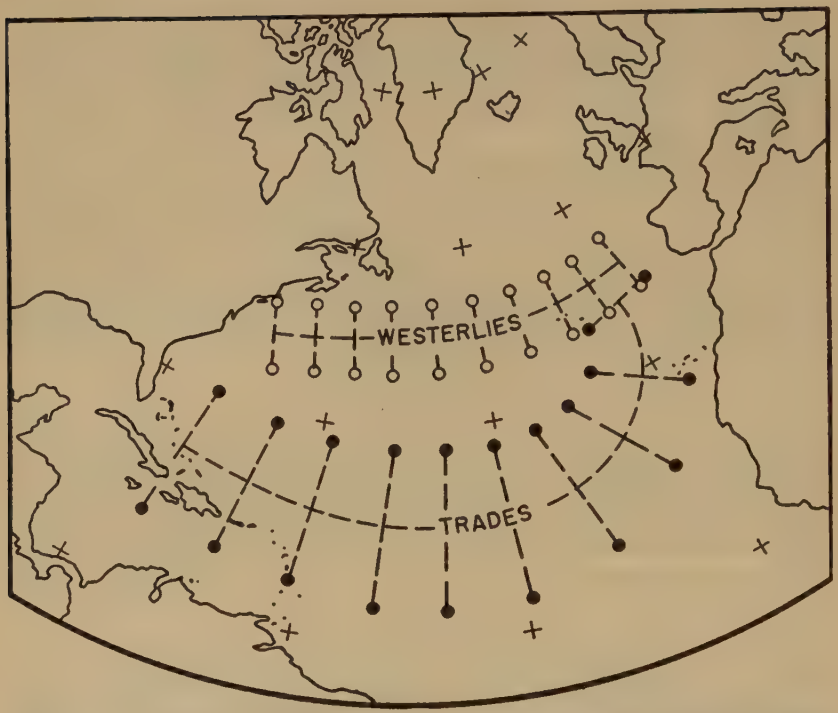

Figure 1. Geostrophic template for measuring wind components at 10 pairs of points in the trades and at 10 pairs in the westerlies. The distance between any pair of points is inversely proportional to the sine of their mean latitude. Components are expressed in terms of millibars of pressure difference.

to the neighborhood of Bermuda. It is remarkably similar to the trades curves.

The much greater current speeds of the Gulf Stream are shown by Fuglister's observed values (bottom curve of Fig. 2) for his segment 4, located just south of Cape Hatteras. In its main features, this curve resembles the preceding ones. It has a large maximum extending from June through August and a small January peak. Here the minima are in February and November, while those of the trades are in April and September through October.

The values of these last two curves in Fig. 2 show no systematic tendency to lag behind those of the trades currents and winds, although they represent areas much farther downstream. With regard to the similarity of the seasonal variations in wind and current speeds, it is noteworthy that the westerlies, which may be considered part of the system, have not been considered.

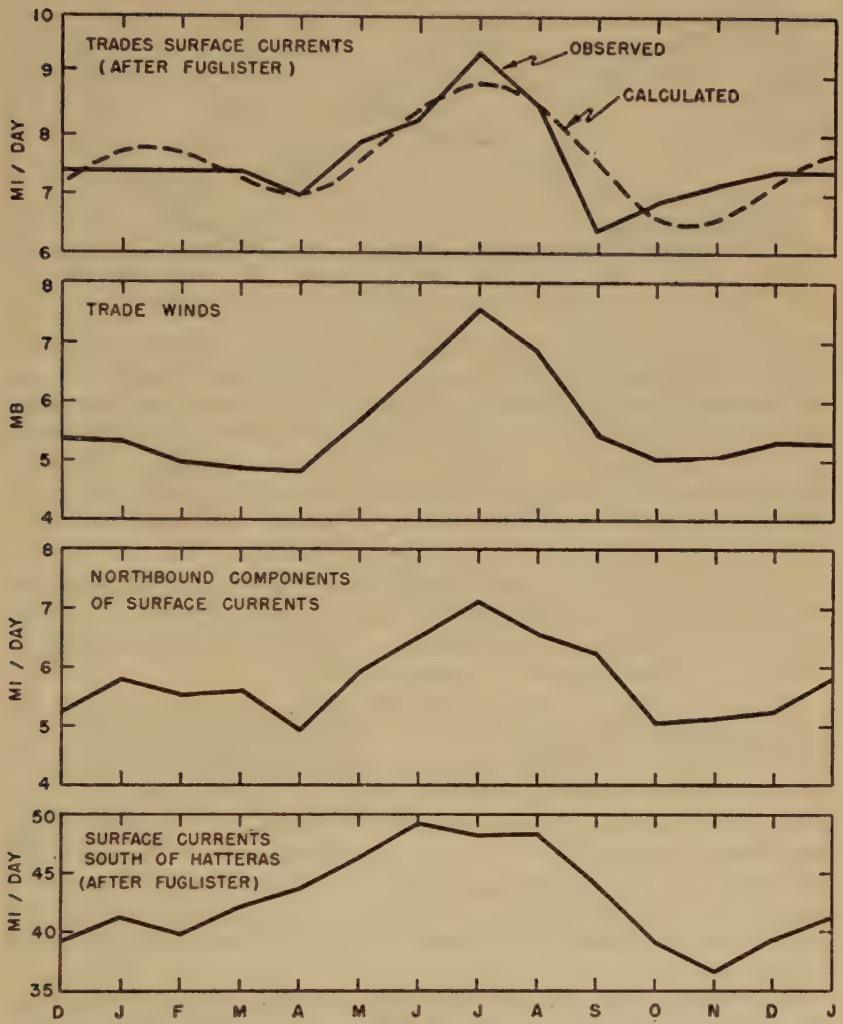

Figure 2. Long-time monthly averages of trades surface currents, template trade wind components, northbound components of surface current for an area extending from the southeast coast of the United States to Bermuda, and surface currents in the Gulf Stream south of Cape Hatteras.

For the westerlies, the template yields a W-shaped curve (Fig. 3), with maxima in January and July and minima in April and September. The rapid decline between July and September closely matches that of the observed trades currents. There is some question here as to

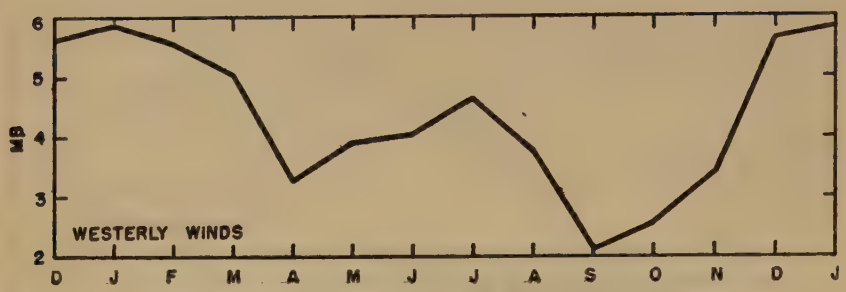

Figure 3. Long-time average monthly west wind components.

the significance of the January maximum because of the gap in the template along the southeast coast of the United States. In an annual average, there is little resultant wind in this area, but seasonally there is a decided shift of resultant wind direction from northerly in winter to southerly in summer. A westerlies template extended southwestward to measure components parallel to the coast would therefore yield lower average values in winter and consequently a curve that would be in closer agreement with the trades.

The effect of the gap is still visible when the trades and westerlies are added to give the values shown in the uppermost curve of Fig. 4. The winter maximum, though less pronounced, is still large enough to be out of line with the winter trades values.

The second curve in Fig. 4 gives the relative slope of sea level between Bermuda and Charleston. It closely resembles the previous curve and therefore shows similar disagreement with the trades in winter. These high winter values may be due to the lowering of sea level at Charleston in response to offshore winds. A tabulation of the percentage frequency of the various wind directions at Charleston for the years 1931–1938 shows that offshore directions are more frequent in the period September through February while the wind stress data of Cochran and Osborn (1950) show a net offshore stress from October through April.

The curve for the height of sea level at Galveston (third curve in Fig. 4) resembles the two previous curves remarkably well, especially in view of the distance from the Gulf Stream. It has a larger amplitude and its spring maximum and summer minimum occur somewhat later. As at Charleston, offshore winds are more frequent in winter.

At Miami the fluctuations in sea level (bottom curve of Fig. 4) show some agreement with the preceding values. Because of the large range, the scale has been halved. The fall maximum is somewhat late, and in the period from March through June the sea level is

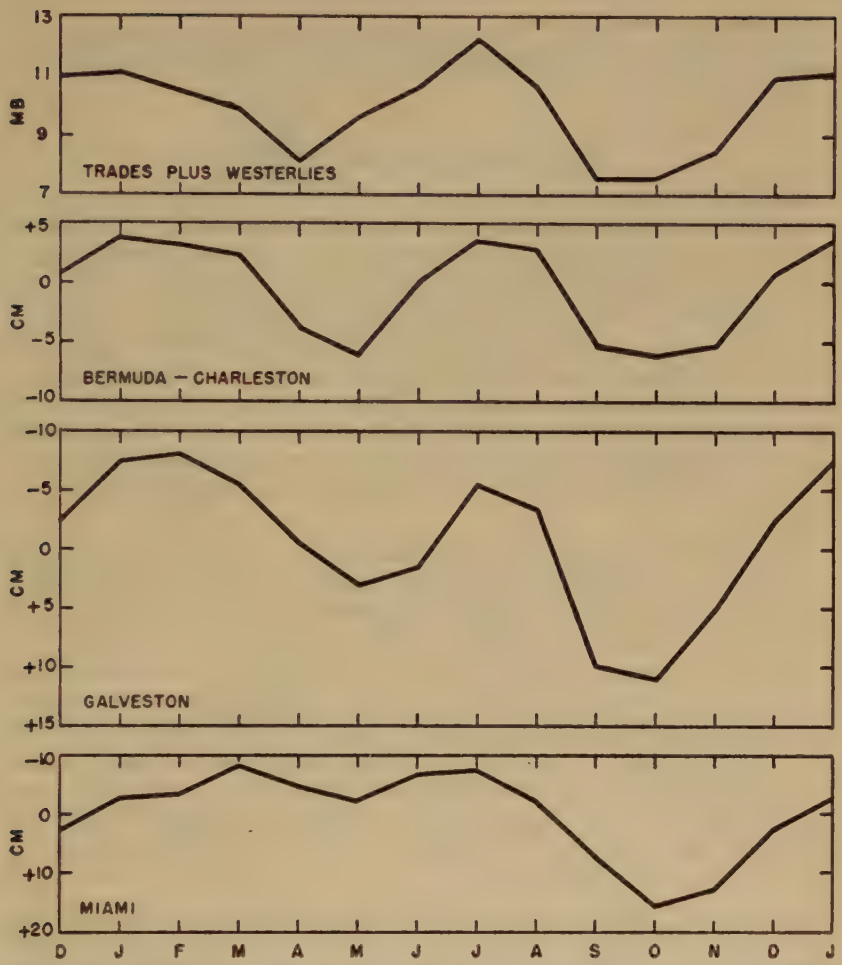

Figure 4. Long-time averages for trades plus westerlies, the relative slope of sea level between Bermuda and Charleston, the height of sea level at Galveston, and the same at Miami. The zero points for the tide gauge height scales were arbitrarily chosen.

too low. Compared to the trades, sea level is too low from December through June. U. S. Weather Bureau (1938) charts indicate a weaker onshore wind component in winter and spring.

It is interesting that the four curves in Fig. 4, representing different factors in different areas, should be so similar. Of greater importance, perhaps, is the possibility that, after consideration of the coastal winds, all of the curves will have essentially the same shape as those

for the trades. A quantitative analysis of the effects of these winds, though necessary to a full understanding of the curves, is beyond the scope of this paper.

SHORT-TIME AVERAGES

Fig. 5 shows three-month running means of trades plus westerlies, the Bermuda-Charleston slope, the height of sea level at Galveston, and the same at Miami. The agreement between the seasonal variations of these values is much poorer than it was in the case of the long-time averages. Yet the main peaks and valleys do show a reasonable correspondence. At Miami the spring values tend to be too low, and in the fall there are lags in the curve; at Galveston there are lags in the curve in spring and summer. These tendencies are in line with the long-time relationships. The Bermuda-Charleston values in this case have as large a range as do those of Galveston and Miami. For averages of periods shorter than three months, the agreements are negligible.

Three-month averages for the trades (not shown) were compared with the above values. The fluctuations in the trades followed those of the other data fairly well in certain periods but not in others. The expected low winter values did not always appear.

The Iselin (1940) Gulf Stream transport data (not shown) were also examined. Compared with the trades, the trades plus westerlies, and the Galveston data, they show no better than fair agreement. The transport figures have a tendency to lag one to three months behind the other data. This may be due to a slower response of the deeper currents to the influence of wind. The Bermuda data are incomplete for this period. Iselin showed good agreement with sea level at Miami and Charleston.

No one- or two-year lags have been noted in any of the above data.

The lesser agreement of the short-time data suggests the influence of extraneous variables whose net effect is less in long-period averages. The more important variables may be: (a) The amount of water entering the system from the South Atlantic and from the coastal waters to the north of the Gulf Stream. (b) The local winds affecting sea level at the tide gauges. (c) Temporary time lags. (d) The migration of average pressure centers across the westerlies section of the template.

Those of lesser importance may be: (e) The ratio of geostrophic wind to sea level stress. (f) The deeper currents. (g) Rainfall and runoff in the vicinity of the tide gauges.

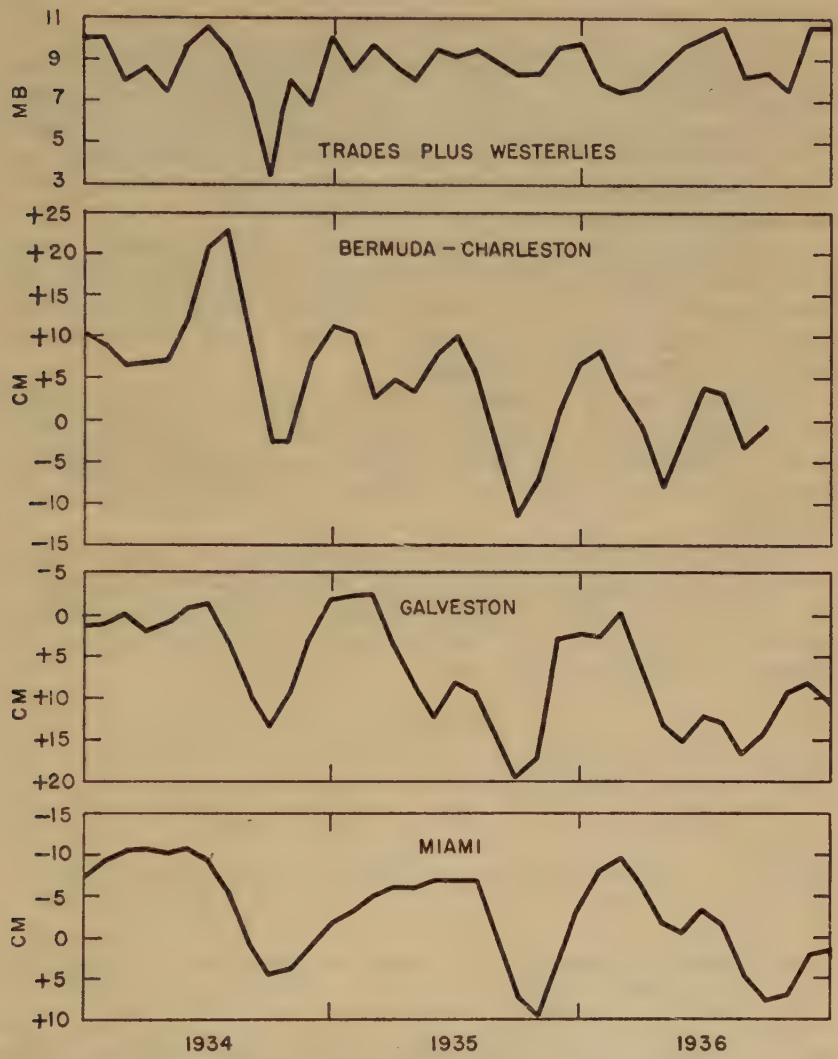

Figure 5. Three-month averages for trades plus westerlies, the relative slope of sea level between Bermuda and Charleston, the height of sea level at Galveston, and that at Miami. The zero points for the tide gauge height scales were arbitrarily chosen.

Special studies of each of these variables may be necessary to a complete understanding of the relationships between winds, tide gauge readings, and currents.

CONCLUSIONS

1. The trade winds (measured by the template method) and the surface currents for an area in the trades zone and for an area off the southeast coast of the United States have similar seasonal fluctuations in long-time monthly averages. In three-month running averages (short period) the agreement of trade wind fluctuations with those of the best available transport data is only fair.

2. The seasonal variation of trades plus westerlies agrees very well in long-time averages and fairly well in three-month running averages with variations in the: (a) Relative Bermuda-Charleston sea level slope; (b) height of sea level at Galveston; (c) height of sea level at Miami from July through February.

3. Adjustments for the influence of local winds at the tide gauges and an extension of the westerlies template along the southeast coast of the United States would result in closer agreement in the long-time averages between the seasonal variations of 2 (above) and those of the trades.

4. A better understanding of the significance of current speed fluctuations, tide gauge values and wind values depends on a study of the effect of extraneous variables and on the availability of a long continuous record of Gulf Stream transport and surface current observations for use as a standard.

REFERENCES

Cochrane, J. D. and P. Osborn
1950. The mean wind stress over the Atlantic Ocean. Rep. Scripps Inst. Oceanogr., No. 15.

Fuglister, F. C.
1951. Annual variations in current speeds in the Gulf Stream system. J. Mar. Res., *10* (1): 1–40.

Hidaka, Koji
1952. Wind-driven current and lateral mixing in a zonal ocean. Geophys. Mag., Tokyo, *23* (4): 487–495.

Iselin, C. O'D.
1940. Preliminary report on long-period variations in the Gulf Stream system. Pap. phys. Oceanogr. Meteorol., *1* (2): 1–40.

Montgomery, R. B.
1938. Fluctuations in monthly mean sea level on the eastern U. S. coast as related to dynamics of western North Atlantic Ocean. J. Mar. Res., *1* (2): 165–185.

Munk, W. H.
1950. On the wind driven ocean circulation. J. Meteorol., *7* (2): 79–93.

Stommel, Henry
1951. An elementary explanation of why ocean currents are strongest in the west. Bull. Amer. Meteorol. Soc., *32* (1): 21–23.
U. S. Navy Hydrographic Office
1946. Current atlas of the North Atlantic Ocean. H. O. Misc. 10688.
U. S. Weather Bureau
1938. Atlas of the climatic charts of the oceans. Washington, D. C.
1943. Northern hemisphere sea level charts, monthly mean pressure. Washington, D. C.
1946. Normal weather maps; northern hemisphere, sea level pressure. Washington, D. C.

THE ROLE OF ORGANIC MATTER IN DETERMINING THE DISTRIBUTION OF PELECYPODS IN MARINE SEDIMENTS[1]

By

RICHARD G. BADER

Department of Oceanography
University of Washington
Seattle, Washington

ABSTRACT

Sediments in the region of Mt. Desert Island, Maine, indicate that their organic content and its state of decomposition, as expressed by $L/R_n \times$ T.O. (where L = refractory organics, R_n = nonrefractory organics, and T.O. = total organics), are primary factors in controlling the distribution of sediment-dwelling pelecypods. The relationship of pelecypod population density to the physical characteristics of the sediments and the depth of overlying water are apparently secondary in importance.

INTRODUCTION

Statement of Problem. This research was undertaken to study the relationships of the physical sedimentary characteristics, the organic content of the sediments, and the pelecypod populations of a present-day near-shore marine environment. From the samples collected and from the data obtained during analysis, an attempt is made to show that the relationship between the bottom-dwelling pelecypods and the sedimentary environment is one of dynamic interdependence between physical sedimentary factors, chemical factors, and microbiology, the latter two being of primary importance. The factors quantitatively considered for this project are: water temperature, salinity, and depth, the median diameter of sedimentary particles, the coefficient of sedimentary sorting, the organic content of sediments, the amount of decomposition of organic material, and the total density of the pelecypod population.

Description of Sampling Areas. The relatively shallow waters of bays and sounds in five areas in the region around Mt. Desert Island, Maine, were selected for study. A total of 27 samples from this general region (see Fig. 1) was examined.

Somes Sound (Area I) is a small but typical fjord about 4.5 miles long and 0.8 of a mile wide at its widest point. It gradually deepens

[1] Data taken from a portion of Ph.D. Dissertation, Univ. of Chicago, 1952.

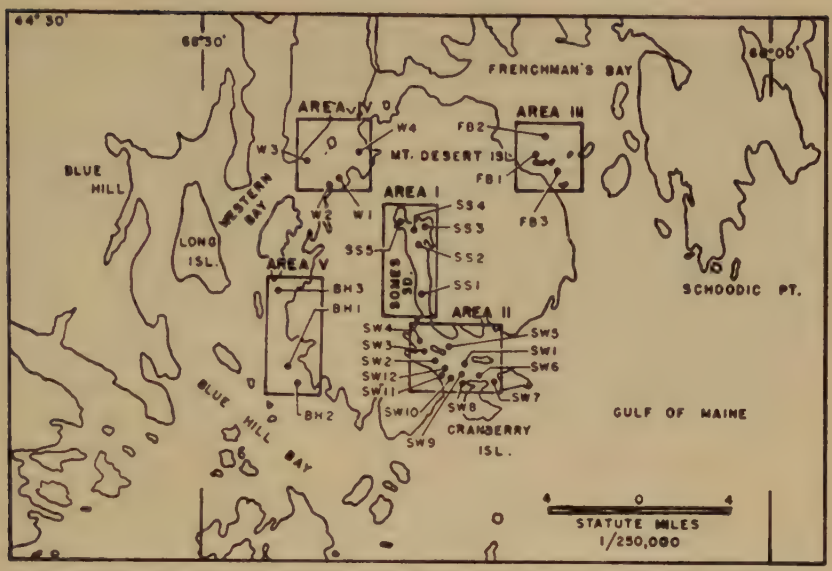

Figure 1. Map of the region of Mt. Desert Island, Maine. The five sampling areas are indicated by the rectangular outlines, the sample locations by the black dots.

southward to a maximum of about 190 feet, then shallows slightly for 0.8 of a mile; the water then shoals from 145 to 30 feet at the sill in 0.6 of a mile. The sides of the Sound are exceedingly steep and at many places the water exceeds 100 feet only a few yards from the western shore. The bottom sediments, except for some rocky and gravelly locations near shore, are essentially dark muds with variable amounts of organic matter ranging from about 1.0 to 8.0%.

Somes Sound opens into a protected bay north of the Cranberry Islands (Area II). Here the water has a maximum depth of about 90 feet, but in most of the bay it ranges between 25 to 50 feet. The deepest portion, probably a small basin, is about one mile southeast of the fjord entrance and 0.2 of a mile south of the northern shore. This bay is protected from open water on the south by the Little and Great Cranberry Islands and a shallow rocky bottom. Eastward it opens into the Gulf of Maine, where the depth gradually increases to 190 feet in about 5 miles. The sediments range from fine muds to gravels, and the organic matter varies from less than 1.0 to more than 3.0%. Many locations have a hard rocky bottom.

Area III, in Frenchman's Bay on the northeastern shore of Mt. Desert Island, is protected from the open part of the Bay by five small islands (Porcupine Islands). In the area sampled, the water attains

a maximum depth of about 95 feet, but there is rapid deepening to the east where there are depths of about 300 feet. The sediments vary from fine muds to gravels, with organic materials ranging from 0.5 to more than 4.0%. In some localities the bottom is dense hard clay and bare rock.

Western Bay (Area IV), off the northwestern shore of Mt. Desert Island, is shallow, with depths attaining a maximum of only 70 feet in a few locations at the southernmost part of the Bay. Its 2.5 mile width is well protected from the sea by Mt. Desert Island. The bottom sediments are composed essentially of soft dark muds, with the organic content often exceeding 4.0%. In a few locations rock bottoms are present.

Blue Hill Bay (Area V), a large body of water containing many islands, is protected from open water by a series of islands from the mainland to the southwestern tip of Mt. Desert Island. The entire Bay is probably a large basin with a single small opening to the south. The depths exceed 330 feet in a few localities. The bottom is exceedingly variable, being composed of soft muds, hard muds, sand, gravel, and bare rock. The organic content is also variable.

Field Investigation. Field investigations from July 15 to November 15, 1950 consisted essentially of a general survey of the area, including the collection of samples and their preparation. From the initial survey it became evident that the great abundance of pelecypods would allow a quantitative consideration of population density. Of the 16 species of pelecypods represented, *Nucula proxima*, *Yoldia limulata*, *Y. sapotilla*, *Vernicardia borealis* and *Astarta undata* were the most numerous and widespread.[2]

Methods of Sampling. A box drag was used to obtain samples of the pelecypod populations. This is a rectangular rigid drag (24″ wide, 48″ long, 6″ high) with five sides enclosed by ⅛-inch mesh wire. The drag, towed slowly over the bottom for a period of one minute at a relatively constant speed, proved most effective in both sands and muds since it collected a sample of adequate size and still prevented the loss of smaller mollusks. Upon completion of each drag, one pint of the sediment was separated for sedimentary analysis. The fauna was then removed from the remaining sediment.

A clamshell bucket and an orangepeel bucket were also used. These two samplers of different capacities retrieved smaller amounts of sedi-

[2] The remaining species were: *Crenella decussata*, *Astarta subaecquilatera*, *Pandora glacialis*, *Cerastoderma pinnulatum*, *Huculana tenuisulcata*, *Desinia discus*, *Macoma balthica*, *Laevicardium mortoni*, *Lyonsia hyalina*, and *Salemya velum*.

ment and fewer animals. Two or three samples from each of these instruments allowed a check on the biological sampling technique and gave duplicate samples for sedimentary and chemical analysis.

At each location water samples for salinity determinations were collected with a Nansen bottle. Depth and temperature recordings were made by means of a bathythermograph.

Preparation of Samples. To minimize chemical changes, the samples collected for organic analysis were prepared immediately. The sample originally separated from the drag was quartered to approximately 200 *g* and all macrofaunal remains were removed. The sample was then dehydrated in an oven at 50° C to curtail bacterial activity and to permit storage without change. A similar procedure was followed for a quartered portion from one of the bucket samples. The remaining samples were air-dried after the removal of all living macroscopic animals.

METHODS OF ANALYSIS

Organic Carbon Determination. The total amount of organic carbon was determined by a semimicro combustion method. In general, a weighed sample of powdered sediment was treated with 2% HCl to remove calcium carbonate, after which it was combusted in a measured volume of oxygen under controlled pressure. The carbon dioxide was determined gravimetrically, and the total amount of organic carbon was then computed. The combustion train, with some minor modifications, was constructed on the principles suggested by Pregl (Roth, 1937), Niederl and Niederl (1942), and Piper (1942).

Proximate Organic Analysis. A quantitative determination of the organic suites present in the sediment samples was obtained by running a series of extractions. The first extraction was accomplished by using ether in a soxhlet apparatus to remove nitrogenous fats and waxes, as well as resin-like materials, ethereal oils and fatty oils from both plant and animal material. The sample was then refluxed in 95% ethyl alcohol to remove the alcohol solubles such as waxes, resins, alkaloids, plant pigments, tannins, and phlobophenes. Then the extract was ignited, and the loss in weight represented the amount of alcohol solubles. The temperature of ignition was about 350 to 400° C, but in spite of this low temperature, some inorganic changes probably occurred. A second extraction was achieved with boiling water to remove compounds such as glucose, mannose, sucrose, other sugars, amino acids, some proteins, some organic acids, starches, and pectins. The extract was ignited and the loss in weight represented the water soluble organic matter in the sediments.

Hydrolysis of various portions of the remaining organic constituents in the sediments was performed with hot and cold concentrated acids. The samples were treated with approximately 100 ml of 2% boiling HCl, which hydrolyzed the hemicellulose. The reducing sugars obtained were determined by volumetric analysis with copper sulphate solution (Scales, 1915; Jackson, 1928). The sediment sample was then treated with 80% H_2SO_4 and autoclaved at 15 pounds pressure, thus hydrolyzing the cellulose portion to glucose. Barium chloride was added to the hydrolyzed filtrate in order to precipitate the sulphate. The extract and barium sulphate were dried to constant weight and combusted in the forementioned combustion train to

TABLE I. Sample Data

	Water			*Sediments*			
Sample	*Water depth (ft.)*	*Bottom Temp. (°F)*	*Salinity (°/₀₀)*	*Median Diameter (mm)*	*Coeff. of sorting (log)*	*Total Organic matter (%)*	*Pelecypod Density*
SS1	85	55	32.5	0.135	0.239	2.30	291
SS2	75	54	32.5	0.017	0.577	0.99	85
SS3	30	54	32.6	0.009	0.620	7.36	0
SS4	33	55	32.6	0.009	0.578	8.85	0
SS5	22	54	32.6	0.007	0.493	7.52	0
SW1	57	54	32.6	0.060	0.631	1.91	470
SW2	27	54	32.6	0.049	0.683	3.55	5
SW3	20	54	32.5	0.105	0.283	1.18	165
SW4	40	54	32.5	0.113	0.476	2.27	21
SW5	52	54	32.5	0.024	0.671	1.89	203
SW6	20	55	32.6	0.275	0.109	0.92	40
SW7	14	54	32.5	0.260	0.094	0.98	48
SW8	35	55	32.6	0.150	0.589	1.28	290
SW9	30	54	32.5	16.800	0.318	1.81	24
SW10	25	54	32.5	0.220	0.093	0.88	142
SW11	20	54	32.5	0.245	0.089	0.74	139
SW12	55	54	32.5	0.078	0.438	3.52	209
FB1	85	50	32.5	0.012	1.260	4.01	72
FB2	87	50	32.5	0.425	0.501	0.51	19
FB3	95	50	32.6	0.055	0.668	2.86	390
W1	8	51	32.5	0.170	0.756	4.18	0
W2	18	50	32.5	0.056	0.812	3.64	0
W3	30	51	32.6	0.009	0.634	3.85	22
W4	70	50	32.5	0.150	0.090	4.26	38
BH1	140	50	32.6	0.227	0.221	0.71	148
BH2	150	51	32.6	0.210	0.141	0.62	32
BH3	75	52	32.6	0.006	1.000	3.49	43

determine the amount of carbon. The cellulose content of the sediment was then computed by applying a factor of 2.49. The steps outlined thus far removed from the sample essentially all of the easily decomposable organic matter.

The final step in the proximate analysis was the determination of the lignin content (the remaining organic matter). Since there is no quantitative method for lignin determination, samples were combusted in the previously mentioned combustion train, and the carbon evolved was multiplied by 1.52 to obtain the amount of lignin or refractory organic matter (Waksman, 1933; Norman, 1937). The total amount of organic matter in each sedimentary sample was then determined by the sum of all of the proximate parts.

Sedimentary Size Analysis. Since all of the bottom samples contain particle sizes ranging from sand to fine clay, the size of the sand particles was determined with sieves while the silt and clay sizes were determined by pipette analysis of a dispersed suspension of the sediment in water (Krumbein and Pettijohn, 1938).

Salinity Determination. The salinity of the water overlying the sediments was determined volumetrically by standard methods (Oxner, 1920; Furman, 1939).

THE PHYSICAL, CHEMICAL, AND BIOLOGICAL RELATIONS

In the 27 samples considered, the water depth ranged from 8 to 150 feet and the median diameter of the sedimentary particles varied from 0.006 to 4.250 mm; one sample had a median diameter of 16.80 mm. The log of the coefficient of sorting[3] ranged from 0.089 to 1.260, and the organic content fluctuated from 0.51 to 8.85%. There was also a wide range in the pelecypod densities, from 0 to 470 individuals per sample. Temperature and salinity exhibited only slight differences.

The pelecypod population, as used in this discussion, refers to the total density of pelecypods, including all species. This procedure was followed because the species of pelecypods which are abundant enough to consider individually show the same general trends as the total pelecypod population. The investigation did not show any major ecological hiatus to the exclusion of one or more species.

Water Depth, Sedimentary Characteristics, and Organic Matter. Before we consider the biological aspects, it is first necessary to consider briefly the various physical relationships and organic content of the

[3] "Coefficient of sorting" is a sedimentary expression for the geometric quartile deviation, i.e., $QD_g = \sqrt{Q_3/Q_1}$ (Krumbein and Pettijohn, 1938).

sediments (see Table I). The median diameter of the sediments and the depth of overlying water gave evidence of a gross decrease in median diameter with increase in water depth.

There was a decrease in the coefficient of sorting with an increase in the median diameter, i.e., the greater the particle size the better the sorting. There were no sediments that had a median diameter of less than 0.10 mm and a sorting coefficient of less than 0.40. Only two samples displayed a median diameter of 0.20 mm or greater with a sorting coefficient that exceeded 0.22.

A poor relationship exists between the total organic content of the sediments and the depth of the water. Despite the wide scatter of points, the median diameter of the sediment generally decreased as the amount of included organic material increased. Only three samples with a median diameter of more than 0.135 mm contained more than 1.50% organic matter, and one sample with a median diameter of less than 0.05 mm contained only 0.99% organic matter. In general, of the size ranges encountered in the samples, the extremely small-size sediments had large amounts of organic matter, the extremely large-size sediments smaller amounts.

Pelecypod Density, Water Depth, Temperature, and Salinity. Fig. 2A shows water depth and total pelecypod density for each sample, and it is apparent that there is no significant linear correlation. It does seem possible, however, that there may be at least a gross increase in the populations per sample as the depth increases. If this is so, it is not consistent, since the group of five points at a water depth of about 80 feet have pelecypod densities of under 100 individuals.

When considering the work of Verrill (1874) and the literature summarized in Allee, *et. al.*, (1949), one expects to find a relationship between animal density and depth of water. If such a relationship does exist in these samples, it is a vague one and is strongly affected by some other significant factor or factors. Because of the small variations in salinity (0.2 °/₀₀) and temperature (4° F), no relationship is apparent between these two factors and the pelecypod populations. Probably the tolerance limits for salinity and temperature have not been surpassed.

Pelecypod Density and Physical Character of the Sediments. The relationship between pelecypod density and median diameter of the sedimentary particles is shown in Fig. 2B. Except in one instance, samples with pelecypod densities greater than 200 individuals fell within a median diameter range of 0.05 to 0.15 mm. Pelecypod densities of less than 100 (with one exception) were correlated with particles of exceedingly small median diameters (less than 0.025 mm), essentially

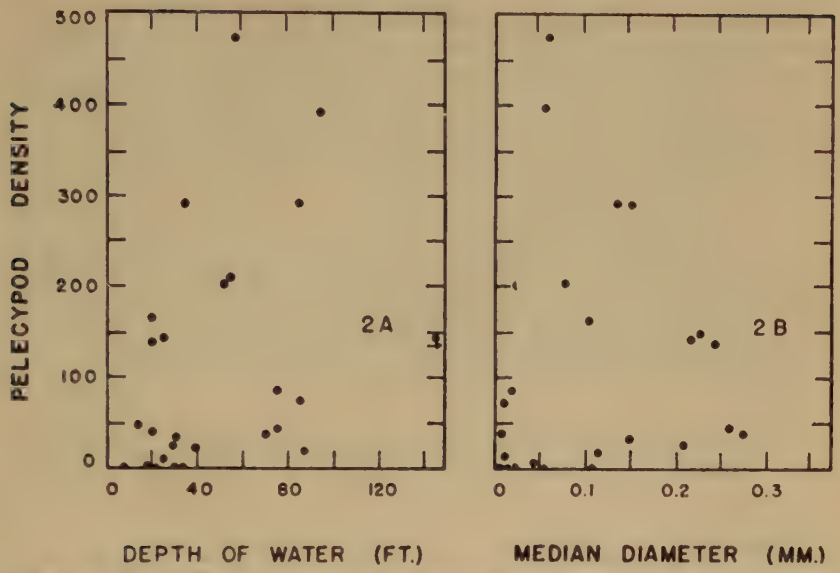

Figure 2A. Relationship between density of pelecypod populations in the sediments (from 0 to 500 individuals) and depth of water at the sample locations. 2B. Relationship between density of pelecypod populations and median diameter of sedimentary particles.

silt and clay. When the median diameter exceeded 0.20 mm, all samples had less than 150 pelecypods. It must be noted, however, that two samples with median diameters of about 0.05 mm contained 0 and 5 individuals, while the two samples containing the greatest number of pelecypods (over 350) also had median diameters of about 0.05 mm. Despite this wide discrepancy, there appears to be an over-all potential toward an increase in pelecypod density as the median diameter decreases and approaches the range of 0.15 to 0.05 mm; beyond this, and toward the extremely fine sizes, there is a sharp drop in the densities. Granted there is an extremely wide scatter of points, but such a relationship is apparent.

There is no obvious correlation between the coefficient of sorting and the pelecypod population. Samples with coefficients between 0 and 0.2, indicating good sorting, had pelecypod densities from 0 to 139. Samples with coefficients of 0.2 to 0.4 (normal sorting) had pelecypod densities between 0 and 291 individuals. When the sorting coefficient increased to 0.6 and 0.8 (poor sorting), the pelecypod density varied from 0 to 470 individuals. The above data suggest that the range in pelecypod densities may increase as the sorting of the sediment gets poorer.

Verrill (1874), Allee (1923a, 1923b), and others referred to in Allee, *et. al.* (1949), have indicated that animal populations are distributed preferentially relative to the physical character of the sediment. The samples in this study seem to show grossly that such a relationship might exist, especially with respect to the median size. Some of the extremely wide deviations indicate a more complex system which requires the consideration of other factors.

Pelecypod Density and Organic Matter. The relationship of pelecypod density to total organic content in the sediments is shown graphically in Fig. 3. It is apparent that the maximum populations are present in sediments containing 1.18 to 3.00% organic matter. However, there are two exceptions: One has 2.27% organic matter with only 21 pelecypods, the other 1.18% organic matter with 24 pelecypods.

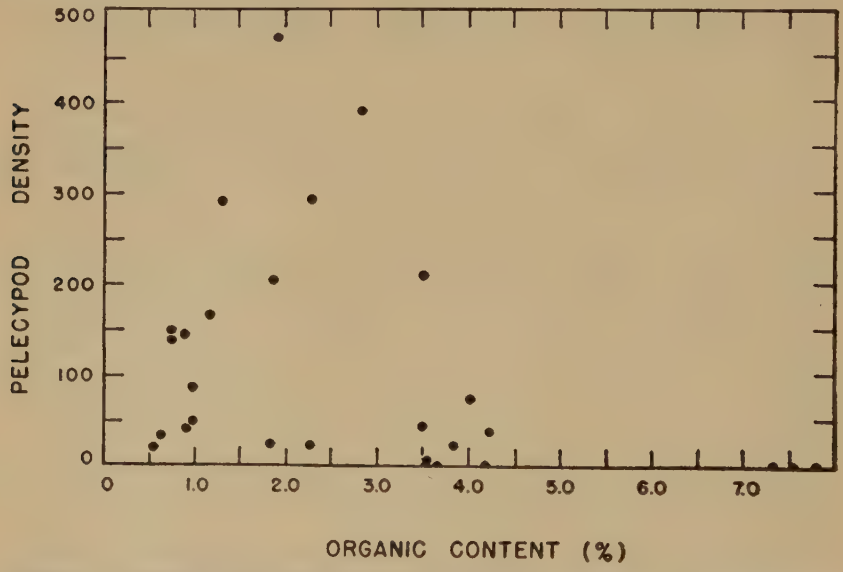

Figure 3. Relationship between density of pelecypod populations and organic carbon content (wt. %) of the sediments. (Note the curvilinear character of the plots when the two samples at about 2% organic material and 20 pelecypods are not considered.)

The next point to consider is the decomposition of the organic matter in the sediments. If the type of organic material is known (Norman, 1937), then it is possible to determine the stage or degree of decomposition. If it is assumed or known that the supply of organic matter in various locations contains the different types of

suites of organic compounds in the same ratio, then the degree of decomposition of the samples may be compared. The lipids, resins, hemicellulose, celluloses, and other carbohydrates and proteins decompose easily and are therefore considered nonrefractory (Waksman and Hotchkiss, 1938; Anderson, 1940), while lignin, which decomposes slowly and at about the same rate in both aerobic and anaerobic environments (Acharya, 1935a, 1935b), is considered refractory.

If a ratio between these two groups is computed, it should indicate the approximate stage of decomposition of the organic matter. As decomposition increases, the amount of lignin will increase relative to the more or less nonrefractory organic compounds. The expression L/R_n (where L = lignin and R_n = total nonrefractory organic matter) will indicate an increase in the degree of decomposition as the numerical value for the expression increases.

In areas where there is a rather high degree of decomposition in a sediment of low organic content, the relative amount of decomposition per unit volume of sediment will be low when compared with an area where the degree of decomposition is the same but the organic content greater. In other words, a coefficient for the degree of decomposition is dependent only upon the actual decomposition, while a coefficient for the amount of decomposition is dependent also upon how much organic matter is available. Therefore, the expression L/R_n, representing the degree of decomposition, has been altered to take into consideration the total amount of organic matter present. The coefficient of the amount of decomposition which has gone on in a unit volume of sediment is represented by the expression $L/R_n \times$ T.O. (where T.O. = total organic content of sample).

Before use can be made of the determined value of the coefficient for the amount of decomposition in each sample, it must be assumed that the over-all ratio of refractory to nonrefractory organic compounds in the organic supply must remain relatively constant though the total amount of organic matter being supplied to the sediments (from whatever source) may vary greatly. If this assumption is fulfilled, then the decomposition coefficient for each sample may be compared with that of other samples. In Fig. 4A the relationship of the decomposition coefficient of organic matter in the sediment is plotted against the pelecypod density. Except for one sample, all of those with a coefficient exceeding 1.0 have pelecypod densities of less than 48 individuals. In view of the sharp break shown in Fig. 4A at a decomposition coefficient of 1.0, a comparison is made between the pelecypod density and the organic content of sediment having a coefficient of 1.0 or less. Fig. 4B clearly indicates an increase in pelecypod

density with an increase in organic content. It is also worth noting here that, upon consideration of this decomposition factor, the two exceptions of low pelecypod density in samples of optimal organic content have been eliminated (see Fig. 3).

TABLE II. Coefficient of Decomposition

Sample No.	*Nonrefractory organic matter** (%)	*Refractory organic matter*† (%)	*Coefficient of amount of decomposition*‡
SS1	1.71	0.59	0.79
SS2	0.74	0.25	0.34
SS3	3.14	4.22	9.86
SS4	5.08	3.77	6.57
SS5	3.62	3.90	8.10
SW1	1.32	0.59	0.85
SW2	2.54	1.01	1.42
SW3	0.90	0.28	0.36
SW4	0.98	1.29	2.96
SW5	1.28	0.61	0.90
SW6	0.64	0.28	0.41
SW7	0.67	0.31	0.53
SW8	0.80	0.48	0.78
SW9	0.70	1.11	2.88
SW10	0.54	0.34	0.55
SW11	0.62	0.12	0.14
SW12	2.45	1.07	1.53
FB1	3.51	0.50	0.57
FB2	0.36	0.15	0.20
FB3	2.12	0.74	0.99
W1	2.55	1.63	2.68
W2	2.11	1.53	2.62
W3	1.89	1.96	3.98
W4	2.06	2.20	4.54
BH1	0.57	0.14	0.18
BH2	0.51	0.11	0.14
BH3	1.58	1.91	4.20

* Sum of ether, alcohol, and water extracts plus hemicellulose and cellulose.

† Lignin and lignoproteins.

‡ $L/R_n \times$ T.O. (L = refractory organics; R_n = nonrefractory organics; T.O. = total organics).

DISCUSSION AND CONCLUSION

Consideration of the organic material in the sediments permits a clarification of the interdependence of environmental factors as related

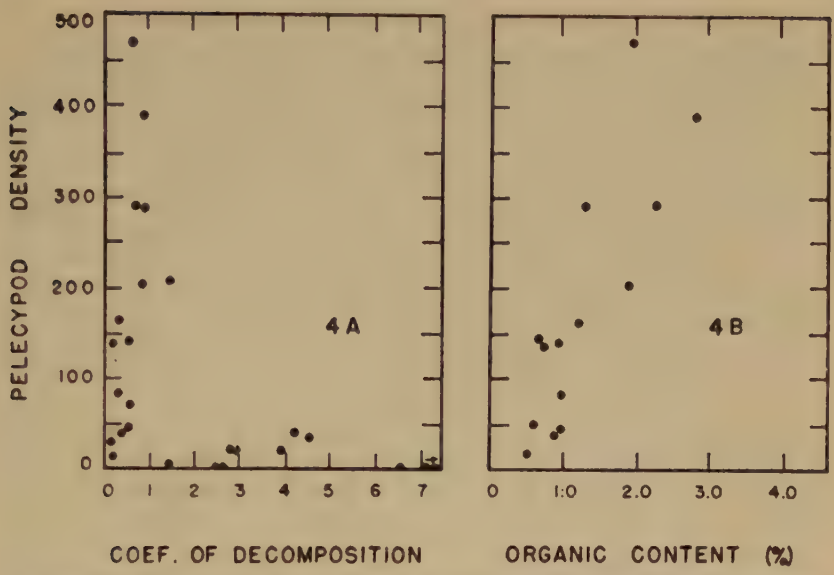

Figure 4A. Relationship between density of pelecypod populations and decomposition coefficient as determined by $L/R_n \times$ T.O. 4B. Relationship between density of pelecypod populations and organic carbon content (wt. %) of the sediments in samples having a decomposition coefficient of less than one.

to pelecypod densities. In undertaking any explanation of the apparent curvilinear distribution of pelecypods in relation to organic matter, it is necessary to consider (1) the feeding habits of the animals, (2) the abundance of food, and (3) the state of decomposition of the food supply.

According to the work of Petersen (1913), Blegvad (1915), and Jensen (1915), many pelecypods use the organic matter in the sediments as a food source. Mitsukuri (1881) and Drew (1899) showed that the palp appendages of the genus *Nucula* and *Yoldia* are functional in scooping up sedimentary detritus during the process of ingestion. In view of this it shall be considered that the organic matter in the samples studied is a primary source of pelecypod nutrition.

The abundance of food naturally affects the potential pelecypod population. If the food supply increases, the population has the potential to increase so long as the food supply is the major limiting factor. Fig. 4B shows an unmistakable increase in pelecypod population as the food supply (i.e., organic matter) increases.

Microbiological decomposition of the organic matter in the sediments occurs in the marine environment. Waksman and Starkey (1931) have shown that natural decomposition of organic matter can produce aldehydes, hydrogen sulphide, methane, and many other toxic products. Reuszer (1933) and Waksman, *et. al.* (1933) have shown that the degree of decomposition of organic matter is correlated with the abundance of bacteria. Liagena and Kuznetzow (1937), ZoBell and Stadler (1940), ZoBell and Feltham (1942), and others have shown that abundant bacterial activity causes a serious drain on the available oxygen supply. From this it can be concluded that the decomposition of the organic material by bacteria is an ecological factor resulting from the production of toxic products and/or the depletion of available oxygen. Fig. 4A shows a sharp drop in the pelecypod density as the amount of decomposition increases.

It is now possible to explain the curvilinear distribution of pelecypods as shown in Fig. 3. The pelecypod density initially increases with an increase in the organic content of the sediment, since the food supply is the major limiting factor. Beyond 3% organic content, the products of decomposition and/or the decline in available oxygen become the limiting variables, and the population decreases. The two exceptions to the curvilinear distribution as shown in Fig. 3 (those with optimum organic contents and low pelecypod densities) support the above contentions; they have decomposition coefficients of 2.88 and 2.96. The rest of the samples in the optimal range of organic content (1.18 to 2.86%) have decomposition coefficients of less than 1.00. The organic matter in these two samples is decomposed to a far greater extent and the population is thus kept at a minimum.

In reality the apparent curvilinear distribution of pelecypod densities represents a composite of the controlling aspects of physical, chemical and microbiological environmental factors. It has been shown that there are some gross correlations between organic content and the physical factors considered. The pelecypod density and the physical characteristics also show some gross relationships. The obvious correlation between pelecypod density and organic considerations makes it apparent that the most important pair of variants is the organic content and its state of decomposition.

The data obtained during this study indicate that greater detail in the determination of ecological variants may be exceedingly profitable. The consideration of micro variants such as bacterial flora, the specific organic chemical compounds, the source of these compounds, the type, rate and amount of decomposition, and many others may develop a clearer understanding of the over-all environment and its relationship to the animal population.

SUMMARY

A general study has been made of a selected portion of the environment of marine sediments and their pelecypod population in the region of Mt. Desert Island, Maine. The environmental factors considered are: water temperature, depth, and salinity, median diameter of the sedimentary particles, coefficient of sedimentary sorting, organic content of sediments, and the decomposition of the organic material.

Salinity and temperature changes vary slightly and do not noticeably affect the populations sampled. The depth of water, as well as the median diameter and sorting of the sediments, are grossly related to the density of pelecypod populations. Finer and poorly sorted sediments of the deeper water have the widest range of pelecypod densities.

The expression $L/R_n \times$ T.O. (where L = refractory lignin, R_n = nonrefractory organics and T.O. = total organic matter) is considered an approximation of the total amount of organic decomposition. Though the physical variants are by no means negligible, the organic content of the sediments and its decomposition, as given by the above expression, apparently control the pelecypod densities of any area. As the organic content (food supply) increases, the pelecypod population increases until bacterial decomposition of the organic material becomes the major limiting factor; then the population decreases.

ACKNOWLEDGEMENTS

The writer is indebted to Dr. H. A. Lowenstam for his suggestions, cooperation, material aid, and interest in this project. Drs. E. C. Olson, F. J. Pettijohn, J. M. Weller, and R. L. Miller gave freely of their time for suggestions and constructive criticism. Appreciation is also extended to Drs. H. C. Urey, S. Epstein, J. L. Hough, B. R. Speicher, and to Mr. N. T. Allen. Thanks are due Messrs. A. Bunker, J. Somes, T. Higgins, and C. Brown of Mt. Desert Island, Maine, and Mrs. M. Bader.

REFERENCES

Allee, W. C.

1923a. Studies in marine ecology. I. The distribution of common littoral invertebrates of the Woods Hole region. Biol. Bull. Woods Hole, *44:* 167–191.

1923b. Studies in marine ecology. III. Some physical factors related to the distribution of littoral invertebrates. Biol. Bull. Woods Hole, *44:* 205–253.

Allee, W. C., A. E. Emerson, O. Park, T. Park, and K. P. Schmidt
1949. The principles of animal ecology. W. B. Saunders Co., Philadelphia. 837 pp.

Anderson, D. Q.
1940. Distribution of organic matter in marine sediments and its availability to further decomposition. J. Mar. Res., *2:* 225–235.

Acharya, C. N.
1935a. Studies on the anaerobic decomposition of plant materials. I. Anaerobic decomposition of *Oryza sativa.* Bio-chem. J., *29:* 528–541.
1935b. Studies on the anaerobic decomposition of plant materials. III. Comparison of the course of decomposition of rice straw under anaerobic, aerobic, and partially aerobic conditions. Bio-chem. J., *29:* 1116–1120.

Blegvad, H.
1915. Food and conditions of nourishment among the communities of invertebrate animals found on or in the sea bottom of Danish waters. Rep. Danish biol. Sta., *22:* 3–88.

Drew, G. A.
1899. Some observations on the habits, anatomy, and embryology of members of the Protobranchia. Anat. Anz., *15:* 493–519.

Furman, N. H.
1939. Scott's standard methods of chemical analysis. 2 vols., D. Van Nostrand Co., Inc., New York. 2617 pp.

Jackson, R. F.
1928. Report on chemical methods for reducing sugars. J. Ass. off. agric. Chem., *11:* 175–178.

Jensen, P. B.
1915. Studies concerning the organic matter of the sea bottom. Rep. Danish biol. Sta., *22:* 1–39.

Krumbein, W. C. and F. J. Pettijohn
1938. Manual of sedimentary petrography. Appleton-Century-Crofts, Inc., New York. 549 pp.

Liagina, N. M. and S. I. Kuznetzow
1937. The determination of the intensity of respiration of some species of water bacteria at various temperatures under laboratory conditions (in Russian, with English summary). Mikrobiologia, *6:* 21–27.

Mitsukuri, K.
1881. On the structure and significance of some aberrant forms of lamellibranchiate gills. Quart. J. micr. Sci., *21:* 595–608.

Niederl, J. B. and V. Niederl
1942. Micromethods of quantitative organic analysis. John Wiley & Sons, Inc., New York. 347 pp.

Norman, A. G.
1937. The biochemistry of cellulose, the polyuronides, lignin, etc. Clarendon Press, Oxford. 232 pp.

Oxner, M.
1920. Chloruration par la methode de Knudsen. Bull. Comm. int. Explor. Mediterr. [Eng. transl. (1946), Woods Hole Oceanogr. Inst., Woods Hole, Mass. 63 pp.]
Petersen, C. G. J.
1913. Valuation of the sea. III. The animal communities of the sea bottom and their importance for marine zoogeography. Rep. Danish biol. Sta., *21:* 40–88.
Piper, C. S.
1942. Soil and plant analysis. Univ. of Adelaide, Adelaide. 368 pp.
Reuszer, H. W.
1933. Marine bacteria and their role in the cycle of life in the sea. III. The bacteria in the ocean waters and muds about Cape Cod. Biol. Bull. Woods Hole, *65:* 48–97.
Roth, H.
1937. Quantitative organic microanalysis of Fritz Pregl. P. Blackiston's Son & Co., Inc., Philadelphia. 271 pp.
Scales, F. M.
1915. The determination of reducing sugars (a volumetric method for determining cuprous oxide without removal from Fehlings solution). J. biol. Chem., *23:* 81–87.
Verrill, A. E. and S. I. Smith
1874. Report of the invertebrate animals of Vinyard Sound and adjacent areas. Rep. U. S. Comm. Fish. (1871–1872), pp. 295–544.
Waksman, S. A.
1933. On the distribution of organic matter in the sea bottom and the chemical nature and origin of marine humus. Soil Sci., *36:* 125–147.
Waksman, S. A., C. L. Carey, and H. W. Reuszer
1933. Marine bacteria and their role in the cycle of life in the sea. I. Decomposition of marine plant and animal residues by bacteria. Biol. Bull. Woods Hole, *65:* 57–79.
Waksman, S. A. and U. Hotchkiss
1938. On the oxidations of organic matter in the marine sediments by bacteria. J. Mar. Res., *1:* 101–118.
Waksman, S. A. and R. L. Starkey
1931. Soil and the microbe. John Wiley & Sons, Inc., New York. 260 pp.
ZoBell, C. E. and C. B. Feltham
1942. Bacterial flora of a marine mud flat as an ecological factor. Ecology, *23:* 69–78.
ZoBell, C. E. and J. Stadler
1940. The oxidation of lignin by lake bacteria. Arch. Hydrobiol. Plankt., *37:* 163–171.

OCEANOGRAPHIC FEATURES OF A SUBMARINE ERUPTION THAT DESTROYED THE KAIYO-MARU No. 5[1]

By

MASITO NAKANO

Meteorological Research Institute and Tokyo University

SANAE UNOKI, MASAO HANZAWA, RYUZO MARUMO AND JIRO FUKUOKA

Central Meteorological Observatory of Japan

ABSTRACT

When Myojinsho Reef erupted in September 1952, tsunami waves were recorded several times by a self-registering wave gauge installed on the southwestern coast of Hachijo Island about 130 km from that Reef. The largest one of these tsunamis appeared on 24 September, and it is presumed that this wave caused the destruction of the KAIYO-MARU No. 5. Results of investigation of these recorded tsunami waves and other phenomena are reported.

INTRODUCTION

Since September 1952, a station for the observation of sea waves has been maintained by the Central Meteorological Observatory of Japan in the vicinity of Port Yayene on the southwestern coast of Hachijo Island (Fig. 1). The station, equipped with a self-registering wave gauge, was established with the aim of investigating the relations between wind waves or swells and atmospheric disturbances such as cyclones or typhoons. In mid-September, Myojinsho Reef erupted, and tsunamis caused thereby were recorded several times by this wave gauge. In the present paper, the results of investigations of these tsunamis are reported, together with other pertinent observations.

RESULTS OF WAVE GAUGE OBSERVATIONS

The wave gauge is of the pressure recorder type and was reconstructed from a statoscope of the type in ordinary use for recording microbarographic oscillations. The pressure change, corresponding to the rise and fall of the sea level, is automatically traced on a roll of paper at a speed of about 33 cm/hr. The device is capable of making a continuous record of waves for about 12 hours. The reducing scale

[1] A surveying ship (211 tons) of the Hydrographic Office, Maritime Safety Agency of Japan.

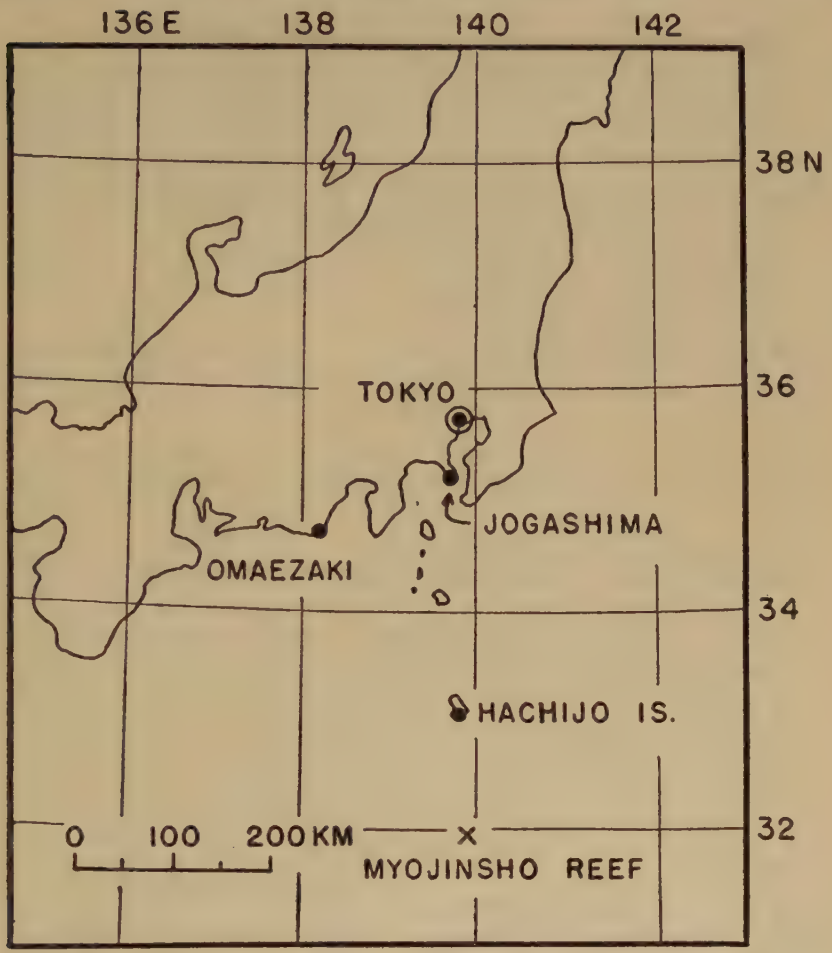

Figure 1. Geographical locations of Myojinsho Reef and Hachijo Island.

of the instrument is about 1/70 for ordinary wind waves or swells but is somewhat less for the tsunamis in question, which have a period of about 1 min or so. A slow-leak device is attached to the instrument to eliminate waves of longer periods, such as tides.

Fig. 2 shows in tabular form the periods[2] in which the observations were taken during the interval of 16–30 September 1952 as well as

[2] In the present paper, the time of observation is always referred to the meridian of 135° E (Japanese Standard Time).

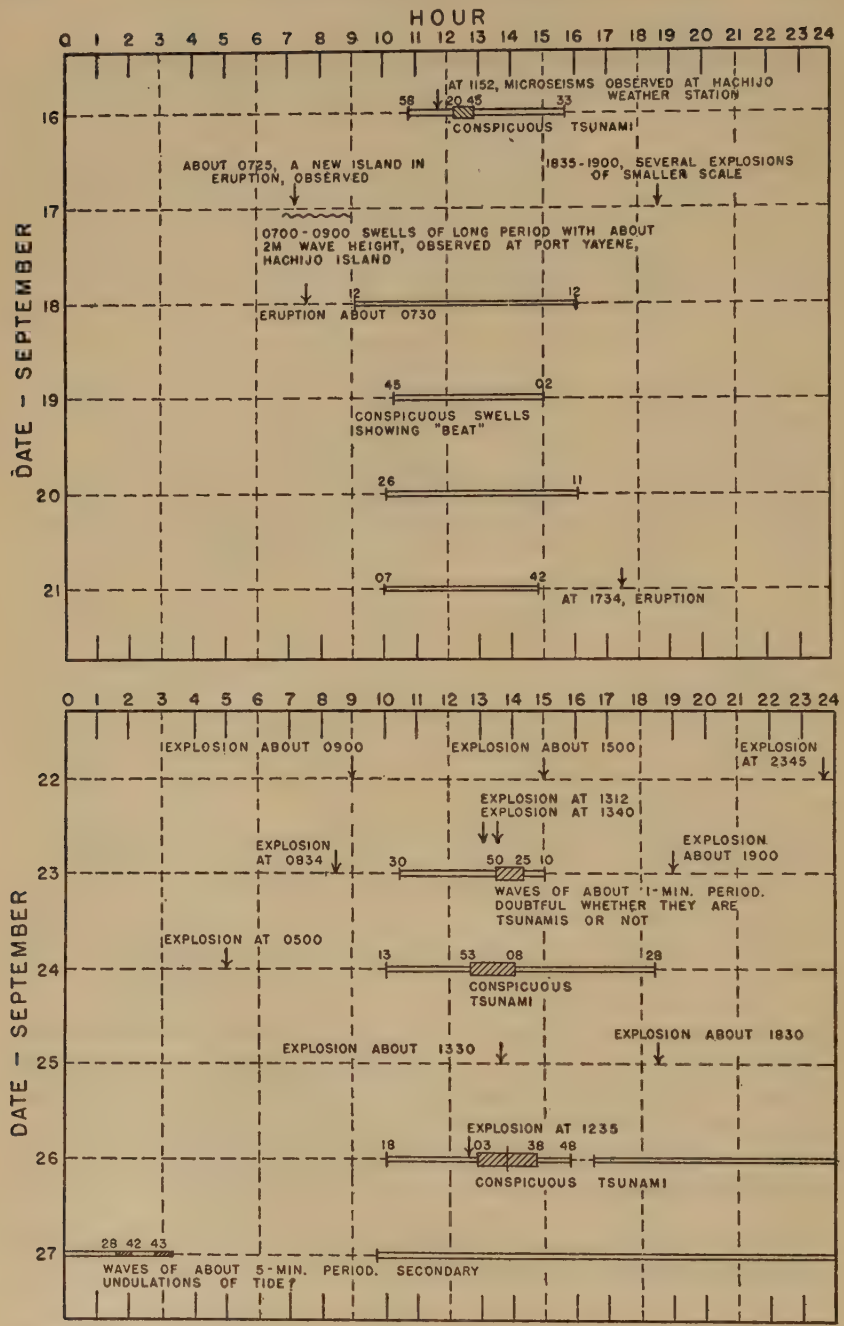
HOUR
0 1 2 3 4 5 6 7 8 9 10 11 12 13 14 15 16 17 18 19 20 21 22 23 24
DATE - SEPTEMBER
16
17
18
19
20
21
AT 1152, MICROSEISMS OBSERVED AT HACHIJO WEATHER STATION
58 20 45 33
CONSPICUOUS TSUNAMI
ABOUT 0725, A NEW ISLAND IN ERUPTION, OBSERVED
1835-1900, SEVERAL EXPLOSIONS OF SMALLER SCALE
0700-0900 SWELLS OF LONG PERIOD WITH ABOUT 2M WAVE HEIGHT, OBSERVED AT PORT YAYENE, HACHIJO ISLAND
12 12
ERUPTION ABOUT 0730
45 02
CONSPICUOUS SWELLS SHOWING "BEAT"
26 11
07 42
AT 1734, ERUPTION
0 1 2 3 4 5 6 7 8 9 10 11 12 13 14 15 16 17 18 19 20 21 22 23 24
DATE - SEPTEMBER
22
23
24
25
26
27
EXPLOSION ABOUT 0900
EXPLOSION ABOUT 1500
EXPLOSION AT 2345
EXPLOSION AT 1312
EXPLOSION AT 1340
EXPLOSION AT 0834
30 50 25 10
EXPLOSION ABOUT 1900
WAVES OF ABOUT 1-MIN. PERIOD. DOUBTFUL WHETHER THEY ARE TSUNAMIS OR NOT
EXPLOSION AT 0500
13 53 08 28
CONSPICUOUS TSUNAMI
EXPLOSION ABOUT 1330
EXPLOSION ABOUT 1830
EXPLOSION AT 1235
18 03 38 48
CONSPICUOUS TSUNAMI
28 42 43
WAVES OF ABOUT 5-MIN. PERIOD. SECONDARY UNDULATIONS OF TIDE?

Figure 2. Results of sea wave observations at Hachijo Island with a self-registering wave gauge.

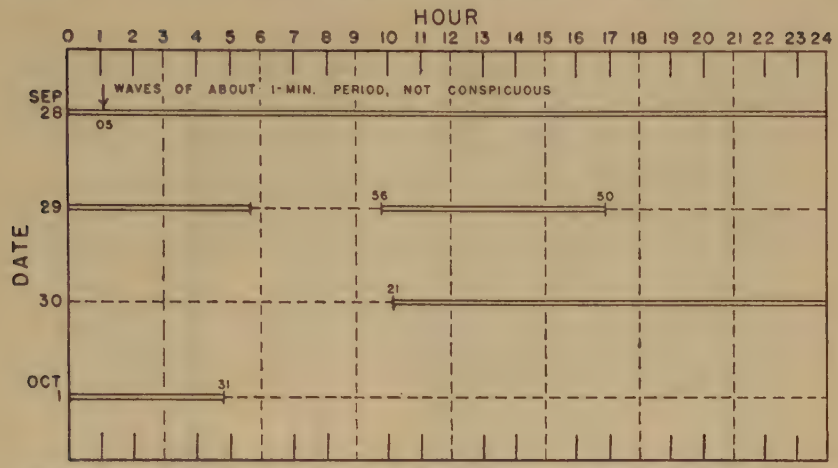

Figure 2 (*Continued*). Results of sea wave observations at Hachijo Island with a self-registering wave guage.

eruptions of Myojinsho Reef and other unusual phenomena in this interval. The thick horizontal line segments indicate the periods in which the records were obtained by the wave gauge, and the hatched portions indicate the periods in which the tsunamis were recorded. The numerals above the horizontal line segments indicate the time (in minutes). In Fig. 2 we see that conspicuous tsunamis appeared on 16, 24 and 26 September and that something like a tsunami occurred on 23 September (see Fig. 3A, B, C, D; a normal record is shown in Fig. 3E). Since records of wind waves and swells were superimposed on those of tsunami waves, the records were smoothed so that the curves represent only the tsunami waves (see Fig. 4). The time marks shown in the above records are those obtained by interpolation. Hence possible errors in time of about $\pm$ 3 min are involved.

(A) On 16 September (see Figs. 3A, 4A), although no one witnessed eruptions, microseisms (or better, seismic surface waves) of maximum amplitude 5 μ and of period 4.1 sec were recorded at 11^h52^m on a portable seismometer installed at the Hachijojima Weather Station. According to seismologists, these microseisms were probably due to an eruption of Myojinsho Reef. If we assume that the velocity of propagation of these microseismic waves is several kilometers per second and that it is the same as that of ordinary seismic waves (surface waves), we may consider that the eruption occurred at about 11^h52^m. Since the tsunami began to occur at Hachijo Island at 12^h20^m, the time taken by the tsunami wave to travel from Myojinsho Reef to the observing station was $12^h20^m - 11^h52^m = 28$ min. The maximum wave height of this tsunami was 56 cm.

(B) On 24 September (see Figs. 3B, 4B), a more conspicuous tsunami was recorded. The eruption which caused it was probably the one

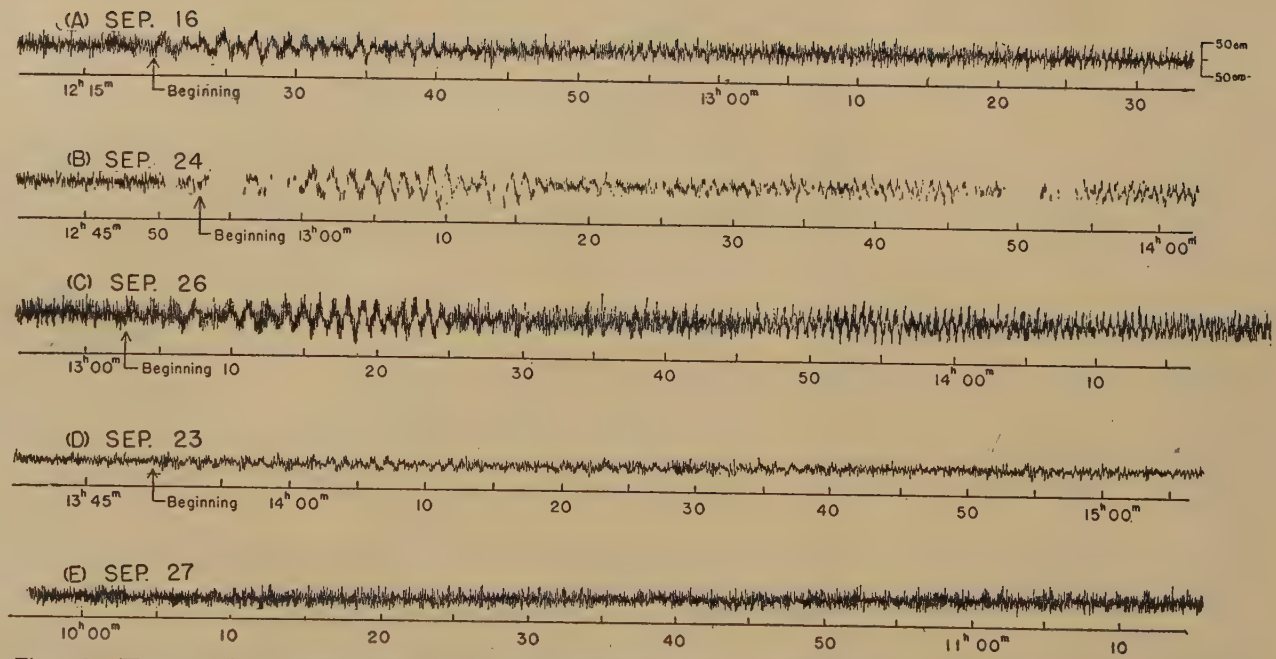

Figure 3. Wave records at Hachijo Island. A, B and C represent tsunamis caused by the eruption of a submarine volcano at Myojinsho Reef. D shows a probable tsunami wave and E a normal record.

which also caused the disaster to the KAIYO-MARU No. 5. Since there were no survivors, no first-hand account of the eruption is reported. The tsunami began at 12^h53^m and the maximum wave height was 92 cm.

(C) On 26 September (see Figs. 3C, 4C), another conspicuous tsunami occurred; its maximum wave height was 71 cm and the time of its first movement was 13^h03^m. In this instance a ship of the Maritime Safety Agency, sent to investigate the fate of the KAIYO-MARU No. 5,

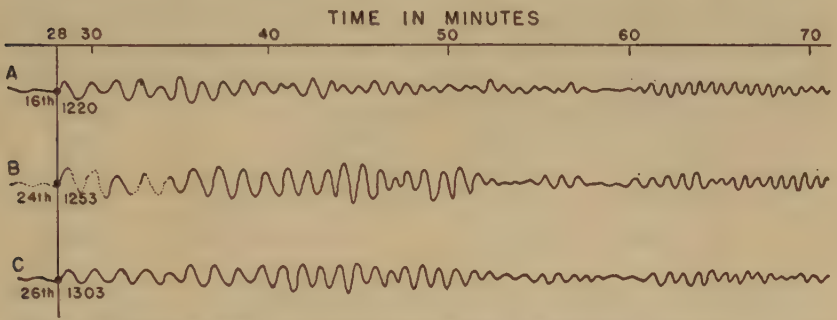

Figure 4. Wave records A, B and C of the tsunamis, obtained by smoothing the actual wave records A, B and C of Fig. 3 to eliminate wind waves and swells.

ascertained that an eruption occurred at Myojinsho Reef at 12^h35^m. The time taken by the tsunami wave to travel from Myojinsho Reef to the observing station on Hachijo Island was $13^h03^m - 12^h35^m = 28$ min, the same value obtained for the one on 16 September.

On 23 September (see Fig. 3D), two eruptions of Myojinsho Reef at 13^h12^m and 13^h40^m were witnessed by members of the Tokyo College of Fisheries on board the SHINYO-MARU. Referring to Fig. 3D, undulations, apparently tsunami waves, began to occur at 13^h50^m. However, when this record is compared with those in Figs. 3A, B and C, we see that the record for 23 September differs from those for 16, 24 and 26 September in wave period as well as in wave height; that is, although at first sight the said undulations for 23 September appear to have been tsunami waves,they might have been the peculiar type of wave which appears when a typhoon or cyclone approaches, or they might have been what Munk (1949) calls "surf beats." Moreover, as regards the determination of the time of beginning of the said undulation, 13^h50^m, it is less clearly defined. Therefore we shall not consider here the observations obtained on this date.

TRAVEL TIME OF TSUNAMI WAVES AND MAGNITUDE OF ERUPTION

In computing the travel time of a tsunami, that is, the time taken by the tsunami wave to travel from Myojinsho Reef to the observing station, we must decide whether it is a shallow, intermediate, or deep wave and whether it propagates with phase or group velocity. Since the depth of water is 200–1400 m and the wave period 30–100 sec, and considering the relative depth (ratio of water depth to wave length), we see that the wave cannot be treated either as a deep or shallow wave (long wave); therefore it must be treated as an intermediate wave (elliptical particle orbits). If we denote the period by τ, the wave length by λ, and the depth of water by d, we have for such waves, according to the Airy theory,

$$\text{phase velocity} \qquad C = \left\{ \frac{g\lambda}{2\pi} \tanh\left(\frac{2\pi d}{\lambda}\right) \right\}^{\frac{1}{2}}, \tag{1}$$

$$\text{group velocity} \qquad C_g = \frac{C}{2}\left\{ 1 + \frac{\frac{4\pi d}{\lambda}}{\sinh\left(\frac{4\pi d}{\lambda}\right)} \right\}, \tag{2}$$

where g is the acceleration due to gravity and $\lambda = C\tau$.

It is found that, within the range of magnitude of the quantities and the distance here considered, computations by equations (1) and (2) yield the following result; the phase velocity C and the group velocity C_g of the intermediate wave differ little from those of the deep water wave.

In Figs. 3A, B and C or Figs. 4A, B and C, we see that the period of the wave which first reached the observing station is about 95 sec. If we consider that this wave proceeded with group velocity, and if we compute the travel time t by the formula

$$t = \int \frac{ds}{C_g} = \sum \frac{\Delta s}{C_g}, \tag{3}$$

we have $t = 32.1$ min. Again, if we consider that this wave travelled with phase velocity, we have $t = 28.5$ min. As stated previously, the actual travel time of the wave was about 28 min as determined for 16 and 26 September. But, as noted earlier, this value has a possible error of about ± 3 min. Consequently it is difficult to reach a definite conclusion as to whether the wave travelled with phase velocity or with group velocity. To ascertain the exact dif-

ference of travel-time within the range of wave period, water depth and distance of travel under consideration, more accurate time-marking would have been necessary.

We are also concerned with the time of occurrence of the volcanic eruption which presumably caused the destruction of the KAIYO-MARU No. 5 on 24 September.[3] If the waves shown in Figs. 3B or 4B (IX/24) are compared with those of Figs. 3A or 4A (IX/16) and 3C or 4C (IX/26), we see that the value of initial wave-period as well as the modes of variation of wave-period and wave-height are very similar. Hence it may be supposed that the travel time was about 28 min. in all cases. Accordingly, the eruption in question presumably occurred at about 24th $12^h53^m - 28^m = 24\text{th } 12^h25^m \pm 6^m$. According to the result of a SOFAR hydrophone observation made by the U. S. Navy, it is estimated that the said eruption on 24 September occurred at about 12^h20^m, which is in good agreement with our result.[4]

Regarding the magnitude of the eruption, Unoki and Nakano (1953, 1953a) have made a detailed theoretical investigation which has shown that the present tsunami is a typical "Cauchy-Poisson wave" generated by a local disturbance over a limited extent of the sea surface. Assuming that the wave was generated by an initial impulse and that the radius of the disturbing source (the area to which the initial impulse was applied) was circular, it was found that the initial radius was about 2.2 km for A, B and C and that the magnitude of the initial impulse was 7.0×10^6, 11.6×10^6, and 8.9×10^6 dyne. sec/cm^2 for A, B, and C respectively.[5] Again, if the initial disturbance was assumed to be an initial elevation, then the radius of the disturbing source was about 2.2 km for A, B, and C, as above, and the magnitude of the initial elevation was 6.3 m, 10.3 m and 8.0 m for A, B, and C respectively.

[3] From navigation and communication, it is presumed that the KAIYO-MARU No. 5 had not yet reached Myojinsho Reef at 10^h on 24 September and that her destruction must have occurred between 10^h and 13^h on that same day.

[4] This information was kindly furnished by Dr. R. S. Dietz of the U. S. Navy Electronics Laboratory, San Diego, Calif.

[5] In the first paper (Unoki and Nakano, 1953), one-dimensional treatment was given to the problem and the effect of friction was neglected, while in the second paper (Unoki and Nakano, 1953a) a two-dimensional treatment was given, with consideration of the frictional factor. Hence the values of the computed quantities for the initial impulse, etc., are not the same in both studies. Naturally the latter values are considered to be closer to reality, and the numerical values of the computed quantities quoted here are those obtained in the second paper.

Moreover, it was found that, in the tsunami of 24 September, the action of the initial impulse exerted much more effect than did the initial elevation. Furthermore, it was known that the energy of the eruption was about 3.0×10^{19}, 7.9×10^{19} and 4.8×10^{19} ergs for A, B, and C respectively. Thus, it is seen that the eruption on the 24th was quite violent.

THE TIME OF DESTRUCTION OF THE KAIYO-MARU No. 5 AS INFERRED FROM DEBRIS

The time of the destruction of the KAIYO-MARU No. 5 may also be inferred from the distribution of the wreckage and debris that remained afloat. From these observations, it was determined that the KAIYO-MARU No. 5 was destroyed during the afternoon of 24 September 1952, a fact which seems to confirm the result deduced from the record of the self-registering wave gauge on Hachijo Island.

In Fig. 5 the abscissa[6] denotes the distance from Myojinsho Reef and the ordinate denotes time; the points correspond to the time and location where debris was found, and it is apparent that these points lie almost within an area limited by two straight lines. If we draw a straight line to represent as nearly as possible the distribution of these points and intersect this straight line with the axis of ordinate, we find that the time when drifting began (equivalent to the time of eruption or disaster) falls between 0^h and 12^h on the 24th. But if we consider Fig. 5 carefully, we notice that some flotsam, such as that indicated by (5), (7), (8) and (10), was driven relatively farther as compared with that indicated by (4), (6), etc. Since the starting time from Myojinsho Reef of all objects is considered to be the same, it is necessary to make a correction for the effect of leeway. According to Yasui (1940), the effect of leeway is expressed by the formula

$$U = k \sqrt{\frac{A}{B}} \cdot W , \tag{4}$$

where U denotes the drifting velocity of a vessel due to the effect of wind, W the velocity of wind, A and B the cross-sectional areas of the vessel above and below the sea surface, respectively, taken in a plane perpendicular to the direction of drift, and k a certain constant. If U and W are measured in cm/sec, the value of k is 0.03. The value of the ratio A/B will differ for different flotsam, but in the present

[6] Here it is assumed that the KAIYO-MARU No. 5 was destroyed in close proximity to Myojinsho Reef.

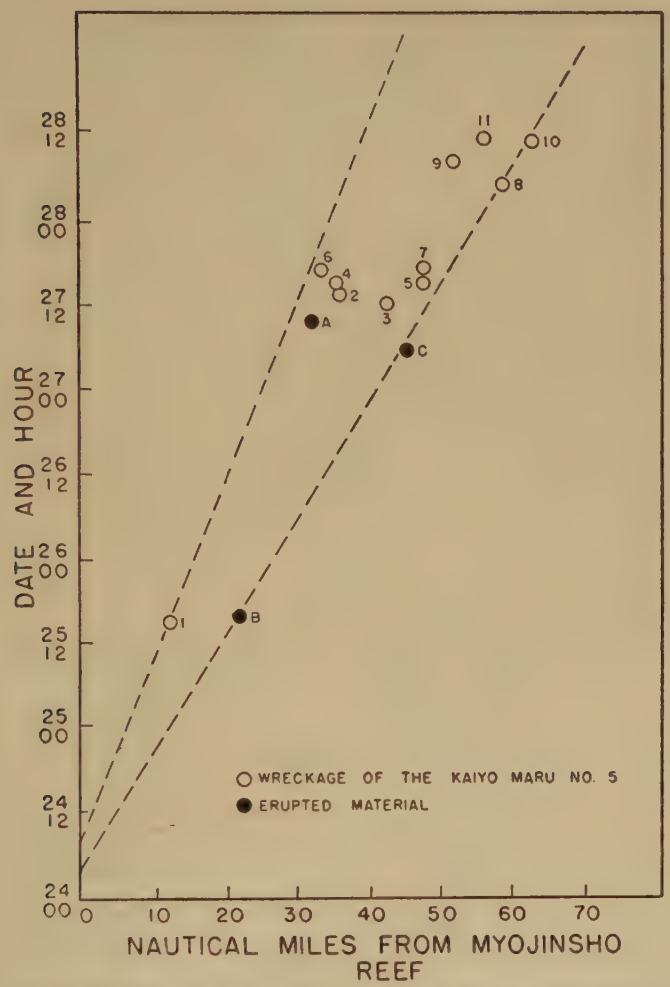

Figure 5. Drifting distance of erupted materials and wreckage from the KAIYO-MARU No. 5 relative to time of drifting. 1. Wooden box, soy keg, angular timber, log, pieces of cork, and numerous timbers. 2. Surveying buoy. 3. Surveying log. 4. Wood from a sampan stern, and a piece of cork. 5. Rack of a sampan, life buoy, and a piece of wood from a vegetable container. 6. Fragment of a life buoy. 7. Fragment of bulwark. 8. Crossbar of bed from operator's room. 9. Four kegs. 10. Part of environs of boat. 11. Part of compass bridge deck. A. Piece of comparatively new wood. B. Volcanic ashes and solidified substances. C. Sulphur and pumice. (Note: Flotsam "A" was picked up by a fishing boat, and it is uncertain whether or not this is part of the KAIYO-MARU No. 5 wreckage.)

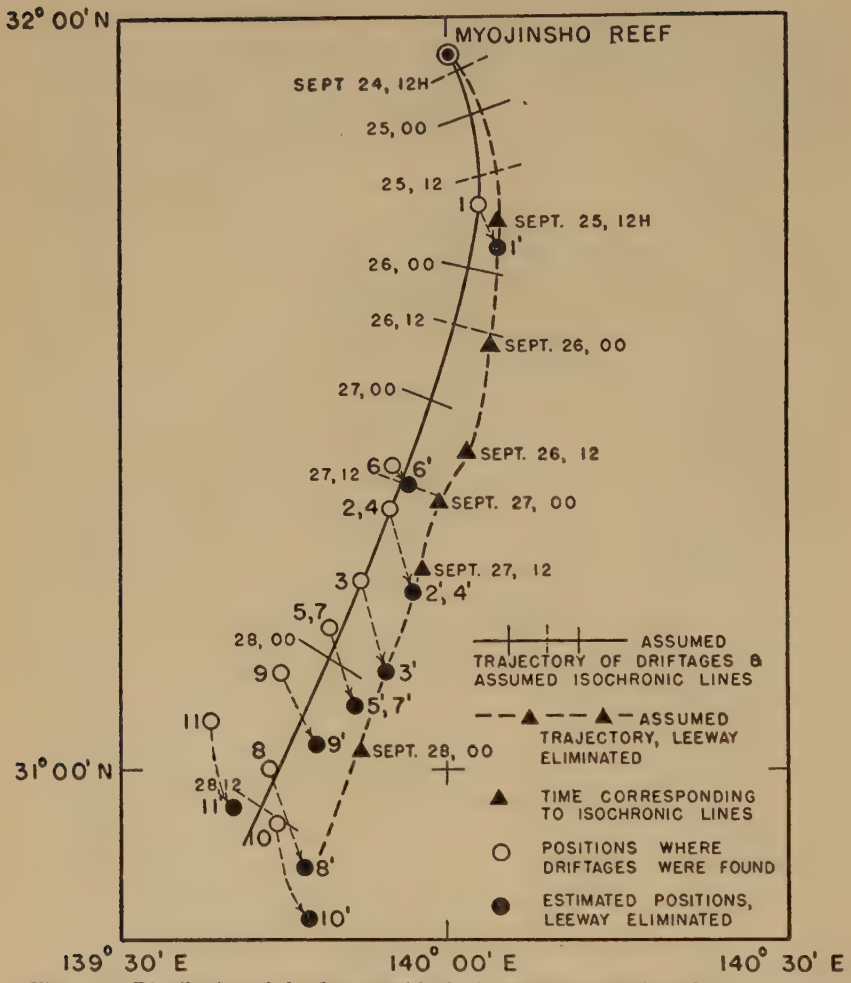

Figure 6. Distribution of the flotsam with the leeway effect eliminated. The numbers applied to the flotsam are in accord with the data of the Hydrographic Office, Maritime Safety Agency of Japan.

case we take, as an approximation, A/B as a constant and equal to $\frac{1}{2}$ for all the flotsam concerned.

By means of weather charts published by the Central Meteorological Observatory of Japan, the wind velocity and direction over the area considered were estimated; and by using equation (4), the effect of leeway was eliminated. In Fig. 6, the small white circles represent the positions where the items of flotsam were actually picked up.

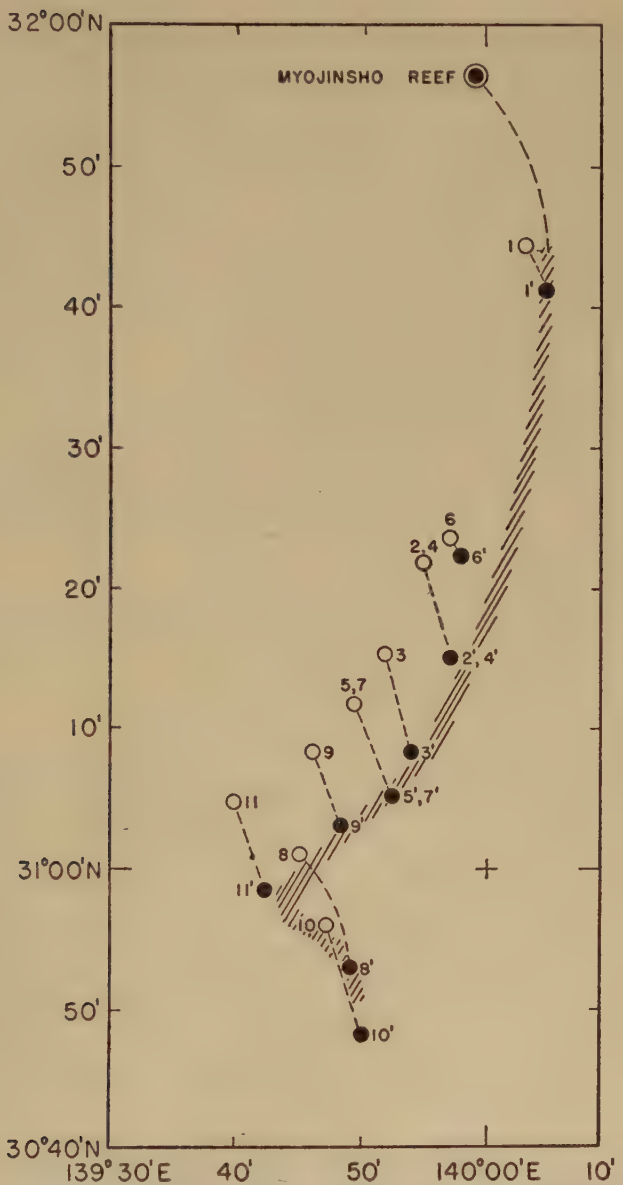

Figure 7. Chart of streamlines of the ocean current, drawn from the estimated positions of flotsam with the effect of leeway eliminated.

If the effect of leeway were nonexistent and if the flotsam had been carried by the general current alone, wreckage would have been found at the positions indicated by the black circles in Fig. 6.

Fig. 7 shows the streamlines of the ocean current in the area concerned; these were drawn from the estimated positions of flotsam after the effect of leeway had been eliminated. Unfortunately the direction of the current is somewhat obscure near 139° 50' E and 31° 00' N because of the fact that there was at that time a stationary front in this vicinity. Since some of the flotsam was situated on the northern side and some on the southern side of the front, some errors were unavoidably introduced when the effect of leeway was calculated.

With the effect of leeway eliminated, Fig. 8[7] is drawn to show the "travel-time curve" of Fig. 5 with corrected values; the values of time and distance correspond to the black circles in Fig. 6. In Fig. 8 we see that the items of flotsam are distributed more or less regularly along a straight line. If we read the value of time at the point where this straight line intersects the time axis, then the starting time of the driftages from Myojinsho Reef occurred during the afternoon of the 24th (about 18^h, we venture to say).

Since there are probably some errors in our estimated values of wind direction and velocity over the sea (the values adopted for k and A/B in the formula $U = k\sqrt{A/B}\,.W$) and of the positions where the flotsam was found, we cannot draw a more detailed conclusion than this from the travel-time curve method used above.

Again we note that the above discussion is based on the assumption that the flotsam came from close proximity to Myojinsho Reef. If the KAIYO-MARU No. 5 met with disaster at some point far apart from Myojinsho Reef, then a major correction would have to be made in our calculations and conclusions. However, at present there is nothing which seems to contradict our assumption. At any rate, the above result of driftage investigation is not inconsistent with the result inferred from the record of the self-registering wave gauge on Hachijo Island. Moreover, if we calculate the velocity of the ocean current from the travel-time curve in Fig. 8, we have approximately 0.7 knot, which is in fairly good accord with the result of observations taken hitherto in this vicinity (Hydrographic Office of Japan, 1948; see also Hanzawa, 1953).

[7] As noted earlier, it is not certain that flotsam "A" in Fig. 5 is a part of the wreckage of the KAIYO-MARU No. 5. Again, it is not certain that the erupted materials "B" and "C" in Fig. 5 were ejected from Myojinsho Reef at the time of the eruption which destroyed the KAIYO-MARU No. 5. Hence, in Fig. 8, A, B and C are omitted.

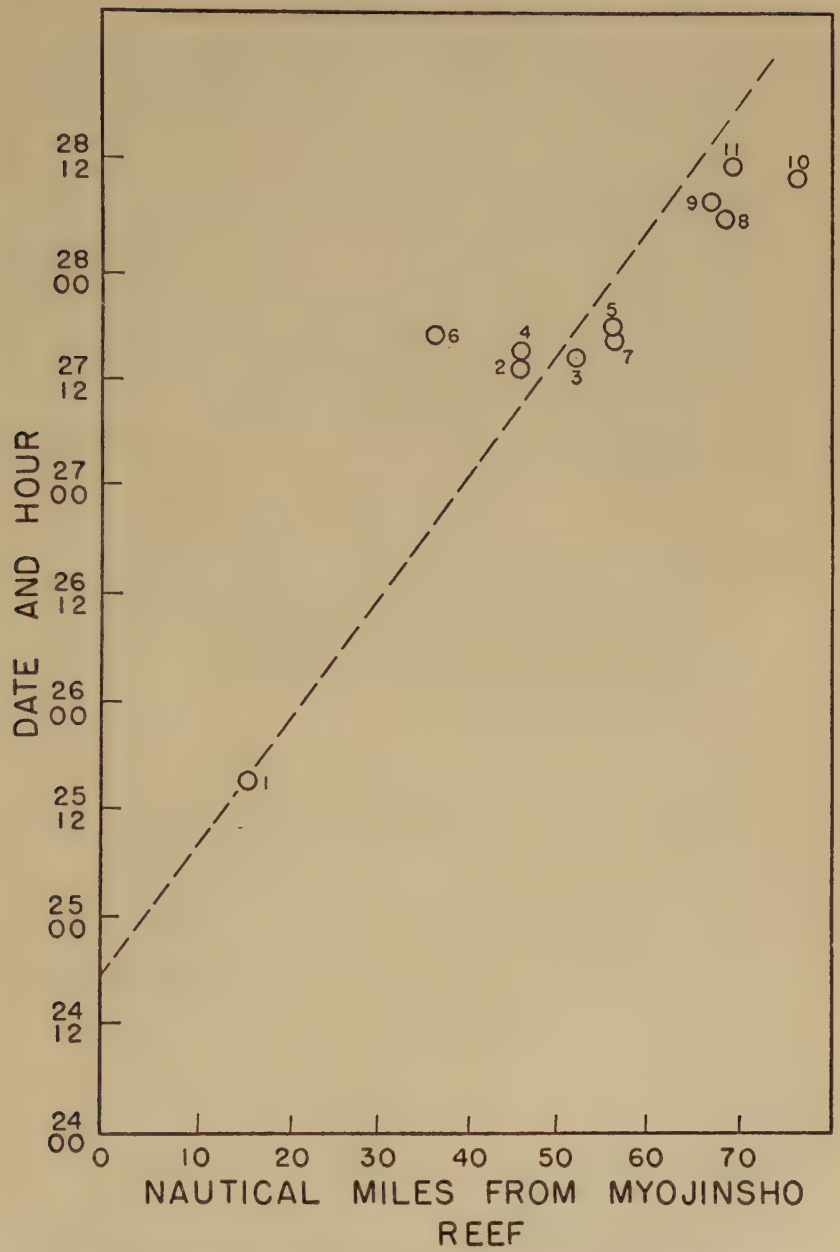

Figure 8. Drifting distance relative to time, corrected for the effect of leeway.

ACKNOWLEDGMENT

In conclusion, we wish to express our thanks to members of Hachijo-jima Weather Station who obtained wave records for us, to the observers and crew of the CHIKUBU-MARU, at whose personal risk data in the danger zone were obtained, to Dr. K. Suda, director of the Hydrographic Office, Maritime Safety Agency of Japan, who kindly gave additional data concerning the disaster of the KAIYO-MARU No. 5, and to Dr. K. Wadati, director of the Central Meteorological Observatory of Japan, for his encouragement and advice. Similar thanks for helpful information and suggestions are due Dr. Y. Kawabata of the Central Meteorological Observatory of Japan, Dr. C. Tsuboi of Tokyo University, and Dr. R. S. Dietz of the U. S. Navy Electronics Laboratory, San Diego, California. And the authors pray heartily for the heavenly bliss of the investigators and crew on board the KAIYO-MARU No. 5 whose precious lives were lost in the southern sea of Japan in the interest of science.

REFERENCES

CENTRAL METEOROLOGICAL OBSERVATORY OF JAPAN, OCEANOGRAPHICAL SECTION
1952. Report of investigations on the disaster of the KAIYO-MARU No. 5 (a surveying ship of the Hydrographic Office, Maritime Safety Agency of Japan) in relation to oceanography (in Japanese). Prepared by Masito Nakano, then Chief of the Oceanographical Section. Oceanogr. Rep. Central Meteorol. Observ. Japan, *2* (4): 295–304.

HACHIJOJIMA WEATHER STATION
1952. Prompt report on the eruption of Myojinsho Reef in September 1952 (in Japanese).

HANZAWA, M.
1953. On the eddy diffusion of pumices ejected from Myojin Reef in the southern Sea of Japan. Rec. Oceanogr. Works Japan, N. S. *1* (1): 18–22.

HYDROGRAPHIC OFFICE OF JAPAN
1948. The results of oceanographical observations taken in the western part of the North Pacific Ocean during 1923–1929 (in Japanese). Kaisho-Jiho, No. 3: 1–15.
1952. The report presented by the Investigation Committee for the Cause of the KAIYO-MARU No. 5 Disaster (in Japanese).

LAMB, H.
1932. Hydrodynamics. 6th ed., Arts 238–240, pp. 384–394.

MUNK, W. H.
1949. Surf beats. Trans. Amer. geophys. Un., *30* (6): 849–854.

NAKANO, M.
1949. On the secondary undulations of tides caused by cyclonic storms (1st paper). Oceanogr. Mag., *1* (1): 13–32.

UNOKI, SANAE AND MASITO NAKANO.
1953. On the Cauchy-Poisson waves caused by the eruption of a submarine volcano (1st paper). Oceanogr. Mag., *4* (4): 119–141.

1953a. On the Cauchy-Poisson waves caused by the eruption of a submarine volcano (2nd paper). Oceanogr. Mag., *5* (1): 1–13.

YASUI, Z.

1940. On the effect of leeway upon a vessel (in Japanese). Umi to Sora (Sea and Sky), *20* (7): 177–181.

APPENDIX

Although these data and observations have no direct bearing on the disaster of the KAIYO-MARU No. 5, we have added them here for the record.

The CHIKUBU-MARU, a weather ship of the Central Meteorological Observatory of Japan, was navigating in waters near Myojinsho Reef from 15^h to 19^h on 21 September 1952 on her passage from Torishima to Tokyo, at which time her crew witnessed an eruption at Myojinsho Reef about $17^h\ 35^m$. Their observations on that occasion are noted herewith. Fig. 9 shows the positions of their stations, the numeral in brackets denoting the time of observation.

(1) APPEARANCE OF THE ERUPTION

15^h20^m; odour of sulphur noted about 22 nautical miles SSE from Myojinsho Reef.

15^h50^m; intense odour of sulphur noted about 17 nautical miles SSE from the Reef.

16^h10^m; column of white smoke trailing westward was seen on the horizon NNW from the ship, about 13 nautical miles from the Reef.

16^h22^m; from the sea surface at the foot of the column of white smoke, a column of black smoke shot upward to a height of about 200 m; this dispersed and turned white subsequently.

16^h30^m; on the sea surface, west of the ship, a stream of yellowish green sulphide spread SSW in the shape of a belt from the direction of Myojinsho Reef.

17^h35^m; column of deep black smoke belched upward from the steam and white smoke, and several seconds later a column of fire appeared.

17^h38^m; this same column of black smoke attained a height of more than 5000 m, and a large quantity of incandescent lava fell into the sea. The surface of the sea swelled up, and the diameter of this swollen portion increased to about 740 m almost instantly.

17^h40^m; volcanic ashes fell from the sky on the deck of the ship, which was then about 5000 m SE from the point of eruption; when these ashes struck the observers' cheeks, the men felt pain, and in the interest of safety, the ship retreated northeastward at full speed.

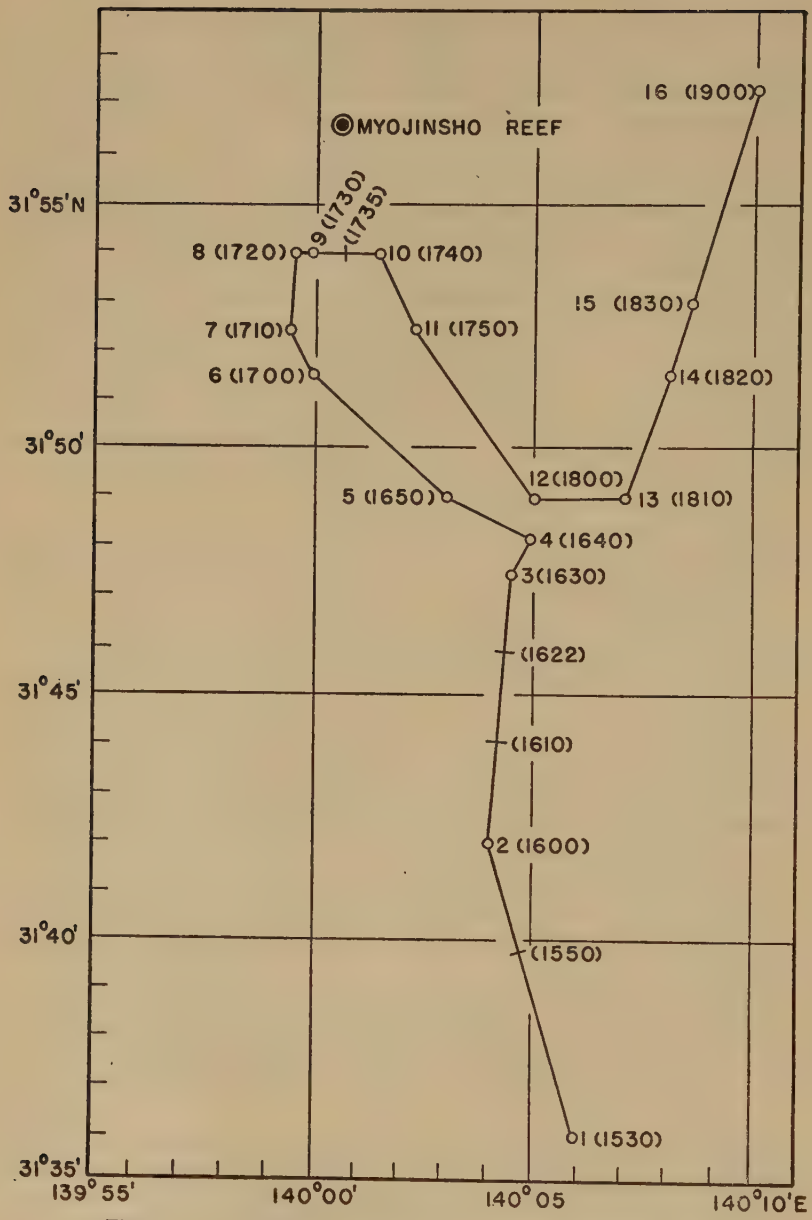

Figure 9. Observation stations occupied by the CHIKUBU-MARU.

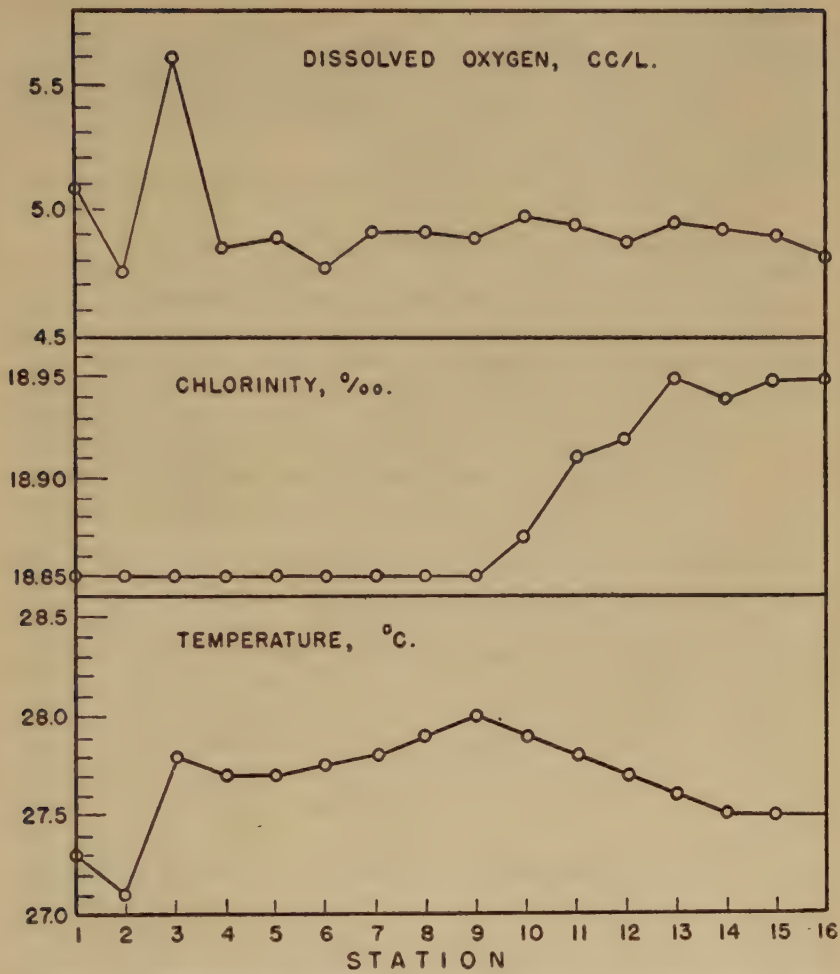

Figure 10. Dissolved oxygen, chlorinity and temperature of the surface water at each station occupied by the CHIKUBU-MARU.

(2) WATER TEMPERATURE, CHLORINITY AND DISSOLVED OXYGEN

Fig. 10 shows the temperature, chlorinity, and dissolved oxygen values of the surface water at each station. The water temperature at stations 6–11, close to Myojinsho Reef, was 27.8°, which is somewhat higher than the temperatures at more distant stations. Apparently this higher temperature was partly due to the heating of the water by various substances ejected from Myojinsho Reef which were carried southward by currents.

The chlorinity values for stations 1–9 are somewhat less than those for stations 13–16. The cause of this discrepancy is not clear at present, but a part of it may be explained qualitatively; possibly water of low salinity spurted from Myojinsho Reef together with other substances, flowed southward with the ocean current, and, by mixing, diluted the surface sea water.[8]

As for the distribution of the dissolved oxygen, no particular tendency is noted.

(3) Floating Mineral Substances and Plankton

Floating mineral substances and plankton organisms from each 100 cc sample of surface-water were examined by the following method. The catch in each water sample was concentrated into 2 cc with a centrifuge, and 0.5 cc of this sample was then examined through a microscope. Brown volcanic dust, presumably small fragments of pumices, were abundant in all samples; a small quantity of pyroxene crystals was also included. Heavier volcanic dusts probably sank rapidly. The quantity of floating mineral substances was greatest at stations 6–11, close to Myojinsho Reef, and least at eastern stations 12–16.

Furthermore, the quantity of plankton organisms was small, amounting to approximately 40 individuals per litre even in samples that were comparatively rich in population. The intercellular substances of organisms such as *Rhizosolenia calcar-avis*, *Coscinodiscus* sp., *Trichodesmium thiebauti* and *Pyrocystis pseudonoctiluca*, had disappeared completely. The scarcity of plankton in the surface water near Myojinsho Reef may have been caused by the injurious action of the eruptive efflux and the subsequent sinking of plankton to lower layers. However, the data are too scanty for definite conclusions.

[8] According to data from observers aboard the Tokyo College of Fisheries boat Shinyo-maru on 23 September, surface chlorinity of the sea adjacent southward of Myojinsho Reef was especially low; H. Niino, a member of the party, suggests that this may have been due to mixing of low salinity water which issued from Myojinsho Reef during its eruption with adjacent water.

ANALYSIS OF A HUGH M. SMITH OCEANOGRAPHIC SECTION FROM HONOLULU SOUTHWARD ACROSS THE EQUATOR

By

R. B. MONTGOMERY

Brown University[1] *and Woods Hole Oceanographic Institution*[2]

ABSTRACT

Observations from a line of stations made in February–March 1950 extending from 5° S to 21° N along meridian 158° W are analyzed, and the results are presented as distributions of sigma-*t*, salinity, oxygen, and phosphate in the vertical section. The method of analysis is partly new and is designed to achieve consistency among the several variables. This section is one of a number made in the central Pacific by the U. S. Fish and Wildlife Service.

Pacific Oceanic Fishery Investigations of the U. S. Fish and Wildlife Service executed during 1950–1952, from the research vessel HUGH M. SMITH, 365 serial oceanographic stations constituting 15 or more meridional sections across the equator in the central Pacific (Cromwell, 1953). The previous temperature-salinity sections crossing the equator in this region were obtained by the CHALLENGER (Wüst, 1929) and CARNEGIE (Sverdrup, et al., 1944), by Operation Crossroads (Barnes, et al., 1948) and by the ALBATROSS (Jerlov, 1953). It is noteworthy that more meridional sections have now been made in the central Pacific than in the equatorial Atlantic or Indian oceans. Cromwell (1953) has discussed the circulation in the central equatorial Pacific by using as examples two of the new sections (172° W January–February 1950, 158° W July–August 1950). The present paper depicts a third section (158° W February–March 1950).

Opportunity for the author to take part in the analysis of these data was arranged through the courtesy of Mr. O. E. Sette, Director, and Mr. Townsend Cromwell,[3] Oceanographer, Pacific Oceanic Fishery Investigations.

[1] Technical Report 5, Office of Naval Research contract N7onr-35811 (NR-083-050) with Brown University, Providence 12, R. I. The cost of producing Figs. 3–6 has been covered in part by this contract.

[2] Contribution No. 664 from the Woods Hole Oceanographic Institution, Woods Hole, Mass.

[3] Now at Scripps Institution of Oceanography, La Jolla, California.

When all of the observations collected so far can be studied together, further important conclusions about the structure and circulation of the ocean can be expected, but such study will be possible only when all of the individual sections have been analyzed. The present paper has the limited objective of giving a reasonably thorough pictorial analysis of a single section.

METHOD

The data for this section consist of bathythermograms and 23 serial stations made during the interval 18 February to 2 March 1950. The stations lie within 28 miles of the meridian 158° W, the northernmost station being 25 miles from Honolulu. Bathythermograph lowerings to a nominal depth of 900 feet were made at the start and finish of each station and at 10-mile intervals between stations. The stations, spaced 60 or 120 miles apart, include serial measurements of temperature and depth by reversing thermometer; the corresponding water samples were chemically measured for salinity, oxygen, and phosphate phosphorus.

The guiding principles of the analysis are (1) to use all of the data and achieve consistency among the several variables and (2) to present the results in such a way that the relations among the several fields are readily visible. In other words, the procedure is to avoid an independent analysis of each variable (temperature, salinity, . . .).

The vertical spacing of the serial observations is too coarse to reveal the structure of the thermocline, but the bathythermograms extend down past the maximum temperature gradient. A temperature-depth curve for each station has therefore been so drawn as not only to pass through the reversing-thermometer points but also to be similar in shape to the bathythermograms for the station, as illustrated in Fig. 1.

The following characteristic curves, also shown in Fig. 1, have been drawn for each station: temperature-salinity, temperature-oxygen, and temperature-phosphate. Each curve passes through the observed points for the station, but the interpolation between points is guided by consideration of observations from adjacent stations of the section and from other stations. (After preliminary drawing of all curves, the graph of each station was superposed on the graphs of the two adjacent stations, and its characteristic curves were adjusted to give as much continuity from station to station as was permitted by the observed points.)

Thus the common scale for the four station curves is temperature; these four curves were chosen because temperature is the only vari-

Figure 1. Depth, salinity, oxygen, and phosphate phosphorus against temperature at station 38, 3°02′N, 157°51′W, 23 February 1950. Observations by reversing thermometer and water bottle are represented by dots. One of the station's two bathythermograms is reproduced as the dashed line.

able observed continuously with depth. The temperature-depth curve and the three characteristic curves determine the continuous vertical distributions of salinity, oxygen, phosphate, and sigma-*t*.[4] The last is conveniently represented by sigma-*t* isopleths printed on the temperature-salinity diagram, as in Fig. 1.

It may be noted that only four such curves can be drawn independently. To draw in addition any of the other four vertical distributions or any of the other seven characteristic curves (temperature against sigma-*t*, oxygen against phosphate, etc.) is undesirable, because, to avoid inconsistency, each additional curve must laboriously be made to agree with those already drawn, and any subsequent adjustment of one curve involves the adjustment of one or more others.

[4] Sigma-*t* (in common use but regrettably nameless) for a point in the ocean is the excess, above one gram per milliliter, of the density of water of the same temperature and salinity but at a pressure of one atmosphere.

With all variables continuously specified for each station vertical, the next question is how best to represent the variables in two-dimensional fields for the vertical section. As with station curves, superfluous fields offer difficulty. Temperature, salinity, and sigma-*t* are interdependent, so representation of all three is undesirable because of the practical difficulty of drawing the three fields so that they agree everywhere. Two of the three and oxygen and phosphate remain to be depicted.

In order to make the relations among these four fields visible, they might all be superposed in one drawing if that were feasible, but experience indicates that no more than two fields can be adequately depicted in one drawing (except for the further addition of very simple fields). To depict all possible pairs combined from the four variables would require six drawings. It may suffice, however, if a particular variable can serve as an adequate reference, to present only the three drawings that depict the reference field in combination with each of the others.

As reference variable, temperature would have advantages, because it can be measured most easily and it can be measured continuously with depth. Sigma-*t*, however, is chosen as reference variable in the present paper. An important consideration influencing this choice is that sigma-*t* more than any other variable approaches a monotonic function of depth at any vertical and therefore has the simplest field.

With sigma-*t* already chosen, salinity is preferable to temperature as the other of these three to be represented. The reason for this choice is that sigma-*t* and temperature are so nearly parallel on a vertical section that the superposed fields are difficult to comprehend, while sigma-*t* and salinity can be superposed and remain clear.

The vertical section of sigma-*t* was constructed first. The serial observations of sigma-*t* were plotted, and the depths of each sigma-*t* isopleth at each station were plotted from the station curves. Instead of being drawn precisely through the points plotted from the station curves, the isopleths were smoothed somewhat but without violation of the observed points. The smoothing might have been achieved in an unobjectionable way by making reasonable adjustments in the station curves while keeping the vertical section consistent with the station curves.

To construct the salinity, oxygen, and phosphate fields, the serial observations and isopleth depths from station curves were plotted as for sigma-*t*. The isopleths were then drawn on a work sheet superposed on the sigma-*t* section. Some liberty was permitted in drawing the isopleths, particularly in allowing them to run more

nearly parallel with the isopleths of sigma-*t*, but again the observed points were not violated.

The sigma-*t* section in Fig. 2 extends down to 1700 m so as to include all observed points, but the vertical scale is too small to show the thermocline to advantage. Figs. 3-6 show the upper 500 m of the four fields on larger vertical scale. The distributions of salinity, oxygen, and phosphate below 500 m are omitted.

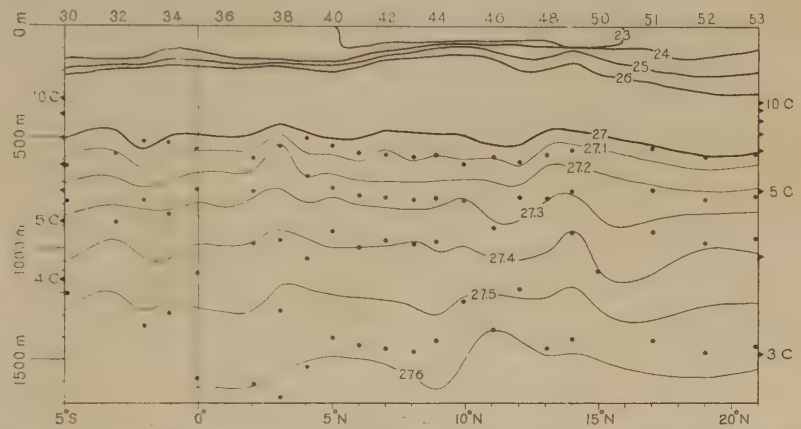

Figure 2. Sigma-*t* in grams per liter. Temperature at ends of section is shown by a tooth for each degree centigrade up to 10 C. Observation points below 500 m are shown by dots; those above 500 m appear in Fig. 3. Station numbers at top. Vertical exaggeration 927.

The field of sigma-*t* alone (Fig. 3) is included in addition to the minimum three drawings (Figs. 4–6). One practical advantage of this repetition is that some of the details of the thermocline shown in Fig. 3 could be omitted from Figs. 4–6.

Although the temperature field is not shown, a rough indication of temperature is provided by marking the depth of each whole degree centigrade at both ends of the section.

The bathythermograms between stations provide valuable information that can be incorporated in sigma-*t* sections. All isothermal layers from all bathythermograms were drawn as vertical lines on the work sheet. These vertical lines served as barriers forbidden to be crossed by the sigma-*t* isopleths, which therefore either avoid vertically isothermal regions altogether or traverse them vertically.

The thermocline on bathythermograms between stations should have been utilized also, but actually it was not. A suitable procedure would be to use all bathythermograms in constructing a temperature section, which would then serve as a guide on which the sigma-*t*

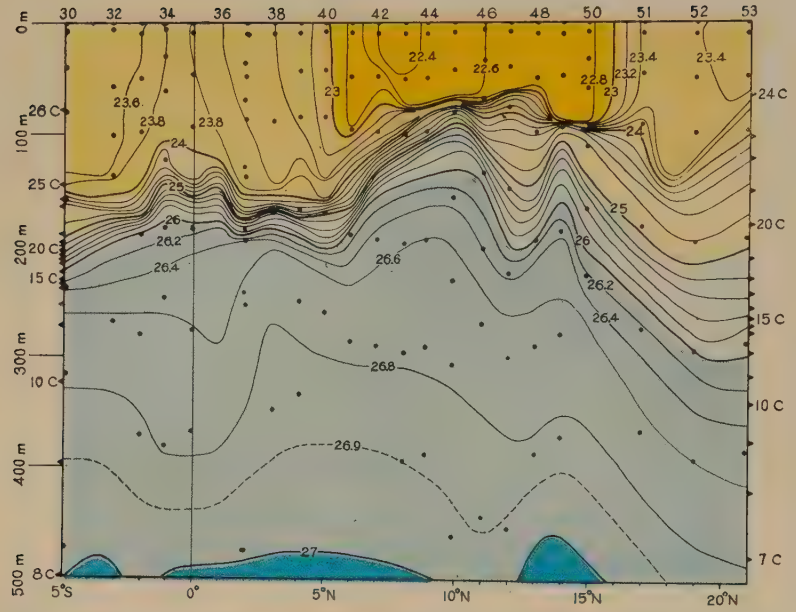

Figure 3. Sigma-*t* in grams per liter. Temperature at ends of section is shown by a tooth for each degree centigrade. Vertical exaggeration 4633.

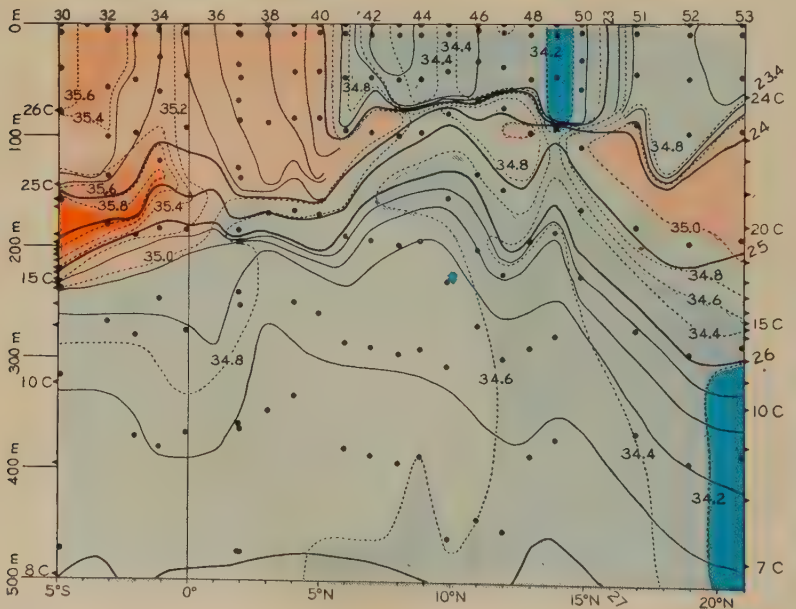

Figure 4. Salinity in per mille. Most of the sigma-*t* isopleths are repeated from Fig. 3 and are labeled at right in grams per liter.

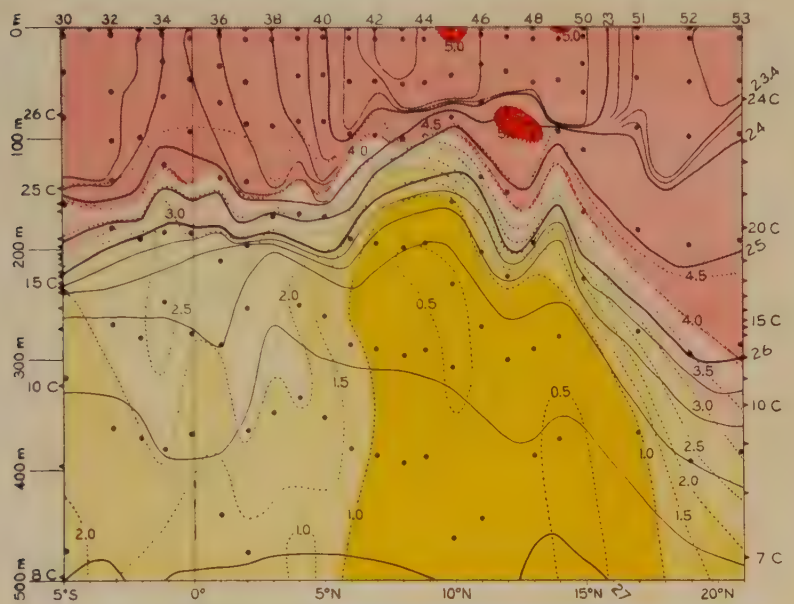

Figure 5. Oxygen in milliliters (NTP) per liter.

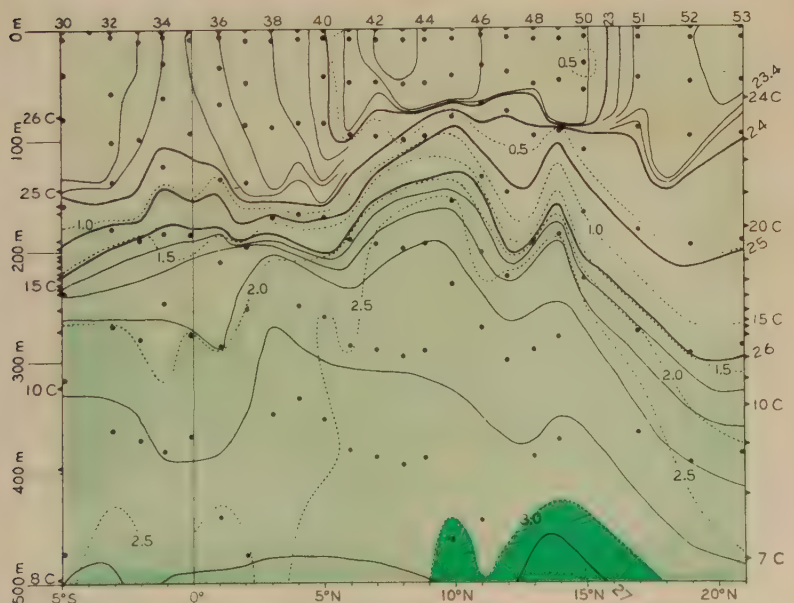

Figure 6. Phosphate phosphorus in microgram-atoms per liter.

section could be superposed while constructing the isopleths. This procedure would place the latitudes of maxima and minima in depth of sigma-*t* isopleths more precisely than they are shown in the present drawings.

DISCUSSION

It is clear from Fig. 3 that bathythermograms in conjunction with rather coarse vertical spacing of serial observations reveal much sharper density gradients and more detail than would the serial observations alone. The horizontal detail also would have been increased if the close spacing of the bathythermograms had been fully utilized. Furthermore, it is clear that, if the salinity, oxygen, and phosphate fields were constructed quite independently of the density field, they would come out markedly different from those in Figs. 3–6, and the four fields would be inconsistent.

Some features of the section may be mentioned, although the primary purpose has been accomplished by presenting the method and pictorial results of the analysis.

Typical of equatorial waters, there is great contrast between the high degree of homogeneity of the surface layer and the large gradients of the thermocline. Bathythermograms are essential for revealing the full magnitude of this contrast.

The sloping thermocline from 5° N to 10° N marks the zone of the Equatorial Countercurrent. The greatest density gradients occur in the upper part of the thermocline near the northern edge of the Countercurrent.

A trough at 12½° N and a ridge at 14° N in the sigma-*t* isopleths of the lower part of the thermocline mark an unusually large disturbance within the North Equatorial Current. At 14° N the layer containing the salinity maximum appears to be absent, as though pinched off, although the water samples are too widely spaced to determine the salinity distribution with certainty.

The salinity maximum in the thermocline south of the equator seems to stop abruptly near the equator. The presence of the maximum proves that there is no transfer of water between the surface layer and the water beneath the maximum. Where the maximum is absent, as it appears to be from 1° N to 5° N, this proof is lacking.

REFERENCES

Barnes, C. A., D. F. Bumpus, and John Lyman
1948. Ocean circulation in Marshall Islands area. Trans. Amer. geophys. Un., *29:* 871–876.

Cromwell, Townsend
1953. Circulation in a meridional plane in the central equatorial Pacific. J. mar. Res., *12:* 196–213.

Jerlov, N. G.
1953. Studies of the equatorial currents in the Pacific. Tellus, *5:* 308–314.

Sverdrup, H. U., F. M. Soule, J. A. Fleming, C. C. Ennis
1944. Scientific results of Cruise VII of the Carnegie during 1928–1929 under command of Captain J. P. Ault. Oceanography—I-A. Observations and results in physical oceanography. Publ. Carneg. Instn., *545:* 156 pp.

Wüst, Georg
1929. Schichtung und Tiefenzirkulation des Pazifischen Ozeans. Auf Grund zweier Längsschnitte. Veröff. Inst. Meeresk. Univ. Berl., N. F., A, 20: 64 pp.

THE STATISTICAL ANALYSIS OF A SEICHE RECORD

By

P. WHITTLE

Applied Mathematics Laboratory, New Zealand D.S.I.R.

ABSTRACT

The series analysed consists of 660 15 sec observations of the water level in a rock channel on the Wellington coast. Both correlogram and periodogram were employed in an attempt to isolate possible discrete components of the spectrum and to characterise the continuous component. Several trains of waves were found, some with phase and amplitude so remarkably stable that they could not be distinguished from sustained oscillations. The two main sets of waves were identified as being due to reflection at the open end of the channel and at the coast of an island parallel with the channel but some 15 chains outside it. The periods of the remaining waves (with one exception) appear to bear a simple numerical relation to the periods of these main trains, and it is suggested that the existence of these minor trains and the surprising permanence of one main train are due to a nonlinear phenomenon associated with the intermittent washing in of water at the top (shore) end of the channel. This mechanism is examined.

The reader is referred to the end of the section on Analysis and Results for a summary of the purely statistical findings.

INTRODUCTION

These data (Fig. 2, curve A) refer to a small seiche on the New Zealand coast. From one point of view they are of local interest only, but on the other hand some of the phenomena observed are of more general importance, since we find statistical evidence for a mixed spectrum and for a certain nonlinear mechanism. The whole question of water wave spectra is a present one. Claims made for the existence of genuine periodicities in ocean waves (Seiwell and Wadsworth, 1949) have been disputed (Pierson, 1952), and interesting theoretical possibilities for the natural occurrence of mixed spectra have been demonstrated (Ursell, 1952). These data, of course, have no direct bearing on the question of ocean waves, since they were not taken in the open sea.

The statistical methods employed appear to be of interest, since they are to some extent new in oceanography. In the Appendix, an attempt is made to explain the correct use of correlogram and periodogram and the conditions under which the application of one or the other or both is appropriate; this Appendix also constitutes in part a reply to a recent article by G. E. R. Deacon (1952).

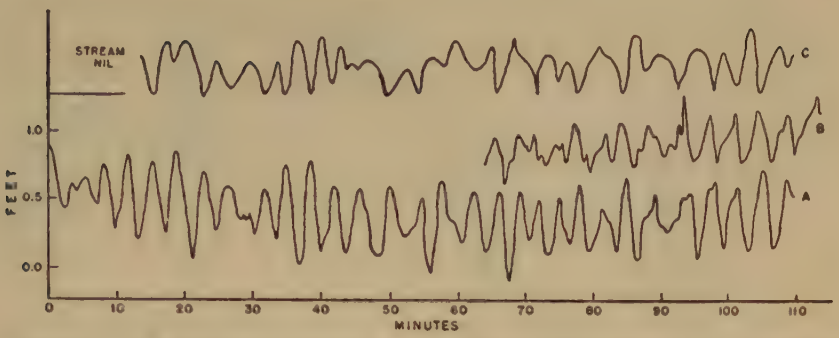

Figure 1. A. Water level in channel; B. Water level at mouth of channel; C. Streaming into top end of channel.

The observations were made by the staff of the Geophysical Observatory, N.Z.D.S.I.R., at a point adjoining Island Bay, Wellington. The site, a channel in the rocks some 5 ch long and about 1 ch wide, contains irregular depths up to about six feet at low water. It runs parallel to a line of breakers outside but is separated from them by a strip of rocks a chain or two wide; at the western (top) end there are two shallow connections with the breakers; the other end opens into the partially sheltered waters of the Bay. At low tide the surf

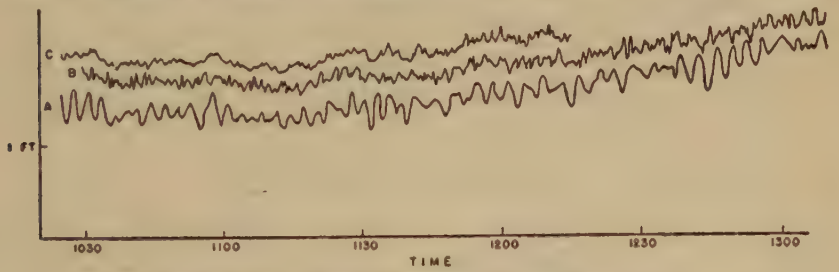

Figure 2. Water level at channel and neighboring points.

periods especially are well filtered out, even with moderate surf outside. Referring to Fig. 1, curve A represents readings at the top end of the channel, curve B represents readings made simultaneously at another point on the channel some 3 ch to the east, and curve C represents a rough estimate of the streaming of water from the western connections into the channel. Although this streaming has often been observed, it has not been noted in the reverse direction. In curve C it is seen that it ceases when the water level is highest and that it is at a maximum when the level is lowest.

In Fig. 2 we have a second set of readings taken at A, the channel; at B, a point on the eastern coast of Island Bay; and at C, a point on

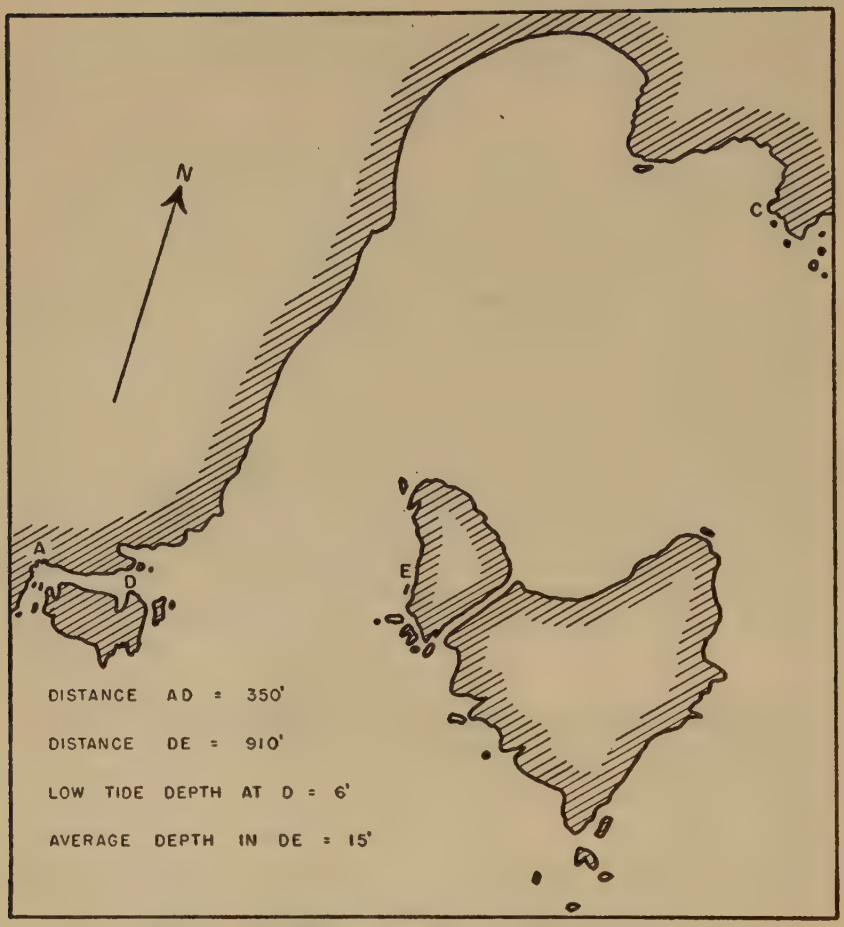

Figure 3. Map of Island Bay, Wellington, New Zealand.

the eastern side of Ohiro Bay; each distance, AB or AC, is about half a mile. The 3–4 minute oscillation which is prominent in curve A is absent from B and C, and therefore it would seen to be attributable to a seiche in the channel.

Although we shall be concerned with only Fig. 2, curve A, the other curves have been included to provide a background. Furthermore, we shall find use later for the observations on the flow into the top end of the channel.

Fig. 3, a map of the district, shows that the channel opens not directly into the sea but into a sound 15 chains wide which is bounded

by the concave shores of the mainland and island. The relevant distances and depths are indicated on the map.

The observations were taken at the turn of the tide so that its effect would be minimal. Nevertheless, it is obvious from Fig. 2 that a gradual trend is present, but this was satisfactorily eliminated by the fitting of a second order polynomial in time. If we denote the terms

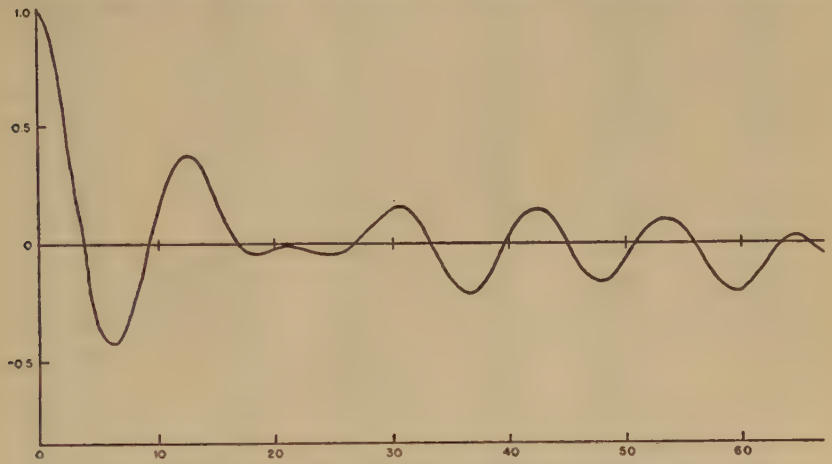

Figure 4. Correlogram of original deviations from trend.

of the series of deviations from trend by $x_1, x_2 \cdots x_n$, then the s^{th} autocovariance of this series is calculated from the formula

$$C_s = \sum_{t=1}^{n-s} \frac{(x_t - \bar{x})(x_{t+s} - \bar{x})}{(n - s)}, \tag{2.1}$$

where $\bar{x}$ is the arithmetic mean of the series and n the number of terms; in this case it is 660. The correlation coefficients, $r_s = C_s/C_o$, are tabulated in Table I, and their graph, the correlogram, is presented in Fig. 4.

A first estimate of the spectrum was obtained by Bartlett's method (Bartlett, 1948, 1950), i.e., by transforming the initial part of the correlogram (strictly, the "covariogram")

$$f_B(\omega) = \sum_{-\sigma}^{\sigma} \left(1 - \frac{|s|}{\sigma}\right) C_s \cos(\omega s). \tag{2.2}$$

Since the sampling variation of the covariances is quite small in the present case, a fairly high value of σ could be taken; the actual value used was 114. The full line in Fig. 5 gives the smoothed estimate of the spectrum thus obtained.

Table I. Correlation coefficients

s	$1000r_s$	s	$1000r_s$	s	$1000r_s$
1	889	41	70	81	−180
2	626	42	132	82	−184
3	285	43	149	83	−152
4	− 41	44	114	84	− 91
5	−289	45	39	85	− 17
6	−418	46	− 50	86	47
7	−421	47	−125	87	83
8	−315	48	−163	88	85
9	−140	49	−151	89	59
10	56	50	− 98	90	13
11	231	51	− 23	91	− 38
12	347	52	50	92	− 80
13	379	53	97	93	− 98
14	332	54	108	94	− 89
15	229	55	83	95	− 57
16	111	56	24	96	− 8
17	18	57	− 53	97	43
18	− 32	58	−130	98	84
19	− 39	59	−187	99	104
20	− 25	60	−207	100	100
21	− 11	61	−183	101	77
22	− 9	62	−128	102	50
23	− 22	63	− 59	103	32
24	− 35	64	0	104	36
25	− 44	65	29	105	69
26	− 36	66	23	106	116
27	− 7	67	− 10	107	157
28	45	68	− 53	108	174
29	100	69	− 85	109	161
30	145	70	− 94	110	124
31	165	71	− 81	111	172
32	144	72	− 53	112	15
33	81	73	− 11	113	− 26
34	− 12	74	33	114	− 40
35	−109	75	66		
36	−184	76	73		
37	−213	77	49		
38	−187	78	− 3		
39	−118	79	− 72		
40	− 23	80	−137		

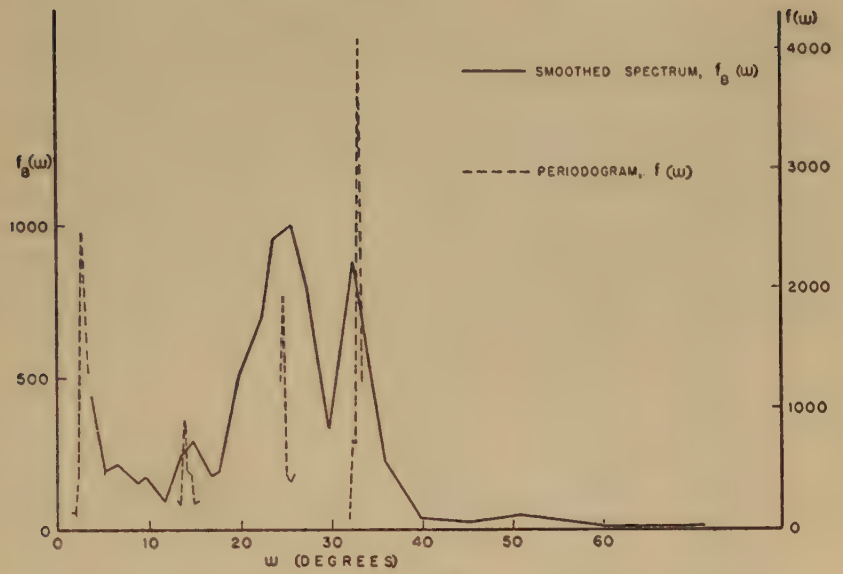

Figure 5.

The preliminary analysis up to this stage was performed by I. D. Dick while he held the post of director of the Applied Mathematics Laboratory.

When the various possible periodicities are investigated we require the direct estimate of the spectrum provided by the periodogram

$$f(\omega) = \frac{1}{n}\left[(\Sigma x_t \sin \omega t)^2 + (\Sigma x_t \cos \omega t)^2\right]$$

$$= \sum_{-n}^{n}\left(1 - \frac{|s|}{n}\right) C_s \cos(\omega s). \qquad (2.3)$$

Calculation of the complete periodogram would be arduous, particularly since the rapid variation of $f(\omega)$ means that about $n/2 = 330$ ordinates would have to be calculated in order to obtain a complete picture. Therefore, since the estimate $f_B(\omega)$ will indicate all but the feeblest periodicities, it will be sufficient to calculate $f(\omega)$ in the neighbourhood of the maxima of $f_B(\omega)$. The most obvious maxima of $f_B(\omega)$ are around $\omega = 2°$, $14°$, $25°$ and $33°$, and the values of $f(\omega)$ in the neighbourhood of these points are tabulated in Table II (see also the thin line in Fig. 5). The unit of angle taken was one millicycle, or $0.36°$. By comparing this with the required minimum value of $360/660 = 0.55°$, we see that there is sufficiently dense covering.

Table II. Periodogram ordinates

ω (*milli-cycles*)	ω (*degrees*)	$f(\omega)$	$\hat{\omega}$ (*degrees*)	$\hat{f}(\omega)$
5	1.80	165		
6	2.16	140		
7	2.52	513		
8	2.88	2608	2.927	2635
9	3.24	1359		
37	13.32	260		
38	13.68	219		
39	14.04	920	14.083	928
40	14.40	485		
41	14.76	464		
42	15.12	156		
43	15.48	174		
68	24.48	1127		
69	24.84	1956	24.790	1977
70	25.20	504		
71	25.56	362		
72	25.92	469		
89	32.04	100		
90	32.40	735		
91	32.76	731		
92	33.12	4092	33.134	4097
93	33.48	1236		

The values obtained were interpolated parabolically in the hope of improving the estimates of the positions and sizes of the maxima of $f(\omega)$; these interpolated values, distinguished by a circumflex, are given in the last two columns of table II.

The further course of the analysis is described in the following section, and readers interested in the statistical side are advised to read the Appendix concurrently.

ANALYSIS AND RESULTS

A start in the analysis is provided by an examination of the correlogram and smoothed spectrum (Figs. 4, 5). In the analysis it is seen that the periods of the waves are of more interest than their frequencies, so for convenience the smoothed spectrum is replotted in Fig. 6 as a function of period, T. [Of course the curve thus obtained has no longer the interpretation of a frequency curve, as have $f(\omega)$ and $f_B(\omega)$.]

The oscillations in the correlogram damp away until about lag 30, after which they maintain a fairly constant amplitude. A period of

about 11 units (the unit of time being the 15 sec observation interval) is evident in the tail of the correlogram, although the oscillation is evidently not a simple one.

Turning to the spectrum, we note two strong peaks that correspond to periods of about 11 and 14, the former being narrow and well defined, the second being considerably broader. Subsidiary peaks are also evident for $T = 25$ and 36, and there is a faint suggestion of a rise between 48 and 50. This rise is little more than a slight increase in curvature, and it would never have been noticed had it not fitted into the rather intriguing pattern: $25 = 11 + 14$, $36 = 2(11) + 14$, and $48 \approx 3(11) + 14$. This is the simple numerical relation men-

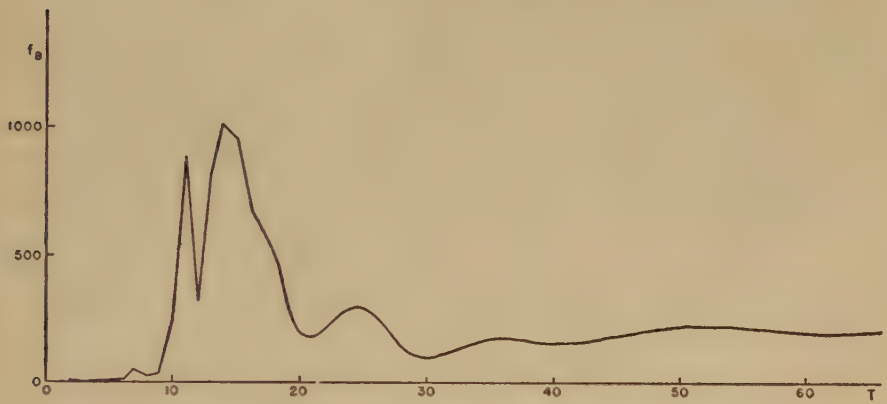

Figure 6. The smoothed spectrum as a function of period.

tioned in the ABSTRACT. Commonly terms corresponding to sums, differences and multiples of *frequencies* occur, but something analogous for *periods* is distinctly more unusual. The phenomenon, if real, recalls the subharmonic response effects of nonlinear mechanics and suggests that there may be a nonlinear mechanism at work.

Finally, we note a rise at the extreme low frequency end of the spectrum which requires investigation. This region of the spectrum, and those around $T = 11$, 14 and 25 were thus "explored" with the help of the periodogram, as described in the preceding section.

An attempt to explain the observed series as being simply generated by an autoregression fails. (The main assumption of such an approach is that the spectrum is completely continuous.) Fitting autoregressions of order $s = 1, 2, 3 \cdots$ and using formula (A.11) to calculate the corresponding residual variances v, the following results are obtained:

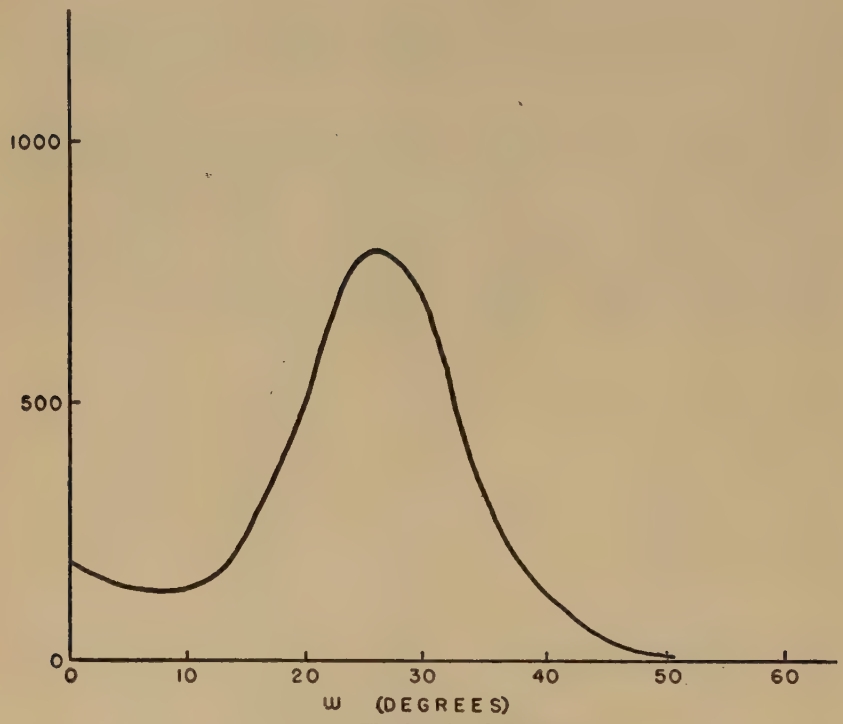

Figure 7. The first fitted spectrum.

s	v	ψ^2	P
0	99.011		
1	20.761	1031.2	<0.0001
2	8.010	628.7	<0.0001
3	7.864	12.5	0.001
4	7.624	20.2	<0.0001
5	7.617	0.6	0.47
6	7.602	1.4	0.25
7	7.576	2.0	0.18
8	7.537	3.3	0.07
9	7.528	0.6	0.47

The third column gives the value of the ψ^2 statistic obtained by comparison of the autoregressions of lags s and $s - 1$ (see A.13), while the figure in the last column gives the significance of the statistic and hence the s^{th} lag term. We see that it is the first four terms which make all of the contribution to the fit and that nothing is gained by

including higher lags. Estimating the coefficients of a fourth order autoregression by (A.9) we obtain the fitted scheme

$$x_t - 1.502x_{t-1} + 0.468x_{t-2} + 0.395x_{t-3} - 0.175x_{t-4} = \varepsilon_t, \qquad (3.1)$$

whose spectrum (calculated from A.7) is shown in Fig. 7.

Agreement with observation is poor; the dip between the two maxima at 11 and 14, which is so characteristic of the observed spectrum, is completely absent. An attempt at improvement was made by fitting all lags up to order 15, but this had an insignificant effect. (The trial was worthwhile, however, since high order lags can often be expected when one deals with mechanisms in which reflection plays a part, and they have been known to occur even in econometric series.)

The hypothesis of a purely continuous spectrum thus seems untenable, and we are forced to the conclusion that wave trains which possess genuine periodicity are present or that there is at least another type of periodicity from that associated with a simple autoregression. We then test the various periodogram peaks, starting with that which bears the greatest ratio to its presumed theoretical value. This is $f(\omega) = 2635$, at $\omega = 2.927°$, or $T = 123$. The theoretical spectrum, $F(\omega)$, is that calculated for scheme (3.1), since this scheme constitutes for the moment our null hypothesis. We have (cf. A.7)

$$F(2.927°) = \frac{7.624}{|1 - 1.502e^{i\omega} + \cdots - 0.175e^{4i\omega}|^2} \qquad (\omega = 2.927°).$$

Thus (cf. A.18) the test statistic g has a value

$$g = \frac{2635}{(191)(330)} = 0.0418$$

whose significance is (cf. A.19)

$$P(g) \approx 330(1 - 0.0418)^{330} = 0.00025.$$

The generally accepted significance level is $P = 0.05$, hence the observed periodogram peak $f = 2635$ is significant, and we conclude that a genuine wave train of period $T = 123 = 30.75$ minutes is present. Now, before we consider the remaining possibilities, we should subtract this component from the series and recalculate the estimate of $F(\omega)$, the continuous component of the spectrum. However, this recalculation has relatively little effect on the central part of the spectrum, hence we can conveniently use the existing $F(\omega)$ to test the next proportionally greatest peak, at $\omega = 33.134°$ $(T = 10.87)$. An analogous calculation to the previous one yields the following quantities:

f	F	g	P
4097	442	0.0281	0.029

The peak is significant. Actually, our test has been conservative, and the significance of the ordinate is far greater than that indicated, for two reasons. First, the spectrum calculated from (3.1) is a sort of envelope to the observed spectrum, and for $\omega > 25°(T < 14)$ it has ordinates of anything up to five times those of what now appears to be the true continuous part of the spectrum; so the apparent g is correspondingly smaller. Furthermore, the probability (A.19) is calculated on the assumption that we have chosen for testing the most significant remaining ordinate in the whole periodogram. It is fairly certain that we have in fact done so, but actually this was not our procedure, since only a small selected portion of the periodogram was calculated. For this reason alone, the significance of the ordinate is greater than that indicated by (A.19).

Be this as it may, the presence of trains with $T = 10.87$ and 123 has been established, and before we test the remaining possibilities we must recalculate our estimate of $F(\omega)$. Applying equation (A.17), we find that the modified autocovariances C_s' will be related to the original C_s's by

$$C_s' = C_s - 7.98 \cos (2.927s)° - 12.42 \cos (33.134s)°. \quad (3.2)$$

Calculating the first few values, we have

s	C_s'	s	C_s'
0	78.7	6	−37.2
1	69.7	7	−41.5
2	49.1	8	−37.3
3	22.4	9	−26.8
4	−3.3	10	−12.3
5	−24.3		

A more complete picture of this correlogram is provided in Fig. 8. Fitting autoregressions of successively increasing order, as before, we obtain the following results:

s	v	ψ^2	P
0	78.700		
1	16.985	1010.5	<0.0001
2	7.619	527.4	<0.0001
3	7.264	31.3	<0.0001
4	7.166	8.9	0.006
5	7.018	13.7	0.0005
6	7.016	0.2	0.65

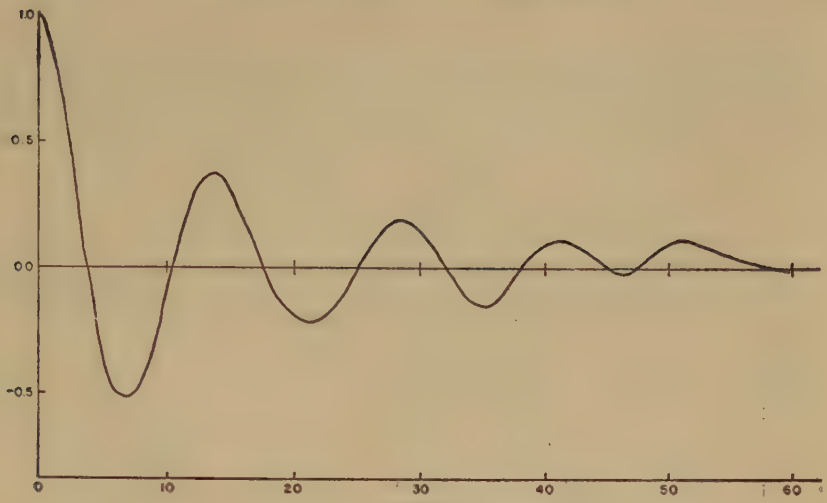

Figure 8.

A fifth order scheme is apparently sufficient; we find the estimated scheme to be

$$y_t - 1.425y_{t-1} + 0.416y_{t-2} + 0.429y_{t-3} - 0.319y_{t-4} + 0.144y_{t-5} = \epsilon_t. \quad (3.3)$$

Now we can rigorously test the peaks at $\omega = 14.083°$ and $42.790°$ ($T = 25.56$ and 14.52). The figures corresponding to those of the previous calculations are:

	T	f	F	g	P
14.083	25.56	928	255	0.0110	>0.1
24.790	14.52	1977	902	0.0066	>0.1

Neither of the peaks is significant, so there is no point in continuing with the smaller peaks at $T = 35$, etc.

Since all of the detectable harmonic components have now been extracted, scheme (3.3) gives the autoregressive representation of the component of the observed series corresponding to the continuous component of the spectrum, y_t. The corresponding spectrum is illustrated in Fig. 9. The curve evidently agrees fairly well with what we would now regard as the continuous component of the observed spectrum in Fig. 5. The peaks at $T = 25, 36 \cdots$ are not evident, but this need not necessarily shake our faith in their reality, since a low order scheme such as (3.3) will reproduce only the broader spectral peaks.

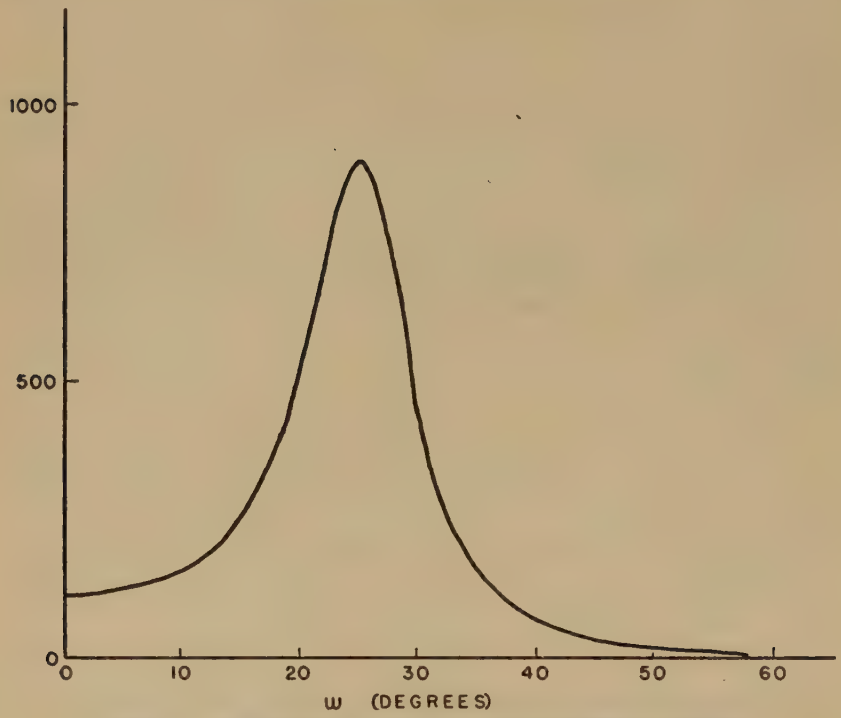

Figure 9. Fitted spectrum of the purely nondeterministic component.

Summing up, then, the following facts have been observed and require explanation:

(1) Sustained waves exist of periods 123 and 10.87 units (1845 and 163 secs) with respective amplitudes 3.00 and 4.99.

(2) The residual component can be expressed largely by the autoregression (3.3), whose energy (see Fig. 9) is mostly accounted for by an impermanent oscillation of approximate period 14 units (210 secs).

(3) The smoothed empirical spectrum definitely indicates subsidiary oscillations of periods 25 and 36 units. These oscillations, not of permanent type, are too regular to be explicable by a simple scheme of type (3.3).

EXAMINATION OF RESULTS

The wave trains of period 10.87 and 14 are readily identified as being due to reflection at the island coast and at the open end of the channel respectively. To see this, we note that the velocity of propagation of tidal waves in water of depth h is

$$V = \sqrt{gh}, \tag{4.1}$$

where g is the acceleration due to gravity. Thus the time of traverse in a channel of length L whose depth increases linearly from 0 to H is approximately

$$\tau = \int_0^L \frac{dx}{\sqrt{gh}} = \sqrt{\frac{L}{Hg}} \int_0^L \frac{dx}{\sqrt{x}} = \frac{2L}{\sqrt{Hg}}, \tag{4.2}$$

and the period of the standing wave produced by reflection at the open end (depth H) of the channel will be

$$T = 4\tau = \frac{8L}{\sqrt{gH}}. \tag{4.3}$$

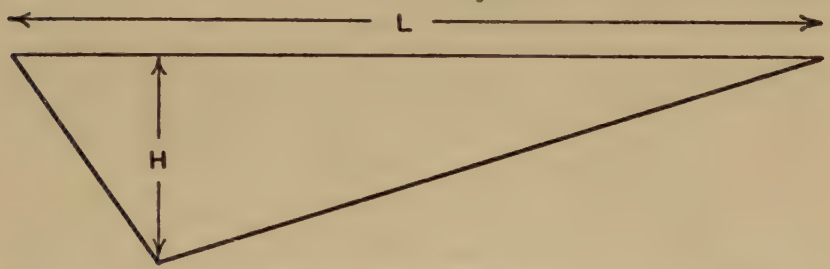

Figure 10. The idealised sea bed.

In our case, we know that the channel has an approximate length of 350 feet and a maximum depth of 6 feet. Assuming that the depth increases linearly, and setting these values in (4.3), we find $T = 202$ secs. This compares well with the observed value of 14 units, or 210 secs.

To calculate the time of traverse to the island, let us assume that the depth increases linearly from each shore to a point of maximum depth H (see Fig. 10). If L now denotes the distance of the island from the top end of the channel, formula (4.2) will still hold, and the period of the standing wave produced by reflection at the island will be

$$T = 2\tau = \frac{4L}{\sqrt{gH}}. \tag{4.4}$$

We know that $L = 1260$ feet, and we shall put $H = 30$ feet, since the average depth in the sound is 15 feet. These values lead to a value of T of 163 secs, which is in precise agreement with the observed value $T = (10.87)(15) = 163$ secs. The good agreement is coincidental and quite undeserved, since formula (4.4) is but an approximation, and the figures for the depths of channel and sound are of the roughest.

This interpretation is also in accordance with the character of the waves; namely, that a wave corresponding to $T = 14$ is fairly diffuse and covers a broadish band of frequencies, while that corresponding to $T = 10.87$ has a well defined period with stable amplitude and phase. We should expect that reflection from the end of the channel would be far from perfect, particularly since the transition from channel to open sea is not the radically discontinuous one postulated in the textbooks. Thus the reflected wave would be smaller in amplitude than the incidental one, and the standing waves in the channel would damp away in a few minutes were it not for the stray energy making its way in from the open sea in the form of chance surges. However, the fact that the wave is dependent upon outside "noise" for its maintenance means that it cannot hold a stable amplitude and phase, and therefore it will not exhibit a pure frequency.

On the other hand, reflection from the island should be efficient, particularly since a small bay on the island coast forms an almost ideal concave reflector directed on the channel mouth! Even so, it is surprising that the standing wave system can maintain its regularity for so long a period as 2½ hours, roughly 60 cycles.

The analysis of the previous section has indicated a relatively sustained wave of period 123 units or 30.75 minutes. We shall not attempt to explain this component, since it almost certainly is not associated with the seiche. The length of its period precludes this, and furthermore the wave appears in records B and C of Fig. 2. which were taken half a mile from the channel. Of course the wave need not be perfectly sustained, since the record contained only five complete cycles.

It has been suggested by R. M. Williams that the remarkable permanence of the oscillation ($T = 10.87$) may be due in part to the intermittent washing in of water at the top end of the channel. Since the flow is largely regulated by the height of water in the channel and hence by existing oscillations, it may be expected that stimulation of this sort would not broaden the natural response frequencies of the channel etc. as much as would stimulation by completely random surges. (As noted in the INTRODUCTION, the flow is always inwards, never outwards, and from the local point of view it is therefore a nonlinear effect. It is well known [see Andronow & Chaikin, 1937] that unforced oscillations which are subject to damping can be maintained only by a nonlinear mechanism, the classic example being the thermionic valve.) It would be interesting to see if this mechanism could possibly explain the periods $T = 25, 36 \cdots$.

Now we shall briefly examine a drastically simplified model of the

mechanism. Suppose that the water level x_t (t continuous) at the top of the channel is governed by the two equations

$$\begin{aligned} L(x_t) &= O \qquad (x_t \geqslant h) \\ L(x_t) &= K \qquad (x_t < h). \end{aligned} \tag{4.5}$$

Here L is a linear operator in t and K a constant that accounts for the flow when the water falls below the critical level h. For concreteness we shall assume that L is a differential operator of order p with constant coefficients

$$L = (D - \alpha_1)(D - \alpha_2) \cdots (D - \alpha_p) \tag{4.6}$$
$$D = \frac{\partial}{\partial t}, \qquad |\alpha| < 1,$$

although the subsequent argument is directly generalisable (to, for example, the case of a difference-differential operator).

We shall define the vectors

$$X_t = \begin{pmatrix} x_t \\ Dx_t \\ D^2x_t \\ \vdots \\ D^{p-1}x_t \end{pmatrix} \qquad P = \begin{pmatrix} \dfrac{K}{\alpha_1\alpha_2 \cdots \alpha_p} \\ \vdots \\ \vdots \\ \vdots \\ \vdots \end{pmatrix} \tag{4.7}$$

and the matrices

$$A = \begin{pmatrix} 1 & 1 & \cdots & 1 \\ \alpha_1 & \alpha_2 & \cdots & \alpha_p \\ \cdots & \cdots & \cdots & \cdots \\ \alpha_1^{p-1} & \alpha_2^{p-1} & \cdots & \alpha_p^{p-1} \end{pmatrix} \qquad \Lambda_t = \begin{pmatrix} e^{\alpha_1 t} & \cdot & \cdots & \cdot \\ \cdot & e^{\alpha_2 t} & \cdots & \cdot \\ \cdots & \cdots & \cdots & \cdots \\ \cdot & \cdot & \cdots & e^{\alpha_p t} \end{pmatrix} \tag{4.8}$$

$$F_t = A\Lambda_t A^{-1}.$$

Further, let us denote the instants of time at which x_t crosses $x = h$ from below by t_{2r}. (r integral) and from above by t_{2r-1}. By piecewise solution of (4.5), we find that the particular integral is

$$\begin{aligned} X_t &= [F_{t-t_{2r}} - F_{t-t_{2r-1}} + F_{t-t_{2r-2}} - \cdots]P \qquad (t_{2r} \leqslant t \leqslant t_{2r+1}) \\ X_t &= [I - F_{t-t_{2r+1}} + F_{t-t_{2r}} - \cdots]P \qquad (t_{2r+1} \leqslant t \leqslant t_{2r+2}) \end{aligned} \tag{4.9}$$

Now, it is x_t which is of interest, not its derivatives, so we shall suppose that

$$F_t P = \begin{pmatrix} \sum_\nu C_\nu e^{\alpha_\nu t} \\ \vdots \end{pmatrix}, \tag{4.10}$$

so that corresponding to (4.9)

$$x_t = \sum_\nu C_\nu [e^{\alpha_\nu (t-t_{2r})} - e^{\alpha_\nu (t-t_{2r-1})} + \cdots] \qquad (t_{2r} \leqslant t \leqslant t_{2r+1})$$

$$x_t = \sum_\nu C_\nu [1 - e^{\alpha_\nu (t-t_{2r+1})}) + \cdots] \qquad (t_{2r+1} \leqslant t \leqslant t_{2r+2}) \,. \tag{4.11}$$

Performing a Fourier analysis of the variable x_t in order to obtain an indication of the frequency ranges in which the energy of oscillation is concentrated, we find from (4.11) that

$$Y(\omega) = \int_{-\infty}^{\infty} e^{i\omega t} x_t dt = \left(\sum_\nu \frac{C_\nu \alpha_\nu}{\alpha_\nu + i\omega} \right) \left(\sum_\nu \frac{e^{i\omega t_{2r}} - e^{i\omega t_{2r-1}}}{i\omega} \right), \tag{4.12}$$

so that the spectrum is

$$|Y(\omega)|^2 = \left| \sum_\nu \frac{C_\nu \alpha_\nu}{\alpha_\nu + i\omega} \right|^2 \left| \sum_\nu \frac{e^{i\omega t_{2r}} - i\omega t_{2r+1}}{i\omega} \right|^2. \tag{4.13}$$

In our case $t_{2r+1} \approx t_{2r}$, since the water falls below the critical level almost as soon as it reaches it (see Fig. 1, curve C). Writing $t_{2r+1} - t_{2r} = \Delta t_{2r}$, we have

$$|Y(\omega)|^2 \approx \left| \sum_\nu \frac{C_\nu \alpha_\nu}{\alpha_\nu + i\omega} \right|^2 \left| \sum_\nu e^{i\omega t} \Delta t_{2r} \right|^2. \tag{4.14}$$

The first factor in (4.13) and (4.14) simply represents the characteristic response of L, while the second factor reflects the essential nonlinearity of the scheme. We see from (4.14) that it is a function of the *recurrence instants* t_{2r}, the instants at which x_t reaches and leaves the critical level, the line of discontinuity, $x = h$. A deeper study of the process thus involves a study of these recurrence times (the intervals between the recurrence instants). This is difficult, and therefore we shall complete the consideration of the phenomenon in a semiempirical manner.

First, it is natural to enquire as to what kind of recurrence times were observed. The only record of these is provided in Fig. 1, curve C. Upon measuring the intervals between the instants of zero flow, we obtain the following observations:

30.4 36.8 12.0 15.2 44.8 19.2 46.4 24.0 24.0 25.6 33.6 22.4 25.6

In general, 13 observations can tell us little, but in this case we do receive one valuable pointer. Upon constructing the histogram of the observations (Fig. 11) we observe a distinct clustering around the value $\tau = 25$. Observations are also grouped in pairs at $\tau = 32$ and 46. This is significant, in the light of what we have already observed. It is suggested that the observed periods of $T = 25, 36 \cdots$ may be associated with the grouping of the recurrence times around the values $\tau = 25, 32 \cdots$. We shall conclude by showing in simple fashion that one can reasonably expect the recurrence times to have just these values.

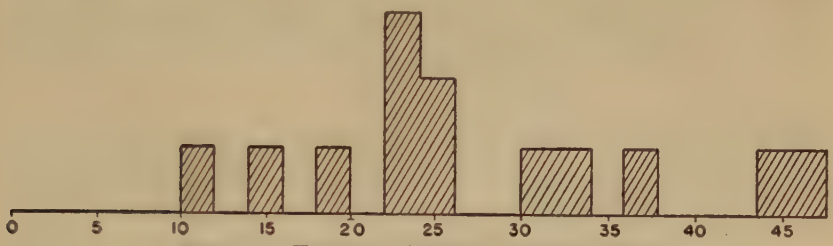

Figure 11. Histogram of observed recurrence times.

Let us suppose that the water is still and level everywhere except at the top of the channel, where there is a momentary accumulation, Let this accumulation of water travel down the channel in a surge, which will be partially reflected at the channel mouth and at the island. These partial reflections will gradually disperse the energy of the surge, but now and again several subsurges will combine to produce a reflected surge of height comparable to the first. If such a major reflected surge arises at time τ after the release of the original surge, then we can reasonably expect that recurrence times τ will occur in the case we have been considering throughout the paper, when the play of waves in the water has reached its stationary state.

Suppose then that the original surge has unit energy, that a fraction k of the energy of any disturbance leaving the channel is reflected back at the mouth, that any disturbance incident on the island is totally reflected, and that any disturbance propagated from the island to the channel is totally accepted. We know that it takes roughly $14/4 = 3.5$ units of time to traverse the channel and $11/2 = 5.5$ units of time to reach the island from the channel top. Thus, 7 units after the release of the surge, a surge of energy k (negative amplitude) will return from the end of the channel, and after 11 units a surge of energy $1 - k$ and positive amplitude will return from the island. In general, the amount of energy returning at time τ and the sign of the corresponding

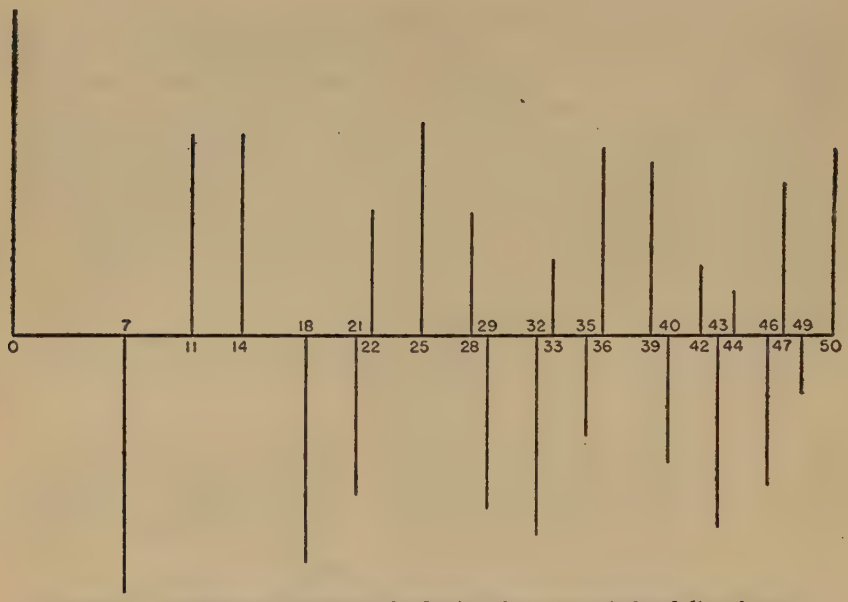

Figure 12. Characteristic response of reflecting planes to an isolated disturbance.

amplitude will be given by the coefficient of u^τ in the Taylor expansion of

$$(1 + ku^7 - (1 - k)u^{11})^{-1}. \tag{4.15}$$

[In effect we are constructing the transient response, or Green function, for the system of three reflecting surfaces shore/channel mouth/island; (4.15) is its power transform.]

Fig. 12 is a graph of the square roots of these coefficients, preserving sign, for the value $k = 0.62$ [a plausible value, deduced from the damping of the appropriate roots of the indicial equation for autoregression (3.3)]. The root is taken because the amplitude of a surge is proportional to the square root of its energy, and it is amplitudes in which we are interested. First we notice that the maximum reflected surge actually occurs at $\tau = 25$ (due to the coincidence of three distinct subsurges) when the amplitude is 0.66 of that of the original disturbance. Large reflections also occur for $\tau = 11$, 14, 36 and 50, taken in order of decreasing magnitude. Few recurrence times smaller than 25 were actually observed, but many explanations could be advanced to account for this.

The actual situation must be far more complicated, but the above argument probably gives some qualitative support to the suggested explanation for the spectral peaks at $T = 25$, 36 and 48.

It is a pleasure to acknowledge the benefit of discussions with Mr. N. Barber, Mr. I. D. Dick, Dr. R. M. Williams, and Mr. R. A. Wooding of the N.Z.D.S.I.R. Thanks are also due Mr. E. W. Jones, who planned and directed the punched card computations.

APPENDIX

Suppose that the series of observations has a theoretical power spectrum $F(\omega)$ when the water surface is measured about its mean level. Suppose further for the moment that this spectrum is purely continuous, so that the total wave power in the range of angular frequency (ω_1, ω_2) may be written simply:

$$\int_{\omega_1}^{\omega_2} F(\omega)d\omega \,. \tag{A.1}$$

Now, the fact that the observations are made at discrete intervals has the consequence that not all waves which occur will appear with their correct frequency (the "aliasing" effect; see Pierson, 1952). In fact, if the interval of observation is taken as time unit, then a harmonic wave of angular frequency $(2\pi s + \omega)$ (s integral, $\omega < 2\pi$) will appear to have frequency ω. Thus we need consider only $F(\omega)$ for the interval $(0, 2\pi)$. Further, a wave of frequency $(2\pi - \omega)$ will also appear to have frequency ω, so that $F(\omega) = F(2\pi - \omega)$, and all information conveyed by $F(\omega)$ is contained in the interval $(0, \pi)$. It is convenient, however, to consider $F(\omega)$ for the full interval $(0, 2\pi)$.

This aliasing effect means that all waves for which $\omega > \pi$ or $T < 2$ are misread. In the present case, then, all waves of period less than 30 secs will not be observed as such. However, the observer stated that, on the particular day considered, the change of level in the channel was so slow that the observations could be regarded as providing a continuous record. That is, the amount of power in the range $T < 2$ was negligible, so that the difference between $F(\omega)$ and the theoretical power spectrum of the continuous record was also negligible.

Now, the periodogram (2.3) provides a direct estimate of the power spectrum, but it is well known that this estimate, for many purposes is almost useless due to its poor sampling properties. Various methods of smoothing the periodogram have been suggested (Bartlett, 1948; Daniell, 1946; Grenander, 1951), Bartlett's proposal being particularly appealing and useful, at least when the spectrum is continuous.

Suppose that we do not need a direct estimate of $F(\omega)$ and that we have advanced so far that we can postulate a functional form for $F(\omega)$, so that it is merely a matter of evaluating the various constants of the function ("estimating the parameters of the model," in statistical

parlance). It has been shown (Whittle, 1952a, c) that estimation on the least square criterion requires that we minimise

$$L = \frac{1}{2\pi}\int_0^{2\pi}\left[\log F(\omega) + \frac{f(\omega)}{F(\omega)}\right]d\omega \tag{A.2}$$

with respect to the various parameters.

We obtain a more convenient form for L if we express it in terms of the correlogram instead of the periodogram, as in (A.2). We know from (2.3) that

$$f(\omega) = \sum_{-n}^{n}\left(1 - \frac{|s|}{n}\right)C_s \cos(\omega s)\,. \tag{A.3}$$

Now, if $[F(\omega)]^{-1}$ has the Fourier expansion

$$[F(\omega)]^{-1} = \sum_s c_s e^{i\omega s} \tag{A.4}$$

[for which we note that $c_s = c_{-s}$, since $F(\omega) = F(2\pi - \omega)$], then (A.2) may be written

$$\begin{aligned} L &= \frac{1}{2\pi}\int_0^{2\pi}\log F d\omega + \sum_{s=-n}^{n}\left(1 - \frac{|s|}{n}\right)c_s C_s \\ &\approx \frac{1}{2\pi}\int_0^{2\pi}\log F d\omega + \sum_{-\infty}^{\infty} c_s C_s\,. \end{aligned} \tag{A.5}$$

In most cases the c's converge quite rapidly as s becomes larger in absolute value, so that it is sufficient to consider the first few terms of the sum in (A.5), usually between 5 and 15. That is, *when fitting a scheme with continuous spectrum we need consider only the first few autocovariances, so that the correlogram is the appropriate tool.* This does not rule out the periodogram completely, since a smoothed periodogram may be very useful in helping to form our hypothesis in the initial stages, which may be particulary the case in oceanographic work. Furthermore, we shall see later that the periodogram is the appropriate tool when dealing with a pure line spectrum, while periodogram and correlogram must be used in conjunction for the treatment of a mixed spectrum. [It may seem pointless to speak of choosing between the two, since they are mathematically equivalent, the one being in fact the Fourier transform of the other. However, for practical purposes the choice makes a great difference, because

the sum in (A.5) is quite readily calculated, while the integral in (A.2) involves an infinity of labour.]

The only model with continuous spectrum with which we shall concern ourselves here is the autoregression, the discrete counterpart of the stochastic differential equation:

$$x_t + a_1 x_{t-1} + a_2 x_{t-2} + \cdots + a_P x_{t-P} = \varepsilon_t \,. \tag{A.6}$$

Here ε_t is the so-called residual or disturbing variate, and the different ε_t's are considered to be independently distributed with zero mean and variance v. For the process (A.6) we have

$$F(\omega) = V|1 + a_1 e^{i\omega} + a_2 e^{2i\omega} + \cdots + a_P e^{iP\omega}|^{-2} \tag{A.7}$$

(see Wold, 1938: 107; Doob, 1944: 257) so that (A.5) becomes

$$L = \log v + \sum_{i=0}^{P} \sum_{j=0}^{P} a_i a_j C_{i-j} \,, \tag{A.8}$$

if in (A.6) we give x_t a dummy coefficient a_0. Minimisation w.r.t. $a_1, a_2 \cdots a_p$ yields the well known Yule-Walker relations (see, for example, Wold, 1938: 178)

$$\sum_{i=0}^{P} a_i C_{i-j} = 0 \qquad (j = 1, 2 \cdots P) \,, \tag{A.9}$$

while minimisation w.r.t. v yields

$$v = \sum_i \sum_j a_i a_j C_{i-j} \,. \tag{A.10}$$

Equations (A.9) and (A.10) together provide estimates of all the parameters of $F(\omega)$. If we denote estimated quantities by a circumflex, setting (A.9) in (A.10) we find that

$$\hat{v} = \frac{\Delta_P}{\Delta_{P-1}}, \qquad \Delta_P = \begin{vmatrix} C_0 & C_1 & \cdots & C_P \\ C_1 & C_0 & \cdots & C_{P-1} \\ \cdots & \cdots & \cdots & \cdots \\ C_P & C_{P-1} & \cdots & C_0 \end{vmatrix} , \tag{A.11}$$

and setting (A.10) in (A.8) we have

$$\hat{L} = 1 + \log \hat{v} \,. \tag{A.12}$$

The importance of these formulae is in test theory. It has been shown (Whittle, 1952a, c) that if, on fitting an extra parameter [e.g. adding a term $a_{p+1} x_{t-p-1}$ to (A.6)], the quantity $\hat{L}$ becomes $\hat{L}_1$, then the statistic

$$\psi^2 = n[\hat{L} - \hat{L}_1] \tag{A.13}$$

is asymptotically distributed as χ^2 with one degree of freedom *if the*

unmodified scheme is the correct one. A substantial value of ψ^2 thus indicates that the extra parameter has definitely improved the fit and is probably necessary to the model, while a value in the neighborhood of expectation indicates that the original scheme is satisfactory.

So much for the purely continuous case. Let us now consider the case of a mixed spectrum. Let $F(\omega)$ denote the continuous component of the spectrum, and let us suppose that the series contains besides a sinusoidal term

$$\sum_{\nu=1}^{q} [A_\nu \sin(\omega_\nu t) + B_\nu \cos(\omega_\nu t)]. \tag{A.14}$$

It has been shown (Whittle, 1952b), then, that the estimation equations for the different A's, B's and ω's are as usual

$$\left.\begin{aligned} A_\nu = \frac{2}{n}\sum_1^n x_t \sin(\omega_\nu t) \qquad B_\nu = \frac{2}{n}\sum_1^n x_t \cos(\omega_\nu t) \\ f(\omega) \text{ has a local maximum } \alpha t\ \omega_\nu \end{aligned}\right], \tag{A.15}$$

while the parameters of $F(\omega)$ are estimated by minimising

$$\begin{aligned} L &= \frac{1}{2\pi}\int \left(\log F + \frac{f}{F}\right) d\omega - \frac{2}{n}\sum_\nu \frac{f(\omega_\nu)}{F(\omega_\nu)} \\ &\equiv \frac{1}{2\pi}\int_0^{2\pi} \log F d\omega + \sum c_s C_s' \end{aligned} \tag{A.16}$$

where

$$C_s' = C_s - \frac{2}{n}\sum_\nu f(\omega_\nu)\cos(\omega_\nu s). \tag{A.17}$$

That is, the discrete components are estimated directly from the periodogram, the estimates of amplitude and frequency thus obtained are used to correct the autocovariances as in (A.17), and $F(\omega)$ is estimated from the modified autocovariances as in the purely continuous case.

The test problem is more complicated, however. Most often one desires to answer in practice the question: "Is a certain peak on the periodogram evidence of a genuine harmonic term in the series, or does it correspond to a relatively broad band of frequencies such as would be generated by a model of type (A.6)?"

We note that there are three types of test problem which correspond to a choice between

(a) including a parameter in $F(\omega)$ or not,
(b) including a certain harmonic term or not, and
(c) including a parameter in $F(\omega)$ or fitting a harmonic term, and we note also that the question put above corresponds to the third of these types of decision. It may be shown that the ψ^2 test, with L calculated from (A.16), will indicate the decision to be made in the first case. However, the ψ^2 test is not applicable to the second case due to the rather peculiar nature of the parameter ω_r, hence this case must be treated by an extension of a Fisher test (1929). Suppose that the observed peak is at ω_r and that $\hat{F}(\omega_r)$ is the estimate of $F(\omega_r)$ when we have *not* fitted this particular harmonic, Then, for large enough n, the probability of obtaining a value of

$$g = \frac{2 f(\omega_r)}{n \hat{F}(\omega_r)} \tag{A.18}$$

greater than that observed is approximately

$$P(g) = \sum_{j=1} (-)^{j+1} \binom{m}{j} (1 - jg)^{m-1}, \tag{A.19}$$

where the summation is continued over all positive brackets and m is the nearest integer to $n/2$. If the observed $f(\omega_r)$ is so large that this probability is less than 0.05, say, then the harmonic must be admitted.

Case (c) may be regarded as a combination of cases (a) and (b); if we have fitted all parameters of $F(\omega)$ which are conceivably necessary and if we still find that a certain periodogram peak is significant by the Fisher test, then the existence of a harmonic term must be admitted. Similarly for the testing of a particular parameter of $F(\omega)$.

The calculations in the section on Analysis and Results provide an illustration of these techniques. The methods are directly generalisable to the treatment of multiple series (Whittle, 1953, 1954), such as occur in oceanography.

REFERENCES

Andronow, A. A. and C. E. Chaikin
1937. Theory of oscillations. Edited English version published by Princeton University Press, 1949.

Bartlett, M. S.
1948. Smoothing periodograms from time series with continuous spectra. Nature, London, *161:* 686.
1950. Periodogram analysis and continuous spectra. Biometrika, *37:* 1.

Daniell, P. J.
1946. Contribution to discussion on stochastic processes. J. R. statist. Soc., (B) *8:* 90.

Deacon, G. E. R.
1952. Analysis of sea waves, in Symposium on Gravity Waves, Nat. Bur. Standards Circ. 521: 209.
Doob, J. L.
1944. The elementary Gaussian processes. Ann. math. statist., *15:* 229.
Fisher, R. A.
1929. Tests of significance in harmonic analysis. Proc. Roy. Soc., (A) *125:* 54.
Grenander, U.
1951. On empirical spectral analysis of stochastic processes. Ark. mat. astr. fys., (1) *35:* 503.
Pierson, W. J.
1952. A unified mathematical theory for the analysis, propagation and refraction of storm generated ocean surface waves. Mineographed publication, Dept. of meteorology, New York University.
Seiwell, H. R. and G. P. Wadsworth
1949. A new development in ocean wave research. Science, *109:* 271.
Ursell, F.
1952. Discrete and continuous spectra in the theory of gravity waves, in Symposium on Gravity Waves, Nat. Bur. Standards Circ. 521: 1.
Whittle, P.
1952a. Some results in time series analysis. Skand. AktuarTidskr., *35:* 48.
1952b. The simultaneous estimation of a time series' harmonic components and covariance structure. Trab. Estad., *3:* 43.
1952c. Tests of fit in time series. Biometrika, *39:* 309.
1953. The analysis of multiple stationary time series. J. R. statist. Soc., *15:* 125.
1954. The statistical analysis of a sunspot series. Astrophys. J., (to appear).
Wold, H.
1938. A study in the analysis of stationary time series. Almquist and Wicksells Boktr., Upsala.

STATIC STABILITY PARAMETERS IN OCEANOGRAPHY[1]

By

M. J. POLLAK

Chesapeake Bay Institute of The Johns Hopkins University

ABSTRACT

The use of static vertical stability criteria in oceanography is discussed and two basic types of such stability parameters are derived. It is shown how these can be determined by using sound velocity as one of the variables. Computation can be simplified by means of a graph.

The concept of static vertical stability in a fluid is a simple one, yet the use of static stability criteria in physical oceanography has been extremely limited. Among the reasons for this situation may be (a) the somewhat haphazard treatment of the subject in the literature and (b) the rather cumbersome computation required for the exact evaluation of the terms involved. This has led to the occasional use of crude approximations to a stability parameter in oceanographic literature, such as the term $10^{-3}\frac{d\sigma_t}{dz}$ (Sverdrup, et al., 1942), or the "coefficient of stability," $\frac{1}{[\rho]}\frac{\partial[\rho]}{dz}$ which appears in Richardson's number (Proudman, 1953).

Since vertical stability is a measure of the restoring force (or the resistance to change) in the vertical direction, it may be expected to have a marked effect on any process involving vertical motion, such as the vertical velocity components of turbulent flow. This fact is generally recognized, and a number of attempts have been made to incorporate a stability term in the vertical eddy coefficients that have been determined theoretically or experimentally for the sea. In view of the continuously increasing attention that oceanographers are devoting to problems of turbulent flow, and because of the evident relationship of vertical stability to nonisotropic turbulence, the present paper is an attempt to remove some of the vagueness that has crept into the concept of stability in physical oceanography.

When a particle of water of unit mass is displaced vertically, it will acquire a vertical acceleration equal to the buoyant force per unit

[1] Contribution No. 14 from the Chesapeake Bay Institute. This work was supported by the Office of Naval Research, the State of Maryland (Department of Research and Education), and the Commonwealth of Virginia (Virginia Fisheries Laboratory).

mass exerted on it by its environment. This acceleration per unit change of geometrical depth is the definition of vertical stability derived by Hesselberg in the last of three papers on the subject (Hesselberg and Sverdrup, 1915; Hesselberg, 1918, 1929). The physical significance of the term remains unaltered if the acceleration is given per unit change of geopotential or per unit change of pressure. This criterion of stability, an acceleration per unit of displacement, is identical to that used in meteorology (Holmboe, et al., 1945), where it is generally written in terms of temperature gradients.

While the above-mentioned definition, in terms of acceleration, is the one conventionally used, any other continuous function which is a parameter of the resistance to deformation of the fluid column would be equally valid. An example of such a function is frequently encountered in meteorology. When the acceleration form of the stability function is transformed into terms of temperature gradients by means of the perfect gas law and when the constant acceleration of gravity is dropped from the expression, we have a function which no longer has the dimensions of an acceleration but which is, nevertheless, an exact parameter of stability.

An alternative definition of stability, one which also has a clear-cut physical meaning, is the amount of energy required to move a particle of unit mass a unit measure of displacement. In both this definition and the one in terms of acceleration, the stability parameter is a function of the difference between the observed vertical mass distribution and the mass distribution corresponding to neutral equilibrium. Consequently, in both of them, a value of zero corresponds to neutral equilibrium, positive values to stable conditions, and negative values to instability.

Stability could also be defined arbitrarily as the ratio of the observed mass distribution to the mass distribution of neutral equilibrium. While such a function lacks the physical meaning of the more conventional expressions, it possesses the advantage of being nondimensional. In terms of this parameter, neutral stability is represented by a value of one, stable equilibrium by values greater than one, and unstable equilibrium by values less than one.

The following section will give the development of some of the stability parameters mentioned, and it will be shown how the velocity of sound can be used as one of the variables for their evaluation. Conventional symbols are used and their units given: h = depth in meters; G = geopotential in dynamic meters (0.1 m^2/sec^2); p = pressure in decibars (10^5 dynes/cm^2); g = acceleration of gravity = 9.81m/sec^2 (assumed constant); T = temperature in °C; S = salinity in ‰;

$\rho = \rho(T,S,p)$ = density in g/cm³; $c = c(T,S,p)$ = velocity of sound in m/sec; subscript $_A$ refers to an adiabatic process.

Let $\frac{d\rho}{dp}, \frac{d\rho}{dG}, \frac{d\rho}{dh}$ be the observed density gradient in a column of water expressed in terms of pressure, geopotential, and geometric depth. Further, let $\left(\frac{d\rho}{dp}\right)_A$ be the density gradient of neutral equilibrium. This is the mass distribution which would exist in an insulated column which has been filled through its open upper end from an infinite reservoir of homogeneous water (T = constant, S = constant, $p = 0$) in a period of time that is sufficiently short to make molecular conductivity negligible. Because water is compressible, $\left(\frac{d\rho}{dp}\right)_A = \frac{\partial\rho}{\partial p} + \frac{\partial\rho}{\partial T}\left(\frac{dT}{dp}\right)_A$. In order to make the adiabatic density gradient comparable to the observed gradient based on other depth measures, the hydrostatic equation can be applied to the above expression. Hence, $\left(\frac{d\rho}{dp}\right)_A = \frac{1}{\rho}\left(\frac{d\rho}{dG}\right)_A = \frac{1}{g\rho}\left(\frac{d\rho}{dh}\right)_A$.

If a unit volume of water is given a vertical displacement corresponding to Δp, the buoyant force on it will be $g\left[\frac{d\rho}{dp} - \left(\frac{d\rho}{dp}\right)_A\right]\Delta p$. Then the corresponding buoyant force on a unit mass will be $\frac{g}{\rho}\left[\frac{d\rho}{dp} - \left(\frac{d\rho}{dp}\right)_A\right]\Delta p$. This latter expression has the dimensions of acceleration irrespective of the measure of vertical displacement used. However, since the force per unit mass is proportional to the increment of displacement, its magnitude is clearly dependent on the units used. For instance, the difference in density between a particle and its environment will not necessarily be the same at a displacement of one meter as it will be at a displacement of one dynamic meter or one decibar. We finally write, force per unit mass per unit pressure equals $\frac{g}{\rho}\left[\frac{d\rho}{dp} - \left(\frac{d\rho}{dp}\right)_A\right]$. Hesselberg's analogous expression in geometric units is his stability term $E'' = \frac{g}{\rho}\frac{\delta\rho}{dh} \equiv \frac{g}{\rho}\left[\frac{d\rho}{dh} - \left(\frac{d\rho}{dh}\right)_A\right]$, in our notation. We thus obtain a set of three stability functions:

(1a) $$E_p = \frac{9.81}{\rho}\left[\frac{d\rho}{dp} - \left(\frac{d\rho}{dp}\right)_A\right] \quad \text{in m/sec}^2\text{/dbar},$$

$$(1b) \qquad E_G = \frac{9.81}{\rho}\left[\frac{d\rho}{dG} - \left(\frac{d\rho}{dG}\right)_A\right] \text{ in m/sec}^2\text{/dyn.m},$$

$$(1c) \qquad E_h = \frac{9.81}{\rho}\left[\frac{d\rho}{dh} - \left(\frac{d\rho}{dh}\right)_A\right] \text{ in m/sec}^2\text{/m},$$

where $E_p = \frac{1}{\rho} E_G = \frac{1.02}{\rho} E_h$.

If we wish to redefine stability in terms of energy per unit mass per unit of displacement, calling this function E^*, it is merely necessary to multiply one-half the E term (in other words, the mean acceleration over the displacement) by the geometric equivalent of the displacement: E_p by $\frac{0.51}{\rho}$ m, E_G by 0.51 m, and E_h by 0.5 m. Thus we have another set of three functions derived from the same basic stability parameter:

$$(2a) \qquad E^*_p = \frac{5}{\rho^2}\left[\frac{d\rho}{dp} - \left(\frac{d\rho}{dp}\right)_A\right] \text{ in (m/sec)}^2\text{/dbar},$$

$$(2b) \qquad E^*_G = \frac{5}{\rho}\left[\frac{d\rho}{dG} - \left(\frac{d\rho}{dG}\right)_A\right] \text{ in (m/sec)}^2\text{/dyn.m},$$

$$(2c) \qquad E^*_h = \frac{4.9}{\rho}\left[\frac{d\rho}{dh} - \left(\frac{d\rho}{dh}\right)_A\right] \text{ in (m/sec)}^2\text{/m}.$$

For purposes of computing the stability E or E^*, the terms in brackets can be written in the following manner:

$$\left[\frac{d\rho}{dp} - \left(\frac{d\rho}{dp}\right)_A\right] = \left[\frac{\partial\rho}{\partial p} + \frac{\partial\rho}{\partial T}\frac{dT}{dp} + \frac{\partial\rho}{\partial S}\frac{dS}{dp}\right] - \left[\frac{\partial\rho}{\partial p} + \frac{\partial\rho}{\partial T}\left(\frac{dT}{dp}\right)_A\right].$$

Combining terms: $\left[\frac{d\rho}{dp} - \left(\frac{d\rho}{dp}\right)_A\right] = \frac{\partial\rho}{\partial T}\left[\frac{dT}{dp} - \left(\frac{dT}{dp}\right)_A\right] + \frac{\partial\rho}{\partial S}\frac{dS}{dp}$.

Except for the use of h in place of p, the three terms, $\frac{\partial\rho}{\partial T}$, $\left(\frac{dT}{dp}\right)_A$, and $\frac{\partial\rho}{\partial S}$ have been tabulated by Hesselberg and Sverdrup (1915). These can be combined with the observed temperature and salinity gradients, $\frac{dT}{dh}$ and $\frac{dS}{dh}$, to obtain the stability functions.

A different type of stability parameter, which has already been mentioned and which is represented by the symbol E_R, is the ratio of the observed to the adiabatic density gradient. Then:

(3a) $$E_{R(p)} = \frac{d\rho}{dp} \Big/ \left(\frac{d\rho}{dp}\right)_A,$$

(3b) $$E_{R(G)} = \frac{d\rho}{dG} \Big/ \left(\frac{d\rho}{dG}\right)_A,$$

(3c) $$E_{R(h)} = \frac{d\rho}{dh} \Big/ \left(\frac{d\rho}{dh}\right)_A.$$

It is immediately apparent that $E_{R(p)} = E_{R(G)} = E_{R(h)}$ and that this parameter is therefore independent of the units used in measuring the density gradients.

It has been pointed out by Bjerknes, et al. (1934) that the adiabatic density gradient $\left(\frac{d\rho}{dp}\right)_A$ is identical to the term which appears in the Laplacian expression for the velocity of sound, $c = \sqrt{\left(\frac{dp}{d\rho}\right)_A}$, and can therefore be represented by $1/c^2$. Since we are dealing with only the total change in p, and since, in both cases, $\rho = \rho(p, T)$ with salinity constant, $\left(\frac{d\rho}{dp}\right)_A$ always represents the same characteristic of the fluid.

The stability can now be expressed in the following forms:

(4) $$E_p = \frac{9.81}{\rho}\left[\frac{d\rho}{dp} - \frac{10}{c^2}\right],$$

(5) $$E_p^* = \frac{5}{\rho^2}\left[\frac{d\rho}{dp} - \frac{10}{c^2}\right],$$

(6) $$E_R = \frac{c^2}{10}\frac{d\rho}{dp}.$$

The coefficient, 10, of $1/c^2$ is a conversion factor resulting from the use of decibars and m per sec in our stability terms in place of dynes and cm per sec. In the comparable expressions for dynamic meters and geometric meters the term $\frac{10}{c^2}$ is replaced by $\frac{10\rho}{c^2}$ and $\frac{9.81\rho}{c^2}$, respectively.[2]

[2] In 1928 the meteorologist Väisälä apparently derived an expression for stability, designated N^2, which is identical to our E_h when the latter is written in terms of sound velocity. Consequently, N has the dimensions of frequency. Väisälä's expression is mentioned in the unpublished notes of a seminar given by Eckart at Scripps

To test the suitability of equations (4), (5), and (6) for practical applications, it was expedient to use the data from Michael Sars Station No. 44 which had been given as an example of stability computation by Hesselberg and Sverdrup (1915) and which is reproduced in Sverdrup, et al. (1942: table 62). The stability term 10^8E, computed by Hesselberg and Sverdrup from their tables, is equivalent to the bracketed term times 10^8 in our expression $E_h = \frac{9.81}{\rho}\left[\frac{d\rho}{dh} - \frac{9.81\,\rho}{c^2}\right]$, or $10^8 E = 10^8 \frac{\rho E_h}{9.81}$.

The stability parameter $\left[\frac{d\rho}{dh} - \frac{9.81\,\rho}{c^2}\right]$ was evaluated as follows. The density, ρ, was determined for atmospheric pressure from Knudsen's (1901) tables for σ_t and was corrected for pressure by means of the tables computed by Ennis (1944). Here it should be pointed out, parenthetically, that the density obtained from Knudsen's σ_t values is actually specific gravity or density in grams per milliliter. Density in grams per cubic centimeter (the units appropriate to dynamic equations) is obtained by dividing $[1 + 10^{-3}\sigma_t]$ by 1.000027 or, approximately, by using the expression $[1 + 10^{-3}(\sigma_t - 0.03)]$. The velocity of sound, c, was determined for atmospheric pressure from Del Grosso's (1952) values and was corrected for depth according to the British Admiralty tables by Matthews (1939). Table I gives the results of this computation, together with the pertinent Michael Sars data.

While the values of $10^8 \frac{\rho E_h}{9.81}$ are not identical with those of $10^8 E$, it is felt that the use of sound velocity in stability computations is validated by these results. The differences between the two tabulated sets of stability parameters can probably be explained on the following grounds.

It will be noted that the largest and least systematic differences occur in the upper 200 m where the depth increments are 50 m or less. With $\frac{\Delta\rho}{\Delta h}$ equal to the mean value of $\frac{d\rho}{dh}$ in the interval Δh, provided ρ is a continuous single-valued function of h, an error of 10^{-5} in $\Delta\rho$

Institution of Oceanography in 1949 and recorded by R. O Reid. Eckart's source is a lecture by Solberg at UCLA in 1946. I have been unable to find the original reference despite a comprehensive search of the meteorological and oceanographic literature.

TABLE I. Michael Sars Station No. 44

(28° 37′ N, 19° 08′ W, 28 May 1910)†

Depth (*m*)	*Temp.* (°C)	*Sal.* (‰)	$10^8 E$ (*Hesselberg and Sverdrup*)	$10^8 \frac{\rho E_h}{9.81}$ (*Pollak*)
0	19.2	36.87		
			−440	−434
10	19.31	36.85		
			−150	−167
25	19.34	36.83		
			− 13	− 15
50	19.24	36.79		
			610	604
75	18.65	36.79		
			390	364
100	18.24	36.78		
			38*	64
150	17.50	36.56		
			270	242
200	16.45	36.40		
			160	160
300	14.52	36.02		
			120	127
400	13.08	35.77		
			150	155
500	11.85	35.64		
			130	134
600	10.80	35.54		
			100	107
800	9.09	35.39		
			89	96
1000	8.01	35.37		
			84	86
1200	7.27	35.42		
			48	50
1400	6.40	35.35		
			26*	29
2000	4.52	35.15		
			11	14
3000	2.84	34.92		
			8	11
4000	2.43	34.90		
			1	3
5000	2.49	34.90		

† First four columns from Sverdrup, et. al. (1942: table 62).

* Recomputed by M. J. P. by means of Hesselberg and Sverdrup's tables (1915).

when $\Delta h = 50$m will produce an error of 20 in the term $10^8 \frac{\rho E_h}{9.81}$. This is the same order of magnitude as the differences found in Table I. A total error of 10^{-5} in $\Delta\rho$ is easily introduced in the determination of the ρ's from temperature, salinity, and depth. In contrast, when $\Delta h = 200$ m, the corresponding error in the stability parameter is only 5. However, the differences are not necessarily due solely to errors in ρ. Values obtained by means of the Hesselberg and Sverdrup tables may also contain small errors as a result of the large intervals in the arguments of those tables and the need for two-way interpolation.

The small systematic differences below 1000 m result from the use of Del Grosso's sound velocity tables in place of Kuwahara's (1939) or Matthews'. Del Grosso's values are based on direct experimental determination and are about 3 m per sec higher than those given in the latter two tables which were derived theoretically from somewhat obsolete and incomplete experimental data on the elastic and thermal properties of sea water (Ekman, 1908; Krümmel, 1907); these latter sets of data are the same ones on which the Hesselberg and Sverdrup stability tables are based. A 3 m per sec increase in sound velocity corresponds to an increase of approximately two units in the term $10^8 \frac{\rho E_h}{9.81}$. However, even with the use of Del Grosso's tables, the present method of stability computation still contains potential sources of error. The pressure corrections for density and sound velocity, taken from Ennis' and Matthews' tables, respectively, are derived from the same data for elastic and thermal properties that are the basis of all the other tables mentioned above. In other words, the only improvement in accuracy which can be claimed for the proposed stability computation stems from the introduction of a more accurate measure of sound velocity under atmospheric pressure. This increased accuracy, however, may be more apparent than real.

Dorsey (1940) raises an interesting point which may have some bearing on the difference between Del Grosso's and Kuwahara's or Matthews' sound velocity tables and therefore on the stability values computed by the above method. In section 34 he states:

> There are no direct determinations of the values of specific heat of water at constant volume, of the ratios of specific heats, or of their differences, but all these can be computed from the observed compressibility, thermal expansion, and specific heat at constant pressure. Values so determined may be called *static* values. They can also be determined from the velocity of sound, in which case they may be described as *dynamic*. Likewise, the increase in temperature

on adiabatic compression may be determined either statically, from the thermal expansion, or dynamically, from the observed drop in temperature that accompanies a sudden release of pressure.

He then points out that, since water probably contains associated molecules of more than one type and since the internal state of a molecule may be affected by gross dynamic changes in the substance, the static and dynamic values of these thermal properties may be expected to differ under certain conditions.

If Dorsey's assumptions are correct for fresh water, we could expect these effects to be even more pronounced in such a complex ionized solution as sea water. Finally, if we extend his reasoning one step further, we might conclude that sound velocities, which have been derived from the static values of thermal properties, would differ from those obtained by direct measurements. The latter values, as exemplified by Del Grosso's data, correspond to sound velocity as a function of the dynamic values of thermal properties. One implication of these ideas is that the term $\left(\frac{d\rho}{dp}\right)_A$ is not a unique function of adiabatic compressibility but is dependent also on the time element involved in the process.

If the suggested theory is true—and the evidence for this is by no means conclusive—it may be necessary to use computed sound velocity values, rather than measured ones, in stability computations. However, as was pointed out previously, the values of the thermal and elastic properties on which Kuwahara's and Matthews' computations are based are not entirely reliable, and hence there is little basis for assuming that their sound velocity tables would give more accurate stability values than Del Grosso's.

In considering the practicability of the proposed method of stability computations, it should be pointed out that the term $\frac{10}{c^2}$ lends itself to graphical presentation as a function of temperature, salinity, and pressure without first determining c. The range of $\frac{10}{c^2} \times 10^8$ is only 100 units, from about 400 to 500. There is little justification for carrying out these values to one more place, since an error of only 0.00001 g/cm^3 in $\Delta\rho$, when Δp equals 1000 dbar, corresponds to an error of 1 in the term $\frac{d\rho}{dp} \times 10^8$. A simple design for such a graph gives $\frac{10}{c^2}$, i.e., $\left(\frac{d\rho}{dp}\right)_A$ for arguments of temperature and salinity at

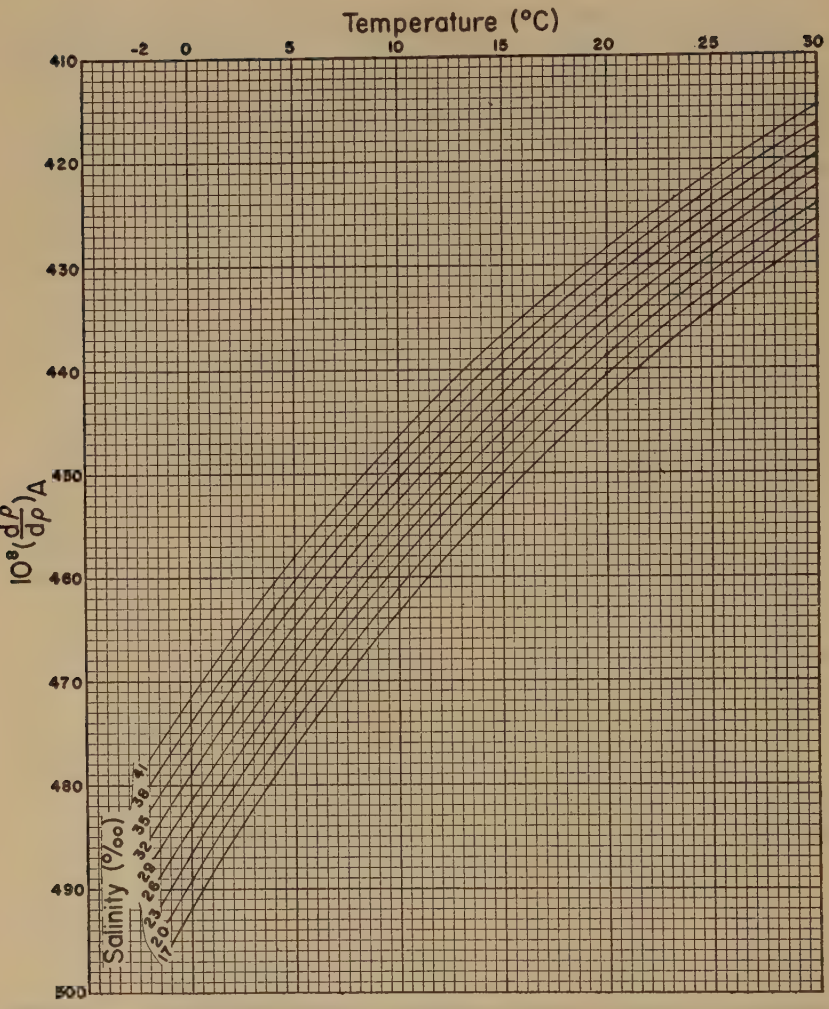

Figure 1. Adiabatic density gradient at atmospheric pressure as a function of temperature and salinity.

atmospheric pressure, with an auxiliary graph for the pressure correction (Figs. 1, 2). Even if the use of sound velocity does not improve the accuracy of stability parameters over that obtainable from Hesselberg's and Sverdrup's tables, the graphical determination of the adiabatic density gradient would probably simplify and speed up the required computations to a considerable extent.

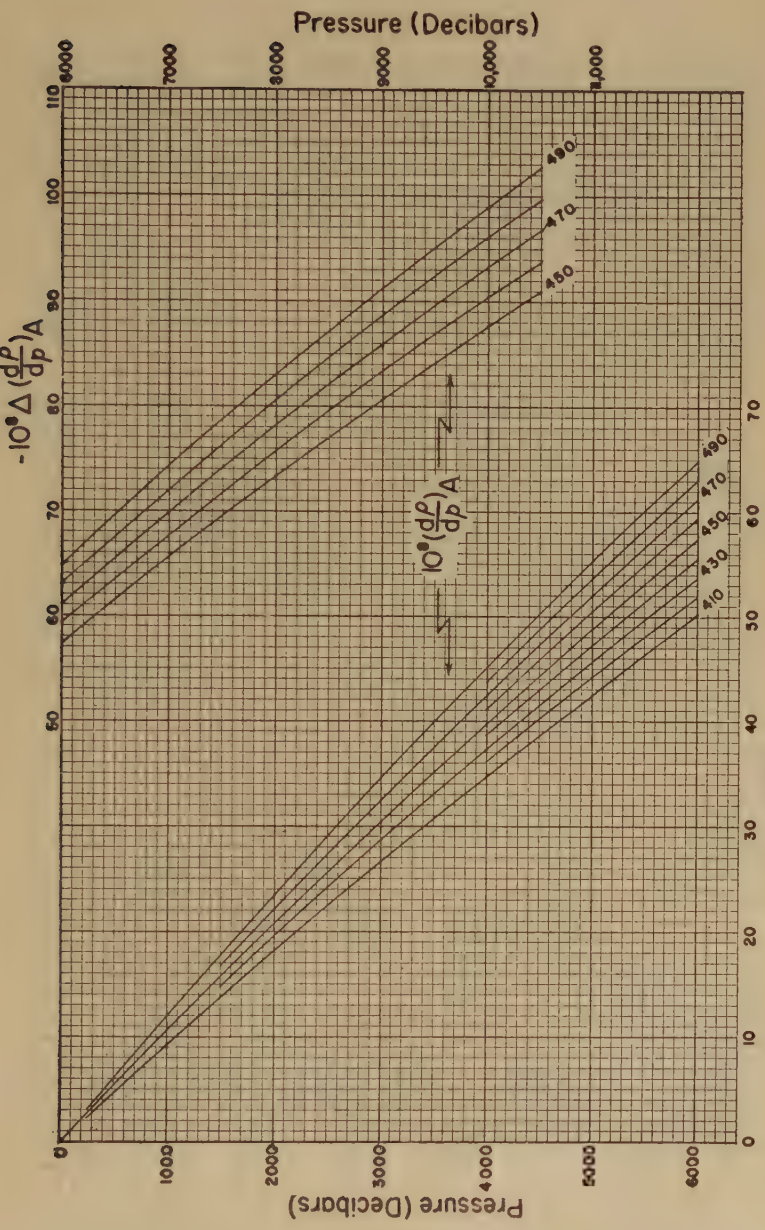

Figure 2. Pressure correction (always subtractive) as a function of pressure and adiabatic density gradient at atmospheric pressure.

REFERENCES

Bjerknes, V., J. Bjerknes, H. Solberg, and T. Bergeron
1934. Hydrodynamique Physique. Les Presses Universitaire de France, Paris. 864 pp.

Del Grosso, V. A.
1952. The velocity of sound in sea water at zero depth. Naval Research Laboratory, Washington, D. C., Rep. 4002. 39 pp.

Dorsey, N. E.
1940. Properties of Ordinary Water-Substance. Reinhold Publ. Corp., New York. 673 pp.

Ekman, V. W.
1908. Die Zusammendrueckbarkeit des Meerwassers. Publ. Circ. Cons. Explor. Mer, 43: 1–47.

Ennis, C. C.
1944. Note on computation of density of sea water and on corrections for deep-sea reversing thermometers. Scientific Results of Cruise VII of the Carnegie. Oceanography-I-A. Observ. Res. Phys. Oceanogr. Publ. Carneg. Instn., No. 545: 23–45.

Hesselberg, Th.
1918. Über die Stabilitätsverhältnisse bei vertikalen Verschiebungen in der Atmosphäre und im Meer. Ann. Hydrogr. Berl., *46:* 118–129.
1929. Die Stabilitätsbeschleunigung im Meere und in der Atmosphäre. Ann. Hydrogr. Berl., *57:* 273–282.

Hesselberg, Th. and H. U. Sverdrup
1915. Die Stabilitätsverhältnisse des Seewassers bei vertikalen Verschiebungen. Bergens Mus. Aarb. 1914–15, No. 15: 1–16.

Holmboe, J., G. E. Forsythe, and W. Gustin
1945. Dynamic Meteorology. John Wiley and Sons, Inc., New York. 378 pp.

Knudsen, Martin
1901. Hydrographical Tables. G. E. C. Gad, Copenhagen. 63 pp.

Krümmel, Otto
1907. Handbuch der Ozeanographie, Bd. 1. J. Engelhorn, Stuttgart. 526 pp.

Kuwahara, Susumu
1939. Velocity of sound in sea-water and calculation of the velocity for use in sonic sounding. Hydrogr. Rev., *16:* 123–140.

Matthews, D. J.
1939. Tables of the velocity of sound in pure water and sea water. Second Ed., H. D. 282, British Admiralty, London. 52 pp.

Proudman, J.
1953. Dynamical Oceanography. Methuen and Co., Ltd., London. 409 pp.

Sverdrup, H. U., M. W. Johnson, and R. H. Fleming
1942. The Oceans. Prentice-Hall, Inc., New York. 1087 pp.

FORMULAS FOR SOUND VELOCITY IN SEA WATER[1]

By

ROBERT T. BEYER

Physics Department, Brown University
Providence 12, Rhode Island

ABSTRACT

Recent measurements by Del Grosso show a discrepancy between computed and observed values of sound velocity in sea water. The basis of Kuwahara's formula has been re-examined. The chief cause of the discrepancy lies in the use of a value for the compressibility of pure water that is too large.

INTRODUCTION

For nearly 15 years, the formulas presented by Kuwahara (1939), or tables derived from them by Stephenson and Woodsmall (1941), have been employed in this country as a basis for computing the velocity of sound in sea water from bathythermographic measurements of temperature, pressure and salinity. These tables have had widespread application in sonar studies, fathometry and, more recently, in sofar work. Similiar tables developed by Matthews (1939) have been employed in Great Britain for similar purposes.

In recent years there have been reported instances of direct sound velocity measurements in which the experimental values of the velocity exceeded Kuwahara's calculated values by several meters per second. The most significant data of this kind are those reported by Weissler and Del Grosso (1951) and by Del Grosso (1952). These observers reported a consistent error in Kuwahara's values of the order of 3–4 m/sec as well as a slightly different expression for the dependence of the sound velocity upon salinity.

Because of the important rôle played by sound velocity in underwater acoustics, it is desirable to re-examine the basis on which the Kuwahara tables were calculated in an effort to determine what velocity values are the most probable.

KUWAHARA'S CALCULATION

The sound velocity V can be expressed in terms of the physical properties of the medium by means of the formula

[1] This work was supported in part by the Office of Naval Research and in part by the Fund for the Advancement of Education.

$$V = \sqrt{\frac{\gamma}{\rho\beta}}, \tag{1}$$

where γ is the ratio of specific heats, ρ the mean density of the medium, and β the isothermal compressibility. An idea of the magnitudes of the quantities involved is useful. For sea water of salinity 35 ‰, at 0°C and zero depth (atmospheric pressure), the values of the quantities in (1), computed from Kuwahara's formulas, are:

$$\rho = 1.02813 \text{ gm/cm}^3; \gamma = 1.000386; \beta = 46.57 \times 10^{-12} \text{ cm}^2/\text{dyne}; \quad V = 1445.5 \text{ m/sec}. \tag{2}$$

The discrepancies reported by Del Grosso are of the order of 3 m/sec or 0.2%. One can look for such discrepancies in errors involved in the measurement of γ, ρ, β or in the formulation of (1) itself.

The derivation of (1) rests on two assumptions: (a) that the amplitude of the wave is infinitesimal and (b) that there is no dissipation in the medium. If the analysis of Lamb (1925) is followed, one obtains for the velocity V_F of a wave of finite amplitude:

$$V_F = V + \xi, \tag{3}$$

where ξ is the particle velocity; for a sinusoidal wave, ξ varies from $+\xi_0$ to $-\xi_0$. The value of ξ_0 can be related to the average acoustic power P transmitted per unit area:

$$P = \tfrac{1}{2}\rho\xi_0^2 V \tag{4}$$

or

$$\xi_0 = \sqrt{\frac{2P}{\rho V}}.$$

For a sound wave of 1 watt/cm², a power considerably in excess of that customarily used for velocity measurements, the data of (2) yield

$$\xi_0 = \sqrt{\frac{2 \times 10^7}{1.028 \times 1.445 \times 10^5}} = 12 \text{ cm/sec}. \tag{5}$$

Thus, the maximum deviation of (3) from the simple expression (1) is smaller by an order of magnitude than the discrepancy observed. Furthermore, in a continuous wave the average value of V_F will be much closer to V, since ξ is alternately positive and negative. Only in measurements on the leading edge of a pulse could variations of the order of (5) be observed. One can therefore neglect errors due to finite amplitude.

The error produced by the neglect of the dispersion due to absorptive processes has been computed by Del Grosso (1952) and were found to be less than 3 cm/sec. Hence such dispersion can be safely neglected. The discrepancies must therefore be accounted for by errors in measurement. Since V is proportional to $\gamma^{1/2}$, $\gamma^{-1/2}$, $\beta^{-1/2}$, it is evident that the measurement for any one of these factors would have to be in error by 0.4% to be responsible for the discrepancy. The mode of calculation of each of these quantities will now be considered.

Density. Kuwahara took his density values for sea water from formulas prepared by Knudsen (1901) and Ekman (1908), whose formulas are quite elaborate and will not be reproduced here since they can be found in Kuwahara's paper.[2] An error of 0.4% in the density would correspond to one of 4 units in the third decimal place. Since measurements are commonly made of $\rho - 1$ rather than of the absolute magnitude of ρ, it follows that such an error would amount to 4 parts in 28 for the datum in (2). It is highly unlikely, therefore, that the gross discrepancy can be due to an error in the density measurement.

Ratio of Specific Heats. The ratio of specific heats γ is also measured in terms of its deviation from unity, usually from the expression

$$\gamma = \frac{1}{1 + \dfrac{T}{Jc_p}\dfrac{\left(\dfrac{\partial v}{\partial T}\right)^2}{\left(\dfrac{\partial v}{\partial p}\right)}}, \qquad (6)$$

where T = absolute temperature, J = Joule's equivalent, c_p = specific heat at constant pressure, and v = specific volume.

As in the case of density, the same argument regarding the gross error applies here but with greater emphasis, since the deviation of γ from unity would have to be a whole order of magnitude greater than it actually is to account for the difference in the Del Grosso and Kuwahara values.

[2] Attention should be called to the fact that, while the expression for the density of pure water $(1 + \Sigma_t)$ is given correctly in that paper, the temperature derivative $\dfrac{\partial \Sigma_t}{\partial T}$ is given incorrectly and will lead to numerical values inconsistent with the remainder of Kuwahara's paper.

Isothermal Compressibility. In view of the foregoing observations, we are left with isothermal compressibility as the only possible source of appreciable error. In fact, this quantity was estimated by Kuwahara to be the least accurate in his formula. Kuwahara took his values for compressibility from a formula devised by Ekman (1908). Ekman measured not only the isothermal compressibility of sea water both on ocean going trips and in the laboratory but also the compressibility of distilled water. His empirical formula was so constructed as to be consistent with the value of the isothermal compressibility of distilled water at 0°C, 1 atmosphere pressure, as deduced from the measurement of Amagat (1893). Ekman's formula was expressed in terms of the mean compressibility μ:

$$\begin{aligned} 10^8\mu = {} & \frac{4886}{1 + 0.000183\,p} - [227 - 28.33\,t - 0.55\,t^2 + 0.004\,t^3] \\ & + 10^{-3}\,p[105.5 + 9.50\,t - 0.158\,t^2] - 1.5 \times 10^{-6}p^2t \\ & - (\sigma_{S00} - 28)[147.3 - 2.72\,t + 0.04\,t^2 \\ & \qquad - 10^{-3}p(32.4 - 0.87\,t + 0.02\,t^2)]10^{-1} \\ & + (\sigma_{S00} - 28)[4.5 - 0.1\,t - 10^{-3}\,p(1.8 - 0.06\,t)]10^{-2}, \end{aligned} \tag{7}$$

where μ is the mean compressibility in reciprocal bars, p is the pressure in bars (10^6 dynes/cm^2) above atmospheric pressure, and t is the temperature in degrees centigrade. The quantity μ is related to the isothermal compressibility by the expression

$$\beta = \frac{\mu + p\,\dfrac{\partial \mu}{\partial p}}{1 - \mu p}, \tag{8}$$

where

$$\sigma_{S00} = -0.069 + 1.4708\,Cl - 0.001570\,Cl^2 - 0.000398\,Cl^3,$$

and the chlorinity Cl is given in terms of the salinity S (both in ‰) by

$$S = 0.030 + 1.8050\,Cl.$$

For a 0.2% error in the sound velocity, the error in β must equal (0.004) 46.57×10^{-6} bar^{-1} $= 0.19 \times 10^{-6}$ bar^{-1} (or 0.19×10^{-12} cm^2/dyne). Such an error would be of the same order of magnitude as that estimated by Ekman for the possible error in his formula.

Thus the accuracy of Kuwahara's formula depends critically upon a measurement of the compressibility of sea water made over 45 years ago and upon a measurement of the compressibility of distilled water made over 60 years ago.

COMPRESSIBILITY MEASUREMENTS

A search of the literature reveals that no direct measurements of the compressibility of sea water have been made since Ekman. Such a measurement, employing more modern techniques, would appear to be desirable.

The compressibility of distilled water has been measured a number of times, in several different ways, since 1893. Before these results are listed, however, it is well to point out how Ekman deduced from Amagat's data a value of β at 0°C, 1 atmosphere (subsequently called β_0), for distilled water. Amagat measured the specific volume change of distilled water at pressures varying from 25 to 900 atmospheres, and the relative error in these measurements is greater at the lower pressures where the deviation of the specific volume from unity is slight. Therefore, Ekman employed only those values at 150 atmospheres and higher. From these he deduced an empirical relation for the pressure dependence and then extrapolated to 1 atmosphere. This relationship is embodied in the first two terms of (7).

It is interesting to note that use of Amagat's values at the lower pressures would have yielded a higher compressibility value and would have caused the computed values of V to be even lower than they are, i.e., the difference between computed and observed values would have been increased. Ekman's selection of the values for β_0 was therefore a fortunate one.

Some more recent values of β_0 are shown in Table I. Tyrer (1913) measured the adiabatic compressibility in the range 1 to 2 atmospheres; a small correction was necessary to obtain β_0. The value attributed to Bridgmann (1913) was obtained by extrapolating his mean compressibilities to atmospheric pressure (as listed in Dorsey, 1940) for the range one to several thousand atmospheres. While the accuracy of this extrapolation is not great, since only four points on the curve were available, the mean compressibility for each pressure range as measured by Bridgmann was less than that measured by Amagat. Hence one would expect the value for β_0 from Bridgmann's data to be less than that of Amagat.

TABLE I. Isothermal Compressibility β_0 of Distilled Water at 0°C, Atmospheric Pressure

Observer	*Year*	β_0 (cm^2 *dynes* $\times 10^{12}$)
Amagat	1893	51.11
Tyrer	1913	49.56
Bridgmann	1913	50.5

No direct measurements have been made of β_0 in recent years. However, a number of observers (Hubbard and Loomis, 1928; Randall, 1932; Lagemann, Gilley and McLeroy, 1953) have deduced its value from measurements of sound velocity (see Table II).

TABLE II. Sound Velocity V_0 and Isothermal Compressibility β_0 in Distilled Water at 0°C, Atmospheric Pressure

Observer	*Year*	V_0 (*m/sec*)	β_0 (*cm²/dynes* $\times 10^{12}$)
Hubbard and Loomis	1928	1407	50.50
Randall	1932	1403.5	50.74
Lagemann, et al.	1953	1408	50.41

From the amount of variation in the values of β_0 obtained by the different observers, it appears to be almost fortuitous that the Amagat-Ekman-Kuwahara velocity values agree with experimental results as well as they do. At the same time, the results of the more recent experimental measurements, both direct and indirect, indicate that the isothermal compressibility of pure water is somewhat less than the value given by Amagat. If one assumes perfect accuracy for all terms in the Ekman equation other than those dependent on β_0, the Del Grosso velocity value at 0°C can be used to compute the magnitude of β_0. A value of 50.92×10^{-12} cm² dyne is obtained. This number lies midway between Amagat's value and that of Randall.

SALINITY DEPENDENCE

From the foregoing discussion it is evident that the gross difference between the Del Grosso data and the computed values of Kuwahara is due to a variation in the measured value of β_0. There remains, however, a slight difference in the salinity dependence for the two cases. The sound velocity V for sea water at 0 C, zero depth, is given (in m/sec) as a function of the salinity S (in ‰) by the two expressions:

$$\begin{aligned} V &= 1445.5 + 1.307(S\text{-}35) - 0.00015(S\text{-}35)^2 \text{ (Kuwahara)}, \\ V &= 1448.6 + 1.25(S\text{-}35) \quad - 0.000002(S\text{-}35)^4 \text{ (Del Grosso)}. \end{aligned} \tag{9}$$

For most salinity values encountered in the ocean, the third term in both of these expressions can be neglected. Since the differences in the first term have already been discussed, this leaves the second term for consideration. Kuwahara obtained this salinity dependence in the form

$$\frac{\partial V}{\partial S} = \frac{1}{2H^{\frac{1}{2}}}\left(2\frac{\partial v}{\partial S} - \frac{v}{H}\frac{\partial H}{\partial S}\right), \tag{10}$$

where

$$H = -\frac{\partial v}{\partial p} - \frac{T}{Jc_p}\left(\frac{\partial v}{\partial T}\right)^2 \tag{11}$$

and

$$\frac{\partial H}{\partial S} - \frac{\partial^2 v}{\partial S \partial p} + \frac{T}{Jc_p}\left\{\frac{1}{c_p}\frac{\partial c_p}{\partial S}\left(\frac{\partial v}{\partial T}\right)^2 - 2\frac{\partial v}{\partial T}\frac{\partial^2 v}{\partial S \partial T}\right\}. \tag{12}$$

The values of c_p used by Kuwahara were taken from an expression deduced by Krümmel (1907) from data on the salinity dependence of c_p at 17.5°C and on the temperature dependence of c_p for distilled water. At first glance this would appear to be a possible source of significant error. However, substitution of numerical values into (9) indicates that the contribution of the second term (which contains $\frac{\partial c_p}{\partial S}$) is almost completely negligible. Since c_p is close to unity in all cases, any error in its absolute magnitude could have only a minute effect on those terms that contain $1/c_p$.

We must still examine the possible effect of the use of a smaller value for β_0. In this case $\frac{\partial v}{\partial p}$ would be correspondingly decreased. Such a drop would result in a decrease in the value of H, thereby increasing $\frac{\partial V}{\partial S}$. Such a consequence would be just opposite to Del Grosso's findings.

Del Grosso, in his report, suggests that the difference in the salinity dependence in the two cases can be attributed to variations in the determination of salinity. Such variations arise from the fact that the concept of salinity is based on the assumption that the relative proportions of different salts in sea water are constant over the entire ocean. Actually, this constancy fails in waters of low salinity, hence the waters used by Knudsen and others to dilute ocean water samples could have actually altered the salt content in a way not observable from chlorinity-salinity measurements. The fact that other sources of error (c_p, β_0) do not contribute to the difference in salinity dependence supports this line of argument.

CONCLUSIONS

There appears to be little doubt that the velocity values of Kuwahara are too low by about 3m/sec. With almost equal certainty, the discrepancy can be attributed to a measurement of the isothermal compressibility of pure water that is slightly too high.

Because of the lack of independent data, one cannot make any definite comment on the slight differences in the salinity dependence in the two cases. Further direct measurements of sea water compressibility would be useful here.

Finally, as a practical step, it is strongly urged that the formula of Del Grosso be employed in all future calculations of sound velocity from BT data.

ACKNOWLEDGMENTS

The author wishes to thank Doctors Ernest R. Anderson and James Stewart of the U. S. Navy Electronics Laboratory, San Diego for many helpful comments and suggestions during the course of this study. The study was carried out during visits at the Navy Electronics Laboratory and at the Physics Department of the University of California at Los Angeles in the summer and fall of 1953.

REFERENCES

Amagat, E. H.
1893. Mémoires sur l'élasticité et la dilatation des fluides jusqu'aux très hautes pressions. Ann. Chim. (Phys.), (6) *29:* 505–574.

Bridgmann, P. W.
1913. Thermodynamic properties of liquid water to 80° and 12000 kgm. Proc. Amer. Acad. Arts Sci., *48:* 307–362.

Del Grosso, V. A.
1952. The velocity of sound in sea water at zero depth. NRL Rep. 4002. 39 pp.

Dorsey, N. E.
1940. Properties of Ordinary Water Substance. Reinhold Publ. Co., N. Y. 673 pp. (see pp. 207–249).

Ekman, V. W.
1908. Die Zussamendrueckbarkeit des Meerwassers nebst Werten fuer Wasser and Quecksilber. Publ. Circ. Cons. Explor. Mer, No. 43: 1–47.

Hubbard, J. C. and A. L. Loomis.
1928. The velocity of sound in liquids at high frequencies by the sonic interferometer. Phil. Mag., (7) *5:* 1177–1190.

Knudsen, Martin
1901. Hydrographical Tables. G. E. C. Gad, Copenhagen. 63 pp.

Krümmel, Otto
1907. Handbuch der Ozeanographie. J. Engelhorn, Stuttgart. 2 vol. 1392 pp. (see p. 279).

Kuwahara, Susumu
1939. Velocity of sound in sea water and the calculation of the velocity for use in sonic sounding. Hydrogr. Rev., *16;* 123–140.

Lagemann, R. T., L. W. Gilley, and E. G. McLeroy
1953. The ultrasonic velocity, density and compressibility of supercooled H_2O and D_2O. J. chem. Phys., *21:* 819–821.

Lamb, Horace
1925. The dynamical theory of sound. Edward Arnold and Co. London. Second edition. 387 pp. (see pp. 177–186).
Matthews, D. J.
1939. Tables of the velocity of sound in pure water and sea water. 2nd ed. Brit. Admiralty Publ. H. D. 282. 29 pp.
Randall, C. R.
1932. Ultrasonic measurements of the compressibility of solutions and of solid particles in suspensions. Bur. Stand. J. Res., Wash., *8:* 79–99.
Stephenson, E. B. and F. J. Woodsmall
1941. The velocity of sound in sea water. NRL Rep. No. S-1722.
Tyrer, Daniel
1913. Adiabatic and isothermal compressibilities of some liquids between one and two atmospheres pressure. J. Chem. Soc., *103:* 1675–1688.
Weissler, Alfred and V. A. Del Grosso
1951. The velocity of sound in sea water. J. acoust. Soc. Amer., *23:* 219–223.

DETERMINATION OF INORGANIC PHOSPHATE IN SEA WATER BY AN ISO-BUTANOL EXTRACTION PROCEDURE[1]

By

CHARLES M. PROCTOR[2] AND DONALD W. HOOD

Texas Agricultural and Mechanical College
Department of Oceanography

ABSTRACT

A method is described for the determination of inorganic phosphate in sea water by extraction of the phosphomolybdate complex into iso-butanol and by reduction in the organic phase with stannous chloride. The color does not fade in 75 minutes. Arsenic and silicate, in amounts ordinarily encountered in sea water, do not interfere. The method is an order of magnitude more sensitive than others in current use and has the same relative accuracy.

INTRODUCTION

Phosphate is intimately involved in the fixation of energy by plants (Calvin, 1953) and in the assimilation, storage, and utilization of food and energy by both animals and plants (McElroy and Glass, 1951, 1952). Phosphorus in the form of phosphate, which is the only form demonstrated so far in protoplasm, thus ranks as one of the trace elements essential to life. The maximum concentration of inorganic phosphate observed in the open sea is 3 μM (micro molar), with 2 μM being the highest concentration generally encountered (Wooster and Rakestraw, 1951). Values of 0.00 μM are often reported, even in areas of great biological activity. This value, however, is below the limit of sensitivity of the Denigés (1920) method for phosphate, as usually employed (Griswold, et al., 1951; Harvey, 1948; Hansen and Robinson, 1953; Robinson and Thompson, 1948a; Rockstein and Herron, 1951; Wooster and Rakestraw, 1951). A more sensitive method is therefore needed to investigate these areas of low phosphate concentration.

[1] Contribution No. 32 from the Department of Oceanography, Texas A. & M. This work was supported in part by the Reynolds Metals Company, the Office of Naval Research (Project NR 083 036, N7onr-487 T.O. 2), and the Bureau of Ships (RE 120219-5), and was presented as a technical report on these projects (Proctor, 1953). A preliminary report was presented at the 8th Southwest Regional Meeting, American Chemical Society, Little Rock, Arkansas, December 5, 1952 (Proctor and Hood, 1952).

[2] Dow Fellow in Chemical Oceanography

The molybdenum-blue method for determination of phosphate, introduced by Osmond (1887), is the basis of nearly all modern microanalytical methods for phosphorus. In Osmond's method the sample is treated with molybdic acid. The resulting phosphomolybdate precipitate is then dissolved with stannous chloride solution to give the phosphomolybdenum blue color. For determination of phosphate in sea water, reference is usually made to the procedure of Denigés (1920). Although visual color comparison methods are still often used in field work and on shipboard (Robinson and Thompson, 1948), the method is usually adapted to the photoelectric colorimeter with modifications to suit the material being analyzed (Griswold, et al., 1951; Harvey, 1948; Rockstein and Herron, 1951; and Wooster and Rakestraw, 1951). Increased sensitivity may be obtained by using a colorimeter absorption cell with a long light path (Harvey, 1948) or by taking a large sample and concentrating it for analysis with standard absorption cells. The latter course is complicated in sea water, since concentration of the sample gives a high salt content which interferes with formation of the phosphomolybdate complex. The present method is based on the observation of Denigés that the phosphomolybdate complex is soluble in organic solvents. The blue color may then be developed by reduction in the organic phase. The phosphomolybdenum blue is thus concentrated without increasing the salt interference, and greater sensitivity becomes practical with standard colorimetric equipment. Interference from citrate, nitrite, fluoride, oxalate (Berenblum and Chain, 1938) and other unspecified ions (Rodden, 1950) are also reduced or eliminated.

METHOD

Reagents. Analytical Reagent (ACS) grade chemicals and distilled water were used throughout.

Sulfuric Acid: 18N and 1.2N.

Wash Acid: 1.2N H_2SO_4 saturated with iso-butanol (i-BuOH) at room temperature (about 10% i-BuOH).

Ammonium Molybdate: 10% solution stored in polyethylene bottle.

Stannous Chloride Solution: 2% in 2.4N HCl. Dissolve 2.3g $SnCl_2 \cdot 2H_2O$ in 20 ml of 12N HCl. Dilute to 100 ml and store in dark bottle with a few pieces of mossy tin. Stable for several months.

Reducing Solution: 2 ml of stannous chloride solution added to 100 ml of wash acid. Mix as needed. Stable for about half a day.

Phosphate Stock Standard: 3mM. 0.408g of KH_2PO_4 added to one liter of distilled water. One ml of CCl_4 was added to prevent growth of molds or bacteria.

Phosphate Working Standards were made as needed by diluting the stock standard with artificial sea water, or with distilled water when required. CCl_4 was used as preservative.

Artificial Sea Water, Lyman and Fleming (1940). For 20 liters use: NaCl, 470 g; $MgCl_2.6H_2O$, 213 g; Na_2SO_4, 78.3 g; KCl, 13.2 g; $NaHCO_3$, 3.84 g; KBr, 1.92 g; NaF, 0.060 g; dissolve in about 15 l of distilled water.

$CaCl_2.2H_2O$, 29.4 g; $SrCl_2$, 0.48 g; dissolve separately in about 2 liters.

H_3BO_3, 0.52 g; dissolve in about 100 ml of hot water.

Add the alkaline earth solution slowly to the solution of salts with vigorous mixing, then add the boric acid. Dilute to 20 l and mix well. A 20 l carboy with siphon tube was used for storage. Final mixing was accomplished by aspirating air through the siphon tube. About 10 ml of CCl_4 were added as preservative.

Iso-Butanol and Iso-Propanol (or ethanol).[3]

Instrument. The Beckman Model B Spectrophotometer with 1 cm Corex cells was used for absorbancy readings. The sensitivity control on the instrument permits readings over most of the range from 0 to 2 absorbancy units (see Fig. 4).

Procedure. 75.0 ml samples of sea water, 0.02 to 10 μM in phosphate (0.04 to 20 γ of P), are run into 200 ml separatory funnels. The samples should be at room temperature. Add 5.0 ml of 18N H_2SO_4 to each, then add 5.0 ml of 10% ammonium molybdate. The samples should be swirled in the flasks while adding these reagents so that local concentrations do not build up. Add 15.0 ml of i-BuOH to each funnel and shake for one minute to extract the phosphomolybdate complex (see Notes 1, 2). Discard the aqueous layer. Back extract the organic layer twice with 25 ml portions of wash acid and discard the aqueous layers (see Notes 2, 3, 4), then add 10 ml of reducing solution and shake for one minute. Discard the aqueous layer and back extract once with 25 ml of wash acid. Mix 3.00 ml of the i-BuOH layer with 0.30 ml of i-PrOH (see Note 5) and read the absorbancy at 730 mμ in a 1 cm Corex cell. The spectrophotometer is set at zero with 3.00 ml of i-BuOH that had been equilibrated with acidified sea water. 0.30 ml of i-PrOH was added to prevent "fog." A reagent blank was obtained with distilled water.

[3] Abbreviations, respectively, are: i-BuOH, i-PrOH, EtOH.

Note 1. Part of the i-BuOH dissolves in the sea water, leaving an organic phase of about 7 ml. The solubility of i-BuOH is temperature dependent, hence samples to be compared must be run at the same temperature.

Note 2. One minute of shaking for the extraction and a half minute for the back extractions seem to be sufficient.

Note 3. The wash acid and reducing solution are saturated with i-BuOH so that concentration of phosphomolybdate in the organic phase should remain constant after extraction. Slight losses of the i-BuOH phase are then unimportant, as a 3.00 ml aliquot is used for absorbancy readings.

Note 4. Broken tip pipettes of 10 and 25 ml capacity were cut off just below the bulb. They made convenient finger pipettes for addition of reducing solution and wash acid respectively. These volumes are not critical.

Note 5. The i-PrOH, or EtOH, prevents separation of water droplets from the i-BuOH solution which might "fog" the absorption cell windows.

Estimation of Absolute Concentration. The phosphate concentration of part of the sample is increased by a known amount, usually 0.5 to 2.0 μM, by "spiking" with a small quantity of concentrated phosphate standard. The absorbancies with and without spike are compared and the phosphate content of the sample is determined by graphical or numerical extrapolation to zero absorbancy (see Fig. 2). The absorbancy increase due to the spike should be the same for all samples and will serve as a check on the method.

EXPERIMENTAL

Spectrum. The absorbancy spectrum of phosphomolybdenum blue in the iso-butanol layer is shown in Fig. 1. Water-saturated i-BuOH with i-PrOH added was used to set the instrument to zero. A spectrum of water-saturated BuOH, with i-PrOH, was determined against butanol and is shown at the bottom of Fig. 1. No appreciable absorption due to the water and i-PrOH was noticed below 900 mμ. The spectrum of i-BuOH was checked against BuOH. No differences between the spectra were found at wavelengths below 900 mμ.

Color Stability. Tests were made of samples of artificial sea water with phosphate added to increase the concentration by 3.0 μM, of distilled water with 3.3 μM of added phosphate, and of Port Aransas channel water with no added phosphate; absorbancies were compared over a four hour period. Table I gives these results. The artificial sea water sample showed considerable fading after the second hour,

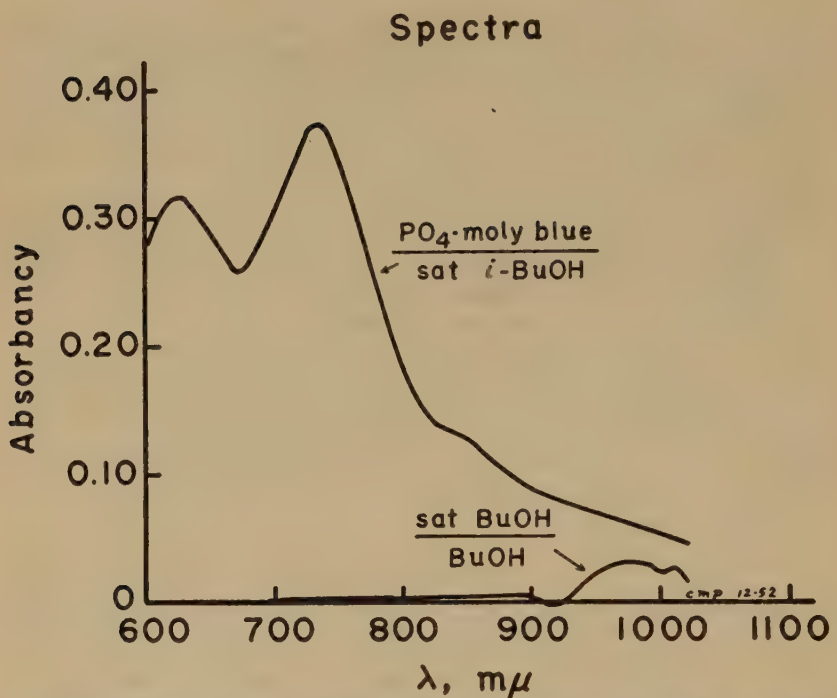

Figure 1. Spectrum of phosphomolybdenum blue against solvent. Absorption maximum is at 730–735 mμ. Spectrum of water-saturated BuOH (with i-PrOH added to prevent "fog") against BuOH shows absorption only above 900 mμ. The spectra of BuOH and i-BuOH were indistinguishable below 900 mμ.

which was not noticed in natural sea water. To check this result, fading tests were made with several concentrations of added phosphate in the natural sea water. The data in Table II indicate that fading is inconsequential in the first 75 minutes.

TABLE I. Color Stability. Absorbancy Change with Time

	Time after reduction (min.)					
	5	*10*	*20*	*60*	*120*	*240*
Distilled water blank	0.003	0.003	0.004	0.005	0.004	0.002
H_2O + 3.3 μM PO_4	0.658	0.661	0.664	0.667	0.663	0.665
Sea Water (Port Aransas)	0.093	0.094	0.095	0.095	0.096	0.096
Artificial S. W. + 3.0 μM PO_4	0.563	0.567	0.571	0.563	0.554	0.538

Sensitivity. The data in Table II have a spread typical of small groups of samples. They have been plotted in Figs. 2 and 3. The mean absorbancy coefficient was found to be 0.19, using the equation

$$A = \log \frac{I_0}{I_t} = Elc$$

where

A = absorbancy (optical density), I_0 = incident light intensity, I_t = transmitted light intensity, E = micromolar absorbancy coefficient, l = length of light path through cell in cm, and c = concentration in micromoles. This is nearly ten times the value of about 0.022 which is the micromolar absorbancy coefficient of some recent

TABLE II. Color Stability. Sea Water from Port Aransas with Added Phosphate

Added PO_4	*30 min.*	*75 min.*
0.00 μM	0.091	0.092
0.10	0.112	0.114
0.20	0.127	0.128
0.30	0.148	0.148
3.00	0.604	0.600

methods that use various reaction conditions adapted to biological and other materials. (Boltz and Mellon, 1947; Griswold, et al., 1951; Wooster and Rakestraw, 1951).

Interferences. Of the substances that interfere with the formation of phosphomolybdenum blue (Boltz and Mellon, 1947), the only ones that are present in sea water in sufficient concentration to cause trouble are: *chloride*, *silicate* and *arsenate*. Chloride in high concentration probably replaces part of the molybdate in the phosphomolybdate complex. Arsenate and silicate form blue molybdate complexes similar to that formed by phosphate.

The chloride effect is shown in Fig. 4. It will be noted that the tests made at 12 and 18‰[4] chloride content are almost indistinguishable but are significantly different from those made with zero chloride. It is possible then to compensate for chloride effects in sea water by using phosphate standards made with artificial sea water or with filtered, low phosphate sea water.

The usual range of silicate in sea water is from 0.0 to about 200 μM (Robinson and Thompson, 1948b). In the first trials of this extraction method, the amount of acid (5 ml of 10N H_2SO_4) and ammonium molybdate (5 ml of 5%) were essentially those used by Berenblum and Chain (1938) for phosphate in biological materials. Some color production by silicate was found under these conditions. By increasing the acid concentration to 18N (final strength in the

[4] ‰ = per mille, parts per thousand.

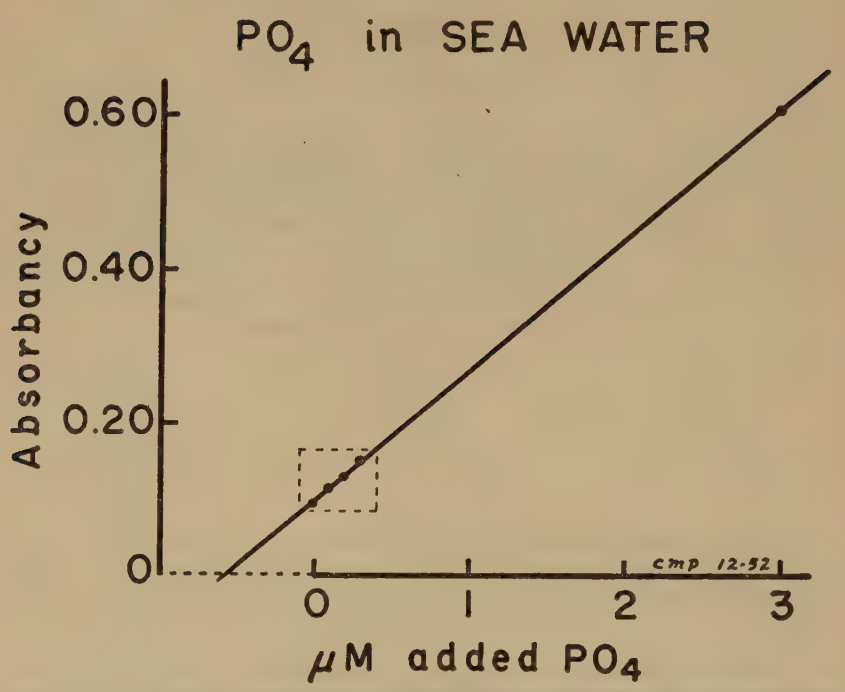

Figure 2. Absorbancy plotted against phosphate added to sea water. The lower part of the line is shown expanded in Fig. 3. By extrapolation to zero absorbancy, the phosphate concentration of the sample was found to be 0.54 μM (intercept on concentration axis is at −0.54 μM).

reaction mixture 1.2N) and by increasing molybdate to 10% (final, 0.6%), silicate interference was eliminated as shown in Fig. 4. The high acidity, and consequently high molybdate concentration (Harvey, 1948), are in marked contrast to the conditions of the Wooster and Rakestraw (1951) method for phosphate in sea water. Wooster and Rakestraw gave no data on silicate interference, but one of us (Proctor, 1953) has found that silicate additions amounting to 40, 80, and 133 μM do not interfere in the Wooster-Rakestraw phosphate determination.

Total arsenic in sea water usually varies between 0.2 and 0.5 μM (Gorgy, et al., 1948). Of this, only part is present as arsenate. Tests were made to determine the absorbancy due to added arsenate. 13 μM arsenate gave an absorbancy increment less than that due to 1 μM of added phosphate. On this basis, the maximum error in phosphate determination, if all the arsenic in sea water were in the form of arsenate, would be only about 0.03 μM. Arsenite, the pre-

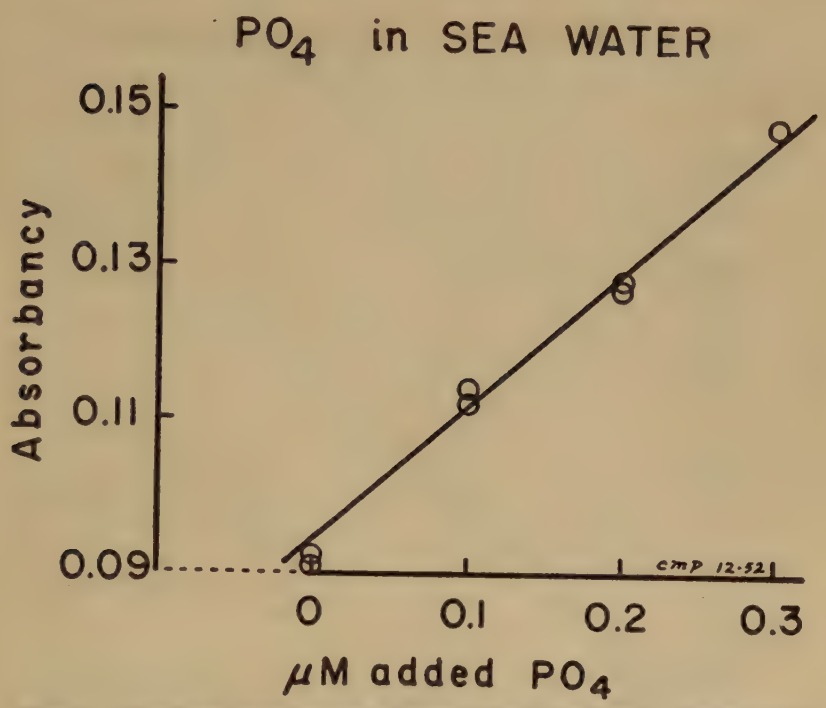

Figure 3. Absorbancy plotted against phosphate added to sea water. This is an expansion of the lower part of the graph shown in Fig. 2. The increase in absorbancy per μM of added phosphate is nearly 10 times that obtained with current methods.

dominant form in sea water, causes a relatively small error (Hansen and Robinson, 1953).

Partition of Acid Between Artificial Sea Water and iso-Butanol. To determine the possible change in acidity due to the extraction procedure, the following test was made at 25°. Artificial sea water, acidified with H_2SO_4, was equilibrated with iso-butanol. The volume of the aqueous layer was 83 ml, of the organic layer 19 ml. Aliquots of each layer were titrated with N/20 NaOH to the methyl orange end point. The acid normality of the aqueous layer was 1.03, the organic layer 0.105. The partition ratio of titratable acids of the kinds present in H_2SO_4 acidified artificial sea water is thus 10:1 between the water and iso-butanol layers. The decrease in acidity from this cause does not affect the determination (see also Harvey, 1948).

Interference by Stopcock Lubricant. Two portions of acidified sea water, with no molybdate, were extracted with i-BuOH in 125 ml

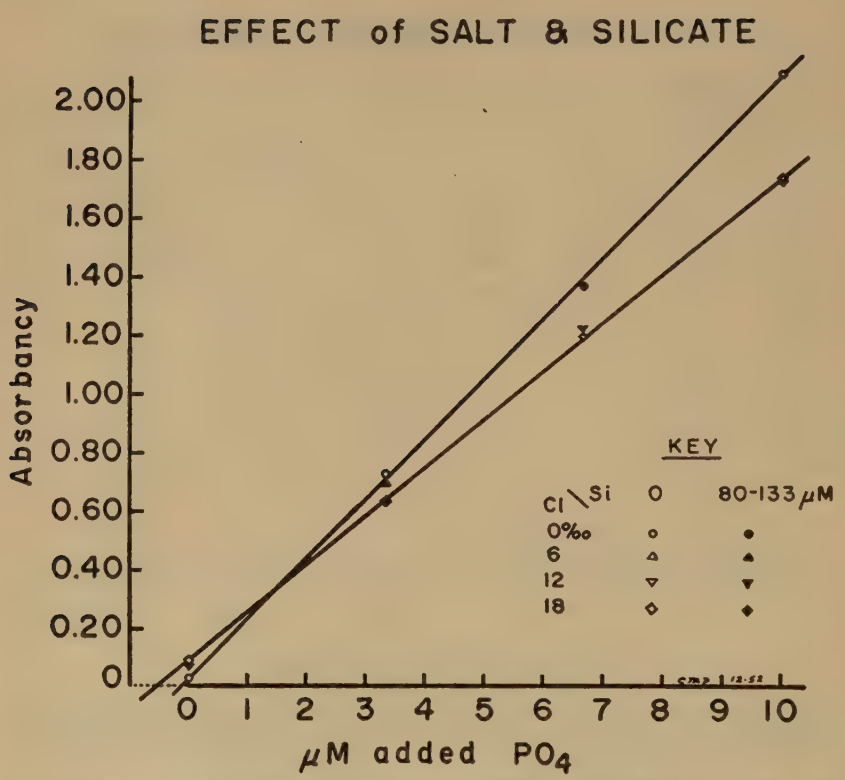

Figure 4. Salt and silicate effects on phosphate determination in distilled water (0 °/₀₀ Cl) and in artificial sea water. Upper line at 0 °/₀₀ chlorinity, lower at 12 and 18 °/₀₀. No difference was noted between 12 and 18 °/₀₀. The data were incomplete at 6 °/₀₀. The effect of 80 to 133 μM silicate was negligible. Note that the graphs are linear over the entire absorbancy range.

pyrex bottles. The bottom of the ground glass stopper of one of these bottles was smeared with *Lubriseal* brand stopcock lubricant (distributed by A. H. Thomas Company, Philadelphia).[5] The absorbancies of the two i-BuOH layers were compared over the spectral range from 600 to 1020 mμ. The difference in absorbancies was zero at each wave length.

DISCUSSION

The method of phosphate analysis presented here is an order of magnitude more sensitive than methods currently in use and has

[5] This is a report of a test run on one sample and does not necessarily constitute an endorsement of the product or a statement of its uniformity.

about the same relative accuracy. It is also subject to fewer interferences (Berenblum and Chain, 1938). It will serve for study of low concentrations of phosphate and of changes in phosphate concentration that are too near the limit of resolution of current methods.

Day to day reproducibility of the method is not as good as could be desired. This is not a serious drawback, however, since it is necessary to run frequent controls with any colorimetric procedure. No difficulty in getting check results within each group of analyses need be expected if each step in the procedure is made routine. Temperature control was not used in these studies. The laboratory temperature usually changed less than one degree during the course of an analysis and no difficulty from this source was experienced. However, samples should be allowed to come to room temperature before extraction.

The phosphomolybdate concentration of the iso-butanol layer should not change after extraction. By having the wash acid and the reducing solution at the same temperature as the extracts and just saturated with iso-butanol, the concentration of the extracts will not change due to iso-butanol dissolving in the wash solutions or by addition of excess iso-butanol.

A single extraction with iso-butanol is sufficient for the analytical procedure. The various aqueous layers from the extraction, washing, and reduction were collected in a jug. This waste mixture was usually colorless or only a faint blue, indicating complete extraction of phosphomolybdate. Phosphate solution added to the waste mixture gave the expected blue color. Since the analytical results were consistent, no further investigation of extraction efficiency was made.

The phosphomolybdate complex is soluble in various organic solvents (Denigés, 1920), including amyl alcohol. The lower solubility of amyl alcohol in water (2.7% at 22°) may be advantageous if large volumes of sea water are to be extracted.

REFERENCES

Berenblum, I and E. Chain
1938. Studies on the colorimetric determination of phosphorus. Biochem. J., *32:* 286–298.

Boltz, D. F. and M. G. Mellon
1947. Determination of phosphorus, germanium, silicon, and arsenic by the heteropoly blue method. Industr. Engng. Chem., Anal. Ed., *19:* 873–877.

Calvin, M.
1953. The path of carbon in photosynthesis. Chem. and Engng. News, *31:* 1622–1625.

Denigés, G.
1920. Réaction de coloration extrememement sensible des phosphates et des arséniates. See applications. C. R. Acad. Sci., Paris, *171:* 802–804.

Gorgy, A., N. W. Rakestraw, and D. L. Fox
1948. Arsenic in the sea. J. Mar. Res., *7:* 22–32.
Griswold, B. L., F. L. Humoller, and A. R. McIntyre
1951. Inorganic phosphate and phosphate esters in tissue extracts. Anal. Chem., *23:* 192–194.
Harvey, W. H.
1948. The estimation of phosphate and of total phosphorus in sea waters. J. Mar. Biol. Ass. U. K., *27:* 337–359.
Hansen, A. L. and R. J. Robinson
1953. The determination of organic phosphorus in sea water with perchloric acid oxidation. J. Mar. Res., *12:* 31–42.
Lyman, J. and R. H. Fleming
1940. The composition of sea water. J. Mar. Res., *3:* 134–146.
McElory, W. D. and B. Glass, editors
1951 & 1952. A symposium on phosphorus metabolism. Volumes I and II. The Johns Hopkins Press, Baltimore. 762 and 930 pp.
Osmond, F.
1887. Über eine Reaction, welche die kolorimetrische Bestimmung des Phosphors in Gusseisen, Stahl, u. s. w. ermoglicht. Bull. soc. chim., Paris, xlvii: 745–748; cf., Ber. dtsch. chem. Ges., *20:* 750c; J. Chem. Soc., *52*: 999.
Proctor, C. M.
1953. Determination of inorganic phosphate in sea water by a butanol extraction procedure. Texas A & M Research Foundation, Project 24, Tech. Rep. No. 7, and Appendix I to Project 40, Final Rep. June 22.
Proctor, C. M. and D. W. Hood
1952. Phosphates in sea water determined by a butanol extraction procedure (abstract). Anal. Chem., *24*: 2016.
Robinson, R. J. and T. G. Thompson
1948a. Determination of phosphates in sea water. J. Mar. Res., *7:* 33–41.
1948b. The determination of silicate in sea water. J. Mar. Res., *7:* 49–55.
Rockstein, M. and P. W. Herron
1951. Colorimetric determination of phosphate in microgram quantities. Anal. Chem., *23:* 1500–1501.
Rodden, C. J., Editor-in-chief
1950. Analytical Chemistry of the Manhattan Project. National Nuclear Energy Series VIII–1. McGraw-Hill, New York. 748 pp. (see pp. 324–328).
Wooster, W. S. and N. W. Rakestraw
1951. Estimation of dissolved phosphates in sea water. J. Mar. Res., *10:* 91–100.

A STUDY OF THE SALT BALANCE IN A COASTAL PLAIN ESTUARY[1]

By

D. W. PRITCHARD

Chesapeake Bay Institute, The Johns Hopkins University

ABSTRACT

Observations of salinity and current velocity taken in the James River estuary are used in this investigation. Time means are taken over several tidal cycles and the nonadvective motions and nonadvective salt flux are related to these means. The analysis shows that in the James River estuary the horizontal advective flux and the vertical nonadvective flux of salt are the most important factors in maintaining the salt balance. The vertical advective flux is of secondary importance but is still significant. The horizontal nonadvective flux of salt is small. In addition, the vertical nonadvective flux of salt is partly related to the magnitude of the oscillatory tidal currents.

INTRODUCTION

The extensive observations of salinity and current velocity, made during the summer of 1950 in the James River estuary,[2] form the basis for the present study of the variation and relative importance of factors that maintain the salt balance. Fig. 1 shows the curves for typical mean salinity vs. depth as well as horizontal mean velocity vs. depth for the James River estuary. The salinity increases horizontally from fresh water at the head of the estuary to approximately 20 ‰ at the mouth of the James where it joins the Chesapeake Bay. The character of the vertical distribution does not change much longitudinally. Consequently the horizontal gradients do not vary appreciably with depth. This indicates that there is appreciable vertical mixing of the upper and lower layers. The lower layers are of higher salinity and flow toward the head of the estuary while the upper layers are of lower salinity and flow seaward.

[1] Contribution No. 16 from the Chesapeake Bay Institute. This work was supported by the office of Naval Research, the State of Maryland (Department of Research and Education), and the Commonwealth of Virginia (Virginia Fisheries Laboratory).

[2] Pritchard, D. W. 1952. Salinity distribution and circulation in the Chesapeake Bay estuarine system. J. Mar. Res., *11:* 106–123.

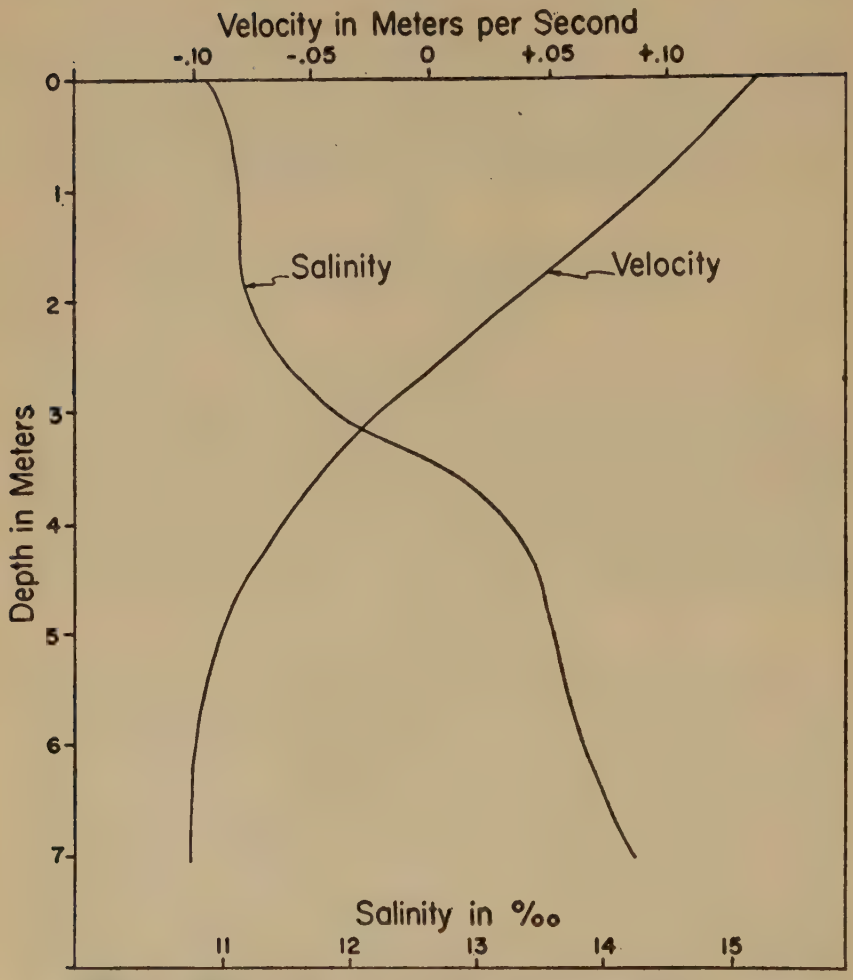

1. Typical mean salinity *versus* depth curve and horizontal mean velocity *versus* depth curve for the James River estuary.

THE BASIC SALT BALANCE EQUATION

Consider a left-handed coordinate system with the origin at the surface in the fresh water at the head of the estuary. The x_1 coordinate is directed down the estuary along the central axis, and the x_2 coordinate points vertically downward; the lateral coordinate x_3 is directed horizontally from the center of the estuary toward the right-hand shore.

Neglecting molecular diffusion, the instantaneous local rate of change of the salt concentration, s, is given by

$$\partial s/\partial t = -\frac{\partial(v_i s)}{\partial x_i} . \tag{1}$$

The instantaneous velocity, v_i, may be expressed as the sum of three terms: (1) a mean velocity $\bar{v}_i$, obtained by averaging over one or more tidal cycles; (2) a tidal velocity U_i, which we assume is directed up and down the estuary and which is given simply by $U_0 \cos \varphi$, where U_0 is the amplitude of the tidal current and φ represents the sum of the angular time argument of tidal period plus a phase angle; (3) a velocity deviation relative to a time average, designated as v_i'. Thus

$$v_i = \bar{v}_i + U_i + v_i'. \tag{2}$$

In a similar manner, the instantaneous value of salinity is expressed by

$$s = \bar{s} + (s)_u + s', \tag{3}$$

where $\bar{s}$ is the time mean salt content, $(s)_u$ the periodic variation in salt content related to tidal motion [assumed to be given simply by $(s)_u = (s)_0 \sin \varphi$], and s' the salinity deviation relative to a time average. Substituting (2) and (3) into (1), and taking the time average over one or more tidal cycles, we have

$$<\partial s/\partial t> = -\frac{\partial}{\partial x_i}(\bar{v}_i\bar{s}) - \frac{\partial}{\partial x_i}<U_i(s)_u> - \frac{\partial}{\partial x_i}<U_i s'> - \frac{\partial}{\partial x_i}<(s)_u v_i'> - \frac{\partial}{\partial x_i}<v_i' s'>. \tag{4}$$

But if U_i is given by $U_0 \cos \varphi$ and $(s)_u$ by $(s)_0 \sin \varphi$, then the mean product $<U_i(s)_u>$ over one or more tidal cycles becomes zero. The terms involving $<U_i s'>$ and $<(s)_u v'_i>$ depend on the correlation between the velocity and salinity deviations on the one hand and the tidal period on the other. Assuming that no such correlations exist, these terms would also vanish with time averages over one or more tidal cycles. (There may well be a direct relation between the tidal period and the root mean square of the velocity deviations. However, this does not imply a correlation between the tidal period and the individual velocity deviations.) Hence (4) becomes

$$<\partial s/\partial t> = -\frac{\partial}{\partial x_i}(\bar{v}_i\bar{s}) - \frac{\partial}{\partial x_i}<v_i' s'>. \tag{5}$$

Note that the terms involving the simple harmonic tidal fluctuations have been eliminated.

Equation (5) states that the local time mean change in concentration results from two terms, one related to the mean advection, the second to nonadvective processes. Oceanographers and meteorologists have called the latter process "diffusion" and have replaced the mean product $<v_i's'>$ by the so-called diffusion terms having the general form $-A_i\,\partial\bar{s}/\partial x_i$.

Equations (1) and (5) apply to an infinitesimal element in the fluid. The nature of the observations makes it convenient to study the salt balance in an element extending across the estuary laterally. In this element the variations in the velocity and salinity in the x_3 direction are neglected and the resulting salt balance equation will differ from the basic equation (1).

Consider the continuity of salt within an element of volume extending across the estuary at level x_2, which has an infinitesimal length dx_1 and an infinitesimal height dx_2. There can be no transport of salt through the ends of the element which are the sides of the estuary. Since the width of the estuary decreases with depth, the area of the top surface of the element is greater than that of the bottom surface. Likewise, the area of the downstream surface is different from that of the upstream surface, since the width of the estuary varies in the longitudinal direction. For such an element it can be shown that

$$\partial s/\partial t = -\frac{1}{w}\frac{\partial}{\partial x_1}(wv_1s) - \frac{1}{w}\frac{\partial}{\partial x_2}(wv_2s), \tag{6}$$

where w is the width of the estuary at the depth x_2. If we now take the time mean of equation (6) in the same manner as was done with equation (1), we obtain

$$\begin{aligned} <\partial s/\partial t> = &-\frac{1}{w}\frac{\partial}{\partial x_1}(w\bar{v}_1\bar{s}) - \frac{1}{w}\frac{\partial}{\partial x_2}(w\bar{v}_2\bar{s}) \\ &-\frac{1}{w}\frac{\partial}{\partial x_1}\{w<v_1's'>\} - \frac{1}{w}\frac{\partial}{\partial x_2}\{w<v_2's'>\}. \end{aligned} \tag{7}$$

For the element under consideration, the equation of continuity is

$$\frac{\partial}{\partial x_1}(w\bar{v}_1) + \frac{\partial}{\partial x_2}(w\bar{v}_2) = 0. \tag{8}$$

Utilizing this relationship, equation (7) becomes

$$(9) \qquad <\partial s/\partial t> = -\bar{v}_1\,\partial\bar{s}/\partial x_1 - \bar{v}_2\,\partial\bar{s}/\partial x_2 - \frac{1}{w}\frac{\partial}{\partial x_1}\{w<v_1's'>\} - \frac{1}{w}\frac{\partial}{\partial x_2}\{w<v_2's'>\}.$$

Note that, as in the case of equation (5), terms involving the harmonic variations due to the tides are absent from equation (9). The variation in the terms of equation (9) and the relative importance of the processes which they represent in maintaining the salt balance are the objects of our study.

THE MEAN LOCAL TIME CHANGE

It is here assumed that the time mean of the instantaneous local time change of salinity, $<\partial s/\partial t>$, is given approximately by the increment of mean salinity change per unit time, that is $\Delta\bar{s}/\Delta t$. The field program in the James River was undertaken during a period when conditions approximated the mean steady state in salinity distribution. During all three periods of investigation the mean local time variation $<\partial s/\partial t>$ was less than 2×10^{-3} g/m³/sec.

THE LONGITUDINAL TERMS IN THE SALT BALANCE EQUATION

There are two longitudinal terms in the salt balance equation, an advective term $\bar{v}_1\,\partial\bar{s}/\partial x_1$ and a nonadvective term $\frac{1}{w}\frac{\partial}{\partial x_1}\{w<v_1's'>\}$. Sufficient velocity and salinity measurements were made in the James River study to evaluate the advective term. To determine the significance of the turbulent mixing term, the following treatment of equation (1) is required.

Consider a segment of the estuary bounded at either end by a cross-section. Designating the total salt content within the segment by $S = \iiint_{Vol} s\,dv$, where V is the volume of the segment, we have from (1)

$$(10) \qquad \frac{\partial S}{\partial t} = \iiint_{\text{Vol}} \frac{\partial s}{\partial t}\,dV = -\iiint_{\text{Vol}} \frac{\partial}{\partial x_i}(v_i s)\,dV = -\iint_{\sigma} v_i s\,d\sigma_i\,,$$

where $\iint_{\sigma} d\sigma_i$ represents the integral over the bounding surfaces of the segment. The time mean of this equation may be taken, following the same procedure which was utilized in obtaining equation (5) from equation (1). We then have

$$\left\langle \frac{\partial S}{\partial t} \right\rangle = - \iint_{\sigma} \bar{v}_i \bar{s} d\sigma_i - \iint_{\sigma} \langle v_i' s' \rangle d\sigma_i. \tag{11}$$

For steady state $\langle \partial S/\partial t \rangle = 0$, and hence

$$\iint_{\sigma} \bar{v}_i \bar{s} d\sigma_i + \iint_{\sigma} \langle v_i' s' \rangle d\sigma_i = 0 . \tag{12}$$

Since the segment under study is bounded by the surface, bottom and sides of the estuary, only the horizontal terms in equation (12) need be considered. Equation (12) becomes

$$\iint_{\sigma} \bar{v}_1 \bar{s} d\sigma_1 + \iint_{\sigma} \langle v_1' s' \rangle d\sigma_1 = 0 . \tag{13}$$

For an evaluation of the first term of equation (13), observations of mean salinity and velocity for nine separate cases are available. It is convenient, both for the present discussion and for later analysis, to consider their first integral in two parts, one term involving the upper layer, where the mean velocity is positive, the other term involving the lower layer, where the mean velocity is negative. The value of the integral $\iint_{\sigma} \langle v_1' s' \rangle d\sigma_1$, as determined from equation (13), was in all cases less than 5% and in six of the nine cases less than 1% of either of the two parts of the first term in equation (13). This means that the salinity balance within a segment bounded by the surface and the bottom is maintained primarily by horizontal advection, the horizontal diffusion being of only slight importance.

The mean value of the term $\frac{1}{w} \frac{\partial}{\partial x_1} \{ w \langle v_1' s' \rangle \}$, as determined from the mean value of the integral $\iint_{\sigma} \langle v_1' s' \rangle d\sigma_1$, was two orders of magnitude less than the horizontal advective term $\bar{v}_1 \, \partial \bar{s}/\partial x_1$. The latter term varied from about 5×10^{-2} g/m³/sec at the surface to -5×10^{-2}g/m³/sec near the bottom. The horizontal nonadvective term was of the order of only 5×10^{-4}g/m³/sec, though its relative importance increased in the upstream direction.

THE VERTICAL ADVECTIVE TERM IN THE SALT BALANCE EQUATION

The second term on the right-hand side of equation (9) involves the mean vertical velocity. This parameter may be computed from the horizontal velocities by means of the concept of volume continuity. For nondivergent flow, $\partial \bar{v}_i/\partial x_i = 0$. Taking the integral of this expression over the volume V and applying Green's formula, we have

$$\iint_{\sigma} \bar{v}_i d\sigma_i = 0 , \tag{14}$$

a statement that the volume of water flowing into the segment bounded by the surface σ must equal the volume of water flowing out of the same segment. Equation (14) may be employed to evaluate the mean vertical velocity as a function of depth from measurements of the horizontal velocity at two sections.

A second method of computation of the mean vertical velocity involves the vertical integration of the equation of continuity in the form of equation (8). The horizontal gradient of the product $(w\bar{v}_1)$ can be found graphically for each depth and the integration can be carried out numerically, by using the boundary condition that the mean vertical velocity must be zero at the surface.

Computations by both methods were carried out for three periods by using three sections in the James River estuary. The calculations were made for depth increments of one-half meter. Though both methods are based on the same continuity concept, the mechanics of application lead to slightly different results. The average of the two computations of the mean vertical velocity for a typical section for the three periods is shown in Fig. 2.

The vertical velocity vs. depth curve is similar at a given station for different periods. The positive vertical velocities near the bottom probably are related to inconsistencies in the observed data, though they are of the correct order of magnitude to be related to the slope of the bottom.

The vertical advective term, $\bar{v}_2 \partial\bar{s}/\partial x_2$, may now be determined from the computed mean vertical velocities and from the observed mean vertical salinity gradients. It is significant only near the boundary between the upper and lower layer, where it attains a value of about 1×10^{-2}g/m^3/sec. On this boundary the horizontal advective term vanishes. At all other depths the horizontal advective term is considerably larger than the vertical term.

THE VERTICAL NONADVECTIVE TERM IN THE SALT BALANCE EQUATION

The remaining term in equation (9) involves the vertical deviation product $<v_2's'>$. Solving for this term, we have

$$<v_2's'> = -\frac{1}{w}\left\{\int w\left[\partial\bar{s}/\partial t + \bar{v}_1\,\partial\bar{s}/\partial x_1 + \bar{v}_2\,\partial\bar{s}/\partial x_2 + \frac{1}{w}\frac{\partial}{\partial x_2}\{w<v_1's'>\}\right] dx_2 + C\right\}. \tag{15}$$

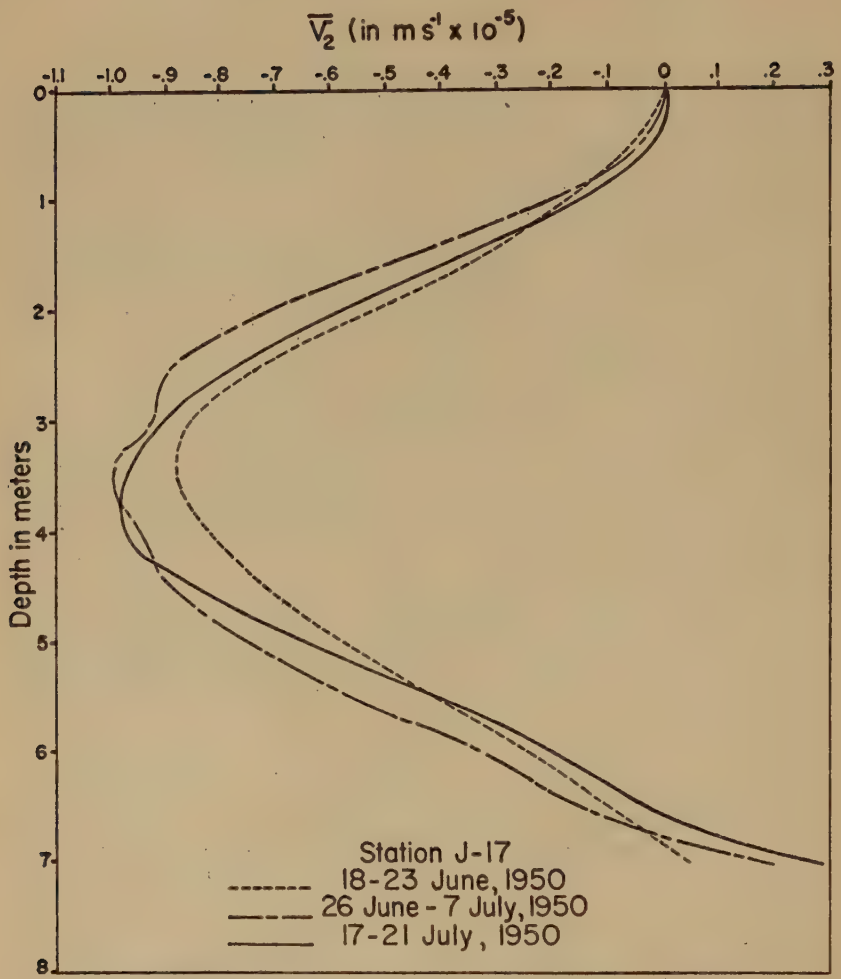

2. Mean vertical velocity *versus* depth for a typical section in the James River for the three different periods as indicated.

This equation may be solved numerically if enough boundary conditions are known to evaluate the constant C. The vertical deviation product should be zero both at the bottom and at the surface (neglecting the effect of rainfall and evaporation at the surface). Only one of these boundary conditions is needed to evaluate C. The consistency of the basic equation (9) and of the analysis of the data may be checked by the degree to which the second condition is met.

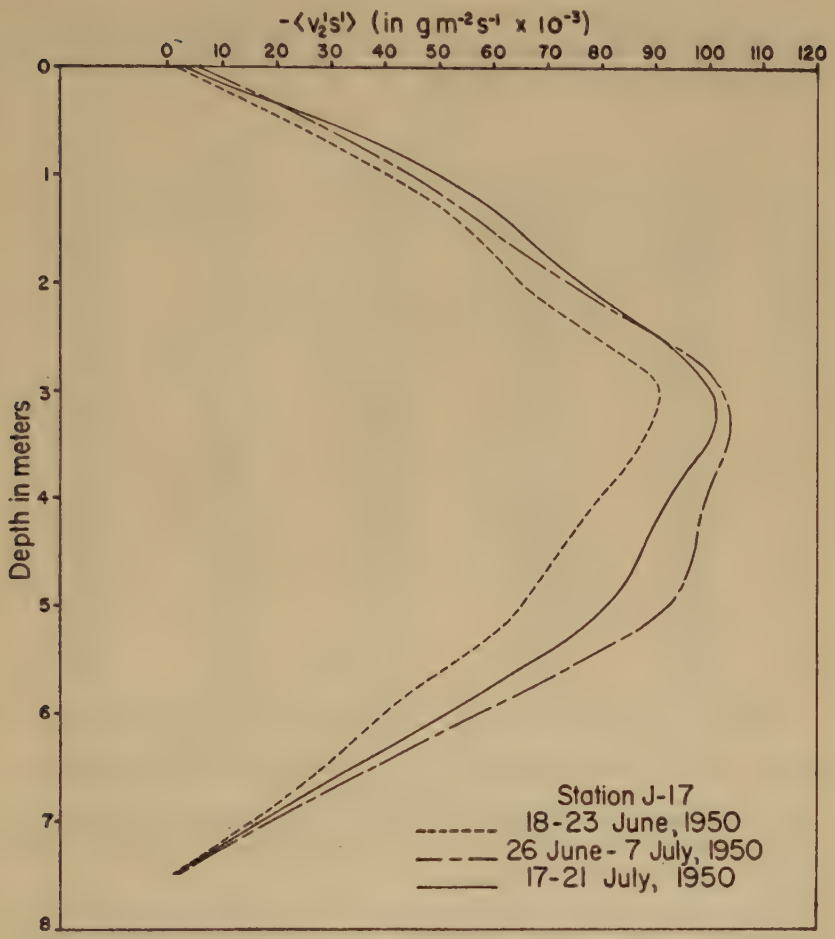

3. The vertical nonadvective flux of salt *versus* depth for a typical section in the James River for the three periods as indicated.

The value of $\langle v_2's' \rangle$ was taken as zero at the bottom boundary, and equation (15) was evaluated for $\langle v_2's' \rangle$ at each half meter interval of depth. The results of this evaluation for a typical section in the James River estuary for three different periods are shown in Fig. 3. The boundary condition at the surface is nearly satisfied in all cases, a result which serves to check the consistency of the form of the salt balance equation used here with the observed data.

It is now possible to discuss the relative magnitude of terms in equation (9). Table I gives the values of the terms for a typical station in the James River estuary.

TABLE I

Depth Meters	$\partial\bar{s}/\partial t$ $g\cdot m^{-3}\cdot s^{-1}$ $\times(10^4)$	$\bar{v}_1\,\partial\bar{s}/\partial x_1$ $g\cdot m^{-3}\cdot s^{-1}$ $\times(10^4)$	$\bar{v}_2\,\partial\bar{s}/\partial x_2$ $g\cdot m^{-3}\cdot s^{-1}$ $\times(10^4)$	$\frac{1}{w}\frac{\partial}{\partial x_1}\{w<v_1's'>\}$ $g\cdot m^{-3}\cdot s^{-1}$ $\times(10^4)$	$\frac{1}{w}\frac{\partial}{\partial x_2}\{w<v_2's'>\}$ $g\cdot m^{-3}\cdot s^{-1}$ $\times(10^4)$
0.0	−4.2	484.0	0.0	1.3	−481.1
0.5	−3.6	407.0	−1.0	1.3	−403.7
1.0	−1.0	326.0	−1.4	1.3	−324.6
1.5	0.0	238.0	−1.9	0.6	−236.7
2.0	−0.1	159.0	−4.2	0.2	−154.9
2.5	0.1	88.0	−21.9	−1.0	−65.2
3.0	0.8	−8.0	−117.0	−0.8	125.0
3.5	2.5	−118.0	−154.8	−0.6	270.9
4.0	4.8	−219.0	−81.0	−0.6	295.8
4.5	15.5	−279.0	−33.8	−0.6	297.9
5.0	14.5	−288.0	−13.7	−0.4	287.6
5.5	10.0	−278.0	−9.2	−0.7	277.9
6.0	10.5	−278.0	−6.7	−1.2	275.4
6.5	11.9	−286.0	−5.2	−0.6	279.9
7.0	12.0	−318.0	+3.5	−1.0	303.5
7.5	12.0	−345.0	+3.5	−0.1	329.6

In Table I it is seen that the horizontal advective term $\bar{v}_1\partial\bar{s}/\partial x_1$ and the vertical nonadvective term $\frac{1}{w}\frac{\partial}{\partial x_2}\{w<v_2's'>\}$ are most important. Of secondary but significant influence is the vertical advective term, $\bar{v}_2\partial\bar{s}/\partial x_2$. The horizontal nonadvective term and the time rate of change are relatively small.

THE RELATIONSHIP BETWEEN THE VERTICAL NONADVECTIVE TERM AND THE TIDE

The computed values of $<v_2's'>$ differ somewhat from place to place and from time to time, with the difference due to location being more pronounced than the difference due to time (Fig. 3). The change in $<v_2's'>$ with time should be related to a corresponding time change in the mechanism which leads to eddy mixing. Since, as stated earlier, the tide is considered to be the most important factor governing the mixing processes, there should be a relationship between the tidal velocities and the magnitude of the vertical deviation product.

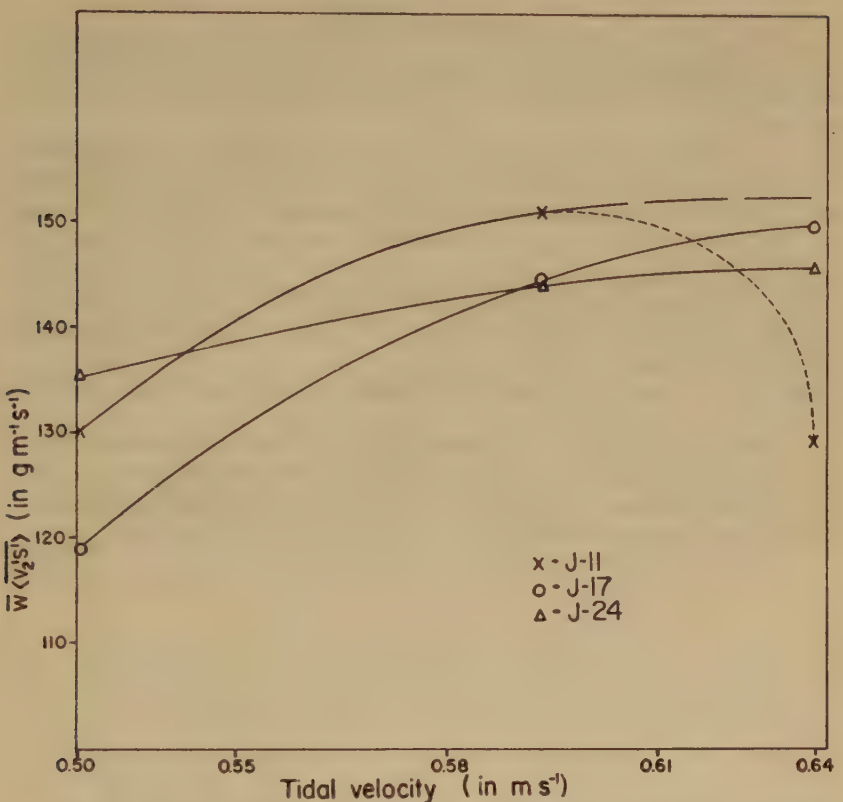

4. The mean value of the vertical nonadvective flux of salt as a function of the amplitude of the tidal velocity for three different sections in the James River.

Predicted magnitudes of the maximum flood and ebb tidal velocities, taken at a reference station near the mouth of the James River estuary during each of the periods under consideration, were obtained from the C&GS tables and were plotted against the mean value of $\langle v_2' s' \rangle$. The relation for each station is shown in Fig. 4. In all but one case there appears to be a definite relation between the tidal velocities and the vertical nonadvective term. This result is significant for two reasons. First, it confirms the hypothesis that the mixing processes are related primarily to tidal action. Second, it suggests the possibility of predicting the eddy diffusion terms from the tidal velocities.

CONCLUSIONS

The following conclusions applicable to the James River and to similar coastal plain estuaries can be made on the basis of the above analysis.

1. If mean conditions over several tidal cycles are considered, equation (9) adequately describes the salt balance. This implies that when the mean values of the parameters are taken with regard to the lateral coordinate, the only lateral terms which need be considered are those related to the divergence of the sides of the estuary.

2. In summer the two most important terms in the salt balance are (a) the mean horizontal advection and (b) the nonadvective vertical flux of salt.

3. Of secondary but significant importance is the mean vertical advection.

4. The nonadvective horizontal flux of salt and the time rate of change of mean salt content are small terms in the salt balance.

5. Some direct relationship exists between the mean magnitude of the vertical nonadvective flux of salt and the tidal velocity.

OBSERVATIONS ON THE STRUCTURE OF RED TIDES IN NEW HAVEN HARBOR, CONNECTICUT[1]

By

SHIRLEY A. MacMILLAN CONOVER

Bingham Oceanographic Laboratory
Yale University

Abstract. Observations were made on noncatastrophic red tides in New Haven Harbor, Connecticut, in the summers of 1952 and 1953. Hydrographic, chemical, and biological factors were measured and weather conditions were taken into account. Oxygen production-consumption experiments and nutrient enrichment experiments were also carried out. High concentrations of red tide organisms, here two species of *Goniaulax*, were found to be associated with stable water masses of inner harbor origin. The configuration of the harbor permits the development and retention of water masses; this tendency is reinforced by large volumes of nutrient-rich fresh water entering the inner harbor, by certain wind patterns, and by high radiation values. Adequate time, illumination, nutrients, and favorable temperatures are essential for red tide development. Stable, discrete, nutrient-rich water masses in the sea adequately meet these conditions.

Introduction and Methods. In July 1952 and June and July 1953, noncatastrophic red tide blooms of *Goniaulax* spp. were observed in New Haven Harbor, Connecticut. Similar blooms are known to have occurred in other years. Cursory examinations were made through most of the bloom periods and more detailed observations were obtained on three occasions at stations shown in Fig. 1.

At a few stations serial observations were made, but at the rest only surface samples were taken. Salinity, temperature, chlorophyll, cell counts, dissolved oxygen, phosphate, and nitrate-nitrite were measured in some or all of the samples. Temperatures were taken with a bucket thermometer; a bathythermograph was also used at some stations. Salinity titrations were made by means of the simplified silver nitrate method suggested by Harvey (1928). Raw water samples were filtered through Whatman No. 42 paper filters and were extracted overnight in 90% acetone for chlorophyll measurements. The amount of chlorophyll was determined by reading the sample in a Klett-Summerson photoelectric colorimeter with a No. 66 filter and comparing the result with a known chlorophyll standard. Raw water samples were preserved with formalin to determine phytoplankton

[1] Work carried out at the Bingham Oceanographic Laboratory under Project NR 163 118 with the Biology Branch, Office of Naval Research.

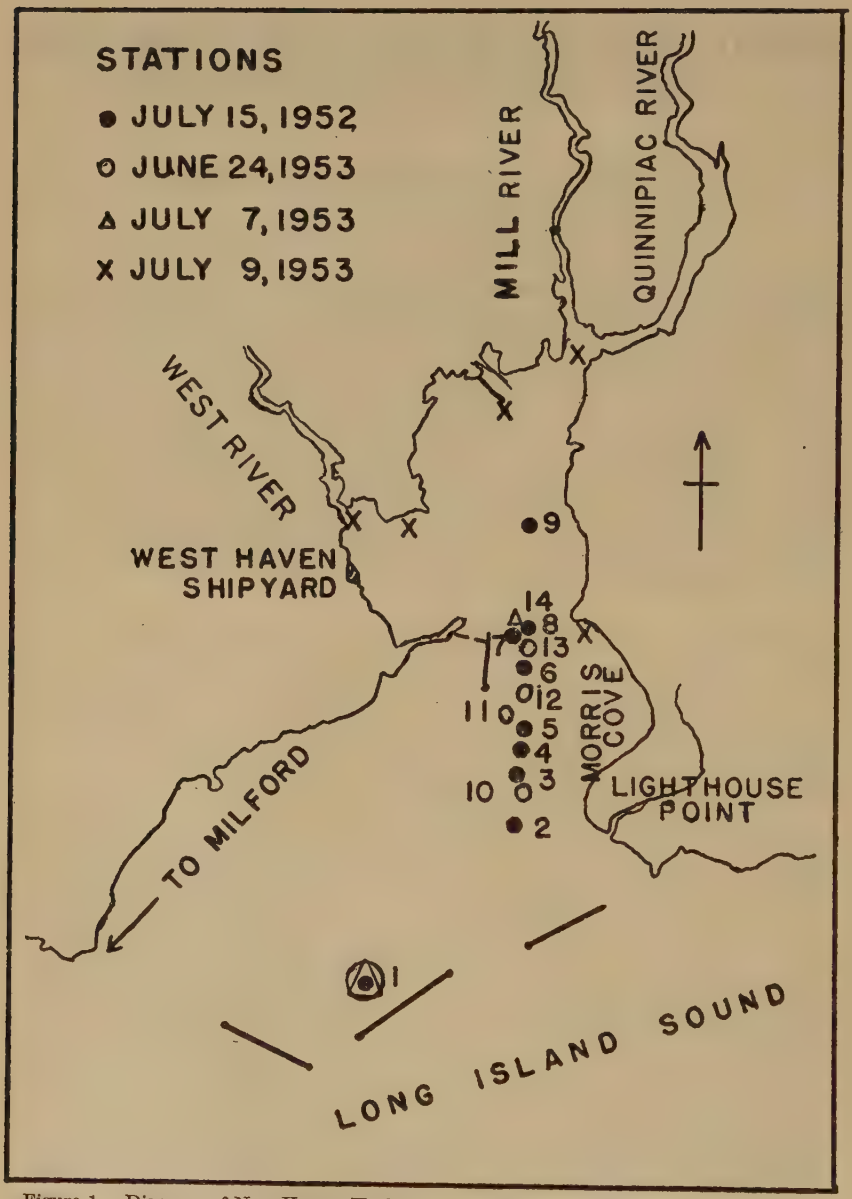

Figure 1. Diagram of New Haven Harbor, showing station positions and other points of reference. Scale: one inch = 1.4 miles.

species and total numbers. Some samples were counted directly; others were allowed to settle and were concentrated before counting. Dissolved oxygen was measured by the Winkler technique. Phosphate was determined by the Denigés-Atkins ceruleomolybdate method; the treated samples were read in the Klett with the No. 66 filter. Water treated with strychnidine-sulfuric acid reagent (Zwicker and Robinson, 1944) was read in the Klett with the No. 54 filter to estimate nitrate-nitrite concentrations.

The light bottle-dark bottle technique was used in 1953 to determine photosynthetic oxygen production. Other experiments were designed to determine the effect of nutrient enrichment and altered salinity on the 1953 blooms. The nutrients were *P*, added as KH_2PO_4, *N*, added as $NaNO_3$, and a soil extract. Since the total *P* and *N* present in the soil extract was not determined, *P* and *N* values in these bottles are marked questionable in Table IV. Salinity was increased by adding more saline Long Island Sound water to the experimental water and was decreased by adding a small quantity of distilled water. All of the experimental bottles were suspended to a constant depth of 0.5 m in Milford Harbor, Connecticut, for two days prior to analysis.

Weather data were obtained from the New Haven Weather Bureau.

General Description. The first red tide, already well developed, was reported on July 14, 1952. On the following day observations showed that it occurred in patches and streaks from the mouth of New Haven Harbor north to the mouth of the West River, where the maximum concentration was found (Fig. 1). From New Haven southwest along the coast to Milford additional streaks were seen in tide rips. The major organism of the bloom was *Goniaulax* sp., probably *Goniaulax africana* Schiller. On the next day (July 16) the bloom appeared as one large patch in New Haven Harbor along the east shore from the mouth of the Quinnipiac River to Morris Cove. At the West Haven Shipyard workmen observed red tide on the west shore and reported that contact with it produced a skin irritation. However, no injury to the marine organisms of the area was observed.

On June 24, 1953, one discrete patch of red tide was observed south of Lighthouse Point; from there into the harbor the concentration of organisms gradually increased, and, so far as could be observed, was greatest off the mouth of West River. This organism, smaller than that observed in 1952, resembled closely the descriptions of *Goniaulax cochlea* Meunier.

The third bloom, again *Goniaulax africana* (?), was observed in its initial stages on July 7, 1953. The water in the main channel of New Haven Harbor was slightly discolored in several places; one small red

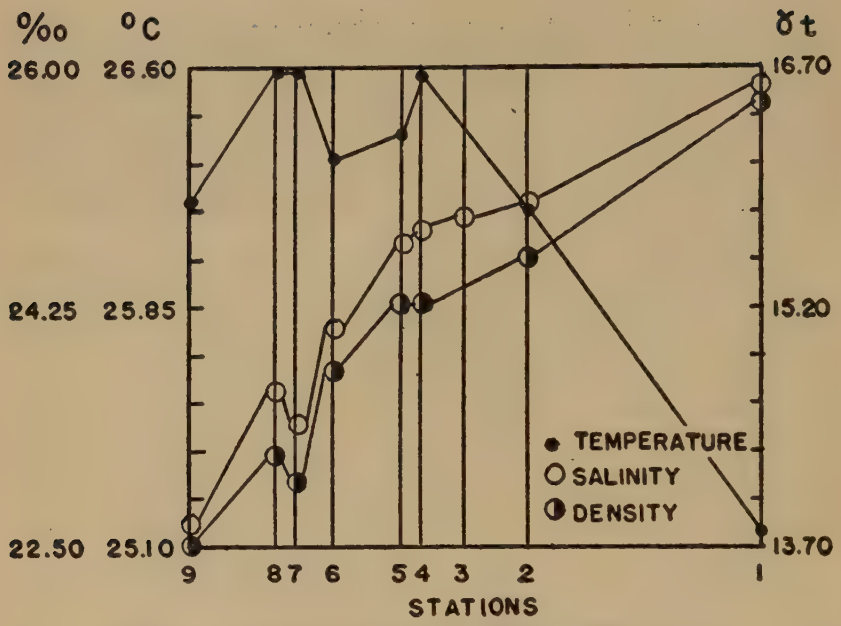

Figure 2. Temperature, salinity, and density data, July 15, 1952.

patch was located in the channel off the mouth of West River. By July 16 a major bloom had developed, and it either continued or recurred throughout the next month.

Hydrography. Examination of the data for July 15, 1952, graphed in Fig. 2, shows that gradients of temperature, salinity, and density existed from the innermost harbor stations to Station 1, where the greatest admixture of Long Island Sound water occurred. The regularity of this gradient was marred, however, by the existence of two patches of high temperature water at Stations 8–7 and 5–4, the first having a distinctly lower salinity as well. These patches were without doubt intrusions of inner harbor water which maintained their identity as discrete water masses by virtue of their density relative to the surrounding waters.

On June 24, 1953 salinity increased and temperature decreased in regular horizontal gradients from the inner harbor to the harbor mouth, uncomplicated by the existence of discrete water patches. Salinity and temperature data for July 7, 1953 suggested a situation similar to that of June 24, but not enough data were obtained to warrent a definite conclusion. Subsurface observations at Station 13 on June 24, 1953 showed that vertical gradients in salinity, temperature, and density were very large (Table I).

TABLE I. VERTICAL SECTION AT STATION 13, JUNE 24, 1953

Depth, m	Temperature, °C	Salinity, ‰	Sigma-t	Extinction coefficient	Chlorophyll, µg/l	Total phytoplankton cell count; millions/l.	Total *Gonialax cochlea* (?) cell count; millions/l.	% red tide organism / total phytoplankton	Oxygen, % saturation	P, µg at/l	N, µg at/l
0.5	19.04	23.80	16.49	2.2	75.8	45.6	44.4	97	131	.66	.20
2.5	17.95	24.37	17.32	1.6	65.6	33.5	31.5	94	117	.68	.23
4.0	16.00	24.95	18.09	1.3	31.0	10.3	8.6	86	86	.83	.08

New Haven Harbor is so shaped that the narrow waist could effectively separate the outer harbor from the inner, thus reducing the active circulation in the latter. The fresh water discharged from the Quinnipiac, Mill, and West Rivers into the inner harbor may have a long period of relative stagnation before it enters active harbor circulation. This would be particularly true if the winds are southerly and hold the water in the inner harbor. Other things being equal, the larger the volume of fresh water entering the inner harbor the larger the discrete water mass and the longer its life. The presence of large horizontal and vertical gradients described above suggests that mixing in any direction would be slow under such stable conditions.

Five days before July 15, 1952 and ten days before June 24, 1953 there were heavy rainfalls; winds on the intervening days were all southerly sea breezes or gentle easterlies. Rainfall and wind data were similar both before and after July 7, 1953. During all of these periods radiation was unusually high, and the average monthly radiation values for July 1952 and for June and July 1953 were close to 120% of normal. In short, weather conditions in New Haven Harbor were optimal for the formation and maintenance of discrete stable water masses during the periods when red tides developed.

Phytoplankton Description. By comparing Fig. 2 with Fig. 3 it is evident that high concentrations of phytoplankton organisms, as measured by plant pigments, total cell counts, and numbers of red tide organisms, were associated on July 15, 1952 with the water masses of inner harbor origin. An additional isolated concentration of organisms was found at Station 2; this might represent either a water mass that had lost its identity in all but organisms or simply a concentration of organisms in a tide rip. Phytoplankton data for June 24, 1954 revealed a regular dilution gradient; the highest con-

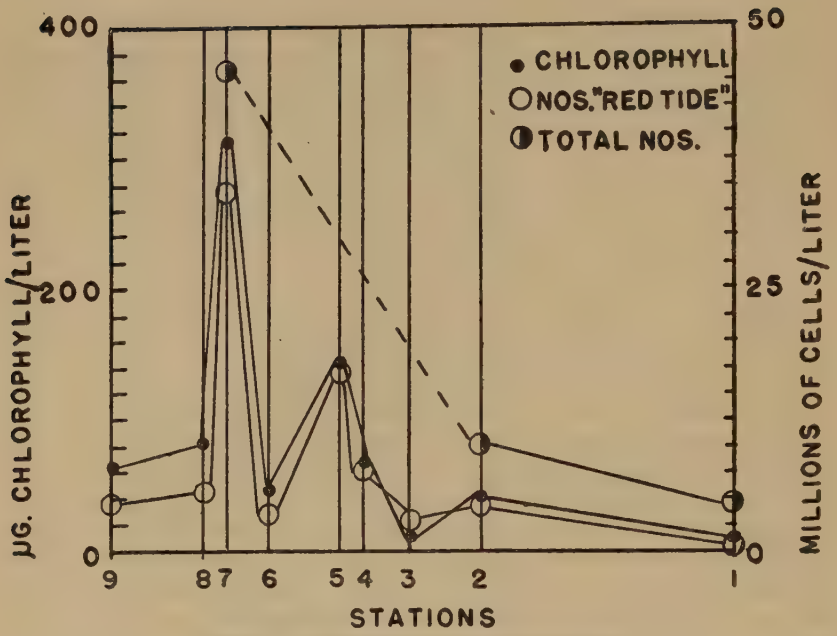

Figure 3. Phytoplankton data, July 15, 1952.

centrations of organisms were found in the inner harbor, with progressive reduction toward the outer harbor entrance.

The data for all samplings have been combined in Figs. 4 and 5, in which micrograms of chlorophyll per liter are plotted against temperature and salinity. The trends in both figures are quite clear; higher phytoplankton concentrations were associated with high temperatures and low salinities.

The phytoplankton cell counts are summarized in Table II. In addition to showing the dilution gradients, these counts show the relationship of the red tide species to other phytoplankton species in the environment. In the inner harbor waters the population was largely made up of red tide organisms while in the outer harbor waters they were only a small proportion of the population, numerically speaking. In Long Island Sound waters, small numbers of these organisms were taken, but it was only in the harbor that blooms developed.

Chemical Description. On July 15, 1952 high phosphate was associated with the fresher waters and with the discrete water masses that contained blooms. Not enough observations were made on

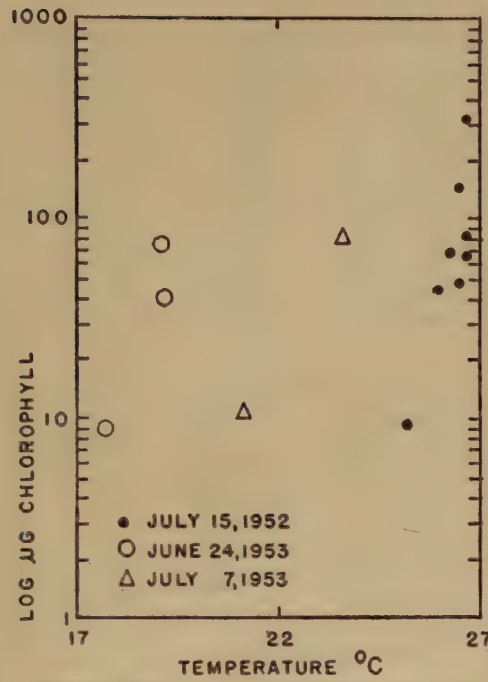

Figure 4 (left) Chlorophyll concentrations plotted against temperature.

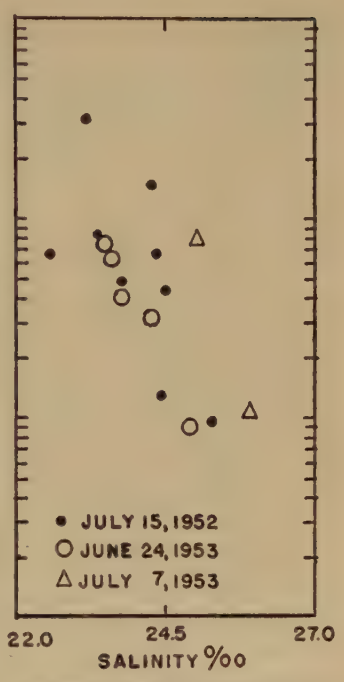

Figure 5 (right) Chlorophyll concentrations plotted against salinity.

nitrates to present a clear picture, but it seems likely that high initial concentrations in the inshore area were lowered by phytoplankton activity (Fig. 6). In the 1953 blooms the concentrations of both phosphates and nitrates were much lower than those associated with the 1952 red tide. In 1953 nitrates ranged from 0.30 to 0.0 µg at/l and *P* from 0.8 to 0.5 µg at/l.

A series of samples was taken on July 9, 1953 at the river mouths and at other shore positions (Fig. 1) in an attempt to determine the nutrient supply entering the harbor. Phosphate was approximately 2.0 µg at/l higher at these shore positions than at Station 1. Nitrate reached significantly higher proportions only under West River influence, the concentrations being 1 and 2 µg at/l higher than those in the outer harbor water. However, it seems doubtful that the West River is normally the only source of nitrate for the inner harbor waters. The other rivers and the harbor shore and shallow bottom could also be sources. When water masses are held in the inner harbor they would store increasing amounts of nutrients derived from the river, shore, and bottom sources.

TABLE II. PHYTOPLANKTON COUNTS

Date	Station	Total cell counts, millions/l	Red tide cell counts, millions/l	% red tide cells / total cells
July 15, 1952	7	46.700	34.963	75
	2	10.220	4.944	45
	1	4.965	.464	9
June 24, 1953	13	45.580	44.400	97
	1	.346	.081	23
July 7, 1953	14	10.670	6.198	58
	1	.304	.024	8

Oxygen was always supersaturated in red tide water, indicating active photosynthesis.

Phytoplankton Experiments. Two experiments were performed to estimate the rate of oxygen production in the blooms. The results are summarized in Table III. For comparison, a value obtained at the height of the Long Island Sound 1953 spring flowering is included. The red tide populations showed very active growth.

Nutrient and salinity experiments are summarized in Table IV. The nutrient experiment of June 24 tested the effects of added nutrients on the growth of *Goniaulax cochlea* (?). Some cell division occurred in the control bottle, but no cell division occurred in the bottle enriched with *P*. *N* had considerable stimulatory effect, and enrichment with soil extract and soil extract+*P*+*N* was even more effective.

The experiments of July 7 were done on *Goniaulax africana* (?). There was little growth in the control bottle. Phosphate had a slight stimulatory effect and nitrate a greater one. The initial salinity was 25.40 ‰; in one bottle this was raised to 26.12 ‰ and in the other it was lowered to 21.30 ‰; both were enriched with *N*. Greatest relative growth of this organism was found in the increased salinity bottle enriched with *N*. Growth declined when the salinity was decreased.

The experiments clearly indicate that nitrogen was a limiting factor. The need for phosphorus was slight or negligible. The soil extract had the greatest stimulatory effect; it almost certainly supplied nitrogen in an amount equal to that in the *N*-enriched bottle. Whether the additional growth was due simply to more nitrogen in any form or to other nutrients is not known.

There is no evidence that the development of blooms in the inner harbor was due to a preference on the part of the organisms for low salinity. It would be inadvisable to put much confidence in the results of a single experiment, but such evidence as is available suggests a preference for higher salinity. Perhaps, then, blooms of these

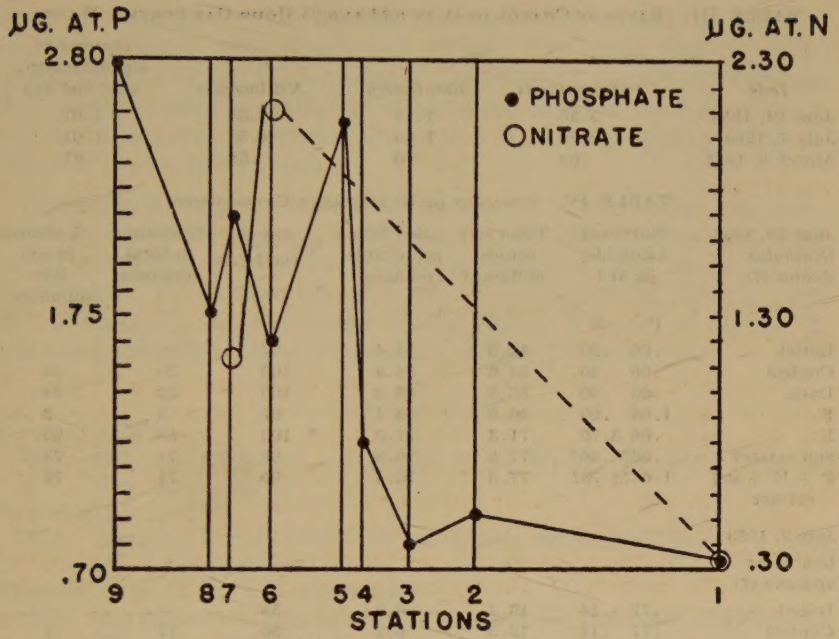

Figure 6. Phosphate *P* and nitrate *N* data, July 15, 1952.

organisms in the inshore waters occur despite low salinity rather than because of it.

Using the greatest growth rates obtained in these experiments, calculations can be made to determine the time required for the development of populations of the magnitude observed in the harbor. Such calculations are artificial at best, since the growth rate can be altered by any of several physical, chemical, and biological conditions. Even so, the calculated required time agrees rather well with the period of time available for bloom development as indicated by data on rainfall, winds, and radiation. It would have taken 14 days for the observed population of *Goniaulax cochlea* (?) to develop at the experimental rate from an initial concentration of one million cells per liter. Nine days would be required for the development of a population of *Goniaulax africana* (?) from one million cells to the level observed in 1952. A slight increase in either the size of the initial population or the growth rate would make the calculated time equal the available time.

Discussion. Slobodkin (1953) has shown that Florida red tides are associated with fresh water masses of high stability in the sea. The

TABLE III. Rates of Change of O_2 in ml/l and 24 Hour Day Surface Water

Date	*Photosynthesis*	*Respiration*	*Net increase*	*Increase in organic matter, mg/l and day*
June 24, 1953	3.36	1.78	1.58	1.67
July 7, 1953	2.22	1.69	1.53	1.61
March 9, 1953	.68	.10	.58	.61

TABLE IV. Summary of Enrichment Experiments

June 24, 1953 *Goniaulax cochlea* (?)	Nutrients available, µg at/l		Total cell counts, millions/l	Red tide cell counts, millions/l	% red tide / total cells	% change in total numbers	% change in red tide numbers
	P	N					
Initial	.66	.20	45.6	44.4	97	—	—
Control	.66	.20	54.6	54.4	100	20	23
Dark	.66	.20	55.5	55.2	100	22	24
P	1.66	.20	46.9	45.4	97	3	2
N	.66	3.70	71.3	71.0	100	58	60
Soil extract	.66?	.20?	77.8	76.8	99	71	73
P + N + soil extract	1.66?	3.70?	77.5	76.4	99	71	73
July 7, 1953 *Goniaulax africana* (?)							
Initial	.77	.14	10.7	6.2	58	—	—
Control	.77	.14	12.5	6.2	50	17	1
Dark	.77	.14	10.0	5.7	57	–6	–8
P	1.77	.14	14.9	10.0	67	40	62
N	.77	3.64	21.0	11.6	55	97	87
Initial for higher S °/oo	.77	.14	3.6	2.1	58	—	—
Higher S °/oo plus N	.60	3.67	7.8	4.4	57	119	115
Initial for lower S °/oo	.77	.14	9.6	5.5	58	—	—
Lower S °/oo plus N	.69	3.63	11.2	4.4	40	16	–20

present work is essentially in agreement with his conclusions except that New Haven red tide organisms have revealed no physiological preference for low salinity.

Because of the configuration of New Haven Harbor, water masses tend to be held in the inner portion. This tendency is reinforced by the fresh water that enters the inner harbor, by southerly winds, and by high radiation values. Such water masses are reservoirs for land-derived nutrients.

The high radiation and the great stability of the water mass that accompanied the observed red tide blooms also provided conditions of light and temperature favorable for active metabolism and cell division in the organisms. Nutrients were evidently adequate for bloom devel-

opment, although by the time the blooms were observed the essential nutrient supplies were nearly exhausted. The rains that preceded the occurrence of red tides probably introduced a supply of nutrients; they also increased the stability of the water mass in the inner harbor, making it resistant to physical dissipation and thus providing adequate time for bloom development.

Acknowledgements. The author wishes to acknowledge the help, advice, and encouragement of Dr. Gordon A. Riley, senior investigator of the ONR project on Long Island Sound, and of Dr. L. B. Slobodkin. Thanks are also due Dr. Victor Loosanoff, director, and Mr. Herman R. Glas, captain of the *Shang Wheeler*, of the U. S. Fish and Wildlife Service Laboratory, Milford, Connecticut.

REFERENCES

Harvey, H. W.
1928. Biological Chemistry and Physics of Sea Water. The MacMillan Co., New York. 194 pp.

Slobodkin, L. G.
1953. A possible initial condition for red tides on the coast of Florida. J. Mar. Res., *12* (1): 148–155.

Zwicker, B. M. G. and R. J. Robinson
1944. The photometric determination of nitrate in sea water with a strychnidine reagent. J. Mar. Res., *5* (3): 214–232.